Isolation and Analysis of the Embryonic Lethal Mutation t^{w18}

Inaugural-Dissertation

to obtain the academic degree

Doctor rerum naturalium (Dr. rer. nat.)

submitted to the Department of Biology, Chemistry and Pharmacy

of the Freie Universität Berlin

by

Lisette Lange

from Berlin

December 2014

The present work was carried out at the Max-Planck-Institute for Molecular Genetics, Department of Developmental Genetics, in Berlin, Germany, between October 2010 and December 2014, under the supervision of Prof. Dr. Bernhard G. Herrmann.

1st Reviewer:

Prof. Dr. Bernhard G. Herrmann

Max-Planck-Institute for Molecular Genetics

Ihnestraße 63-73

14195 Berlin

2nd Reviewer:

Prof. Dr. Rupert Mutzel

Freie Universität Berlin

Königin-Luise-Straße 12-16

14195 Berlin

Date of Defense: 29.05.2015

To Matthias and our little one.

Contents

Abbreviations

AP	alkaline phosphatase
A-P	anteroposterior
AP-MS	affinity purification coupled with mass spectrometry
AVE	anterior visceral endoderm
BAC	bacterial artificial chromosome
bp	base pairs
cDNA	complementary DNA
ctrl	control
DIG	digoxigenin
DNA	deoxyribonucleic acid
DVE	distal visceral endoderm
E	embryonic day
EMT	epithelial-mesenchymal transition
EmVE	embryonic VE
ESC	embryonic stem cell
EtOH	ethanol
ExE	extraembryonic ectoderm
FC	fold change
Flp	Flippase
FPKM	fragments per kilobase of transcript per million mapped reads
FRT	Flp recombination target
GO	gene ontology
H&E	hematoxylin and eosin
HRP	horse radish peroxidase
ICM	inner cell mass
kb	kilobase(s)
LB	Luria Broth
LC-MS/MS	liquid chromatography tandem mass spectrometry
MeOH	methanol
mRNA	messenger RNA
n.a.	not affected
neo	neomycin phosphotransferase-encoding gene
NGS	next generation sequencing
4-OHT	4-hydroxytamoxifen
pA/polyA	polyadenylation signal

PCC	Pearson correlation coefficient
PCR	polymerase chain reaction
PP2A	protein phosphatase 2A
PS	primitive streak
qPCR	quantitative realtime PCR
RIN	RNA integrity number
RT	room temperature
SDS PAGE	sodium dodecyl sulfate polyacrylamide gel electrophoresis
SH-tag	Strep-tag II and HA epitope
snRNA	small nuclear RNA
Tcd	*t* complex distorter
Tcr	*t* complex responder
TRD	transmission ratio distortion
U	unit
UTR	untranslated region
VE	visceral endoderm
WISH	whole-mount *in situ* hybridization
w/o	without
wt	wild-type
YAC	yeast artificial chromosome

1 Abstract

t haplotypes are naturally occurring variants of a ~40 Mb region on the proximal portion of mouse chromosome 17 which can affect embryonic development, among other things. The t^{w18} haplotype carries a lethal factor which causes defects in cell lineage differentiation during gastrulation, resulting in embryonic lethality between E8.5 and E10.5. Previous work identified a large deletion in the t^{w18} haplotype presumed to contain the gene causing the homozygous phenotype. In this work, using next generation sequencing and PCR analyses, the borders of this deletion were precisely mapped. This revealed a region of 4.3 Mb containing 74 genes, among which *Ppp2r1a* was identified as a candidate gene. *Ppp2r1a* encodes for the scaffolding subunit Aα of protein phosphatase PP2A. Loss of *Ppp2r1a* function was shown to phenocopy the t^{w18} homozygous phenotype. In addition, expression of *Ppp2r1a* from a BAC transgene introduced into the t^{w18} homozygous background was able to rescue gastrulation defects and overcome embryonic lethality. Taken together, these results confirm *Ppp2r1a* as the gene responsible for the t^{w18} phenotype.

Gene expression profiling of E6.5 embryos revealed a function for PPP2R1A in regulating Wnt and Nodal signaling. In embryos lacking *Ppp2r1a*, dysregulation of these pathways resulted in failure to induce the mesendodermal cell fate, and enhanced cell adhesion, causing cells to become trapped in the primitive streak. An *in vitro* mass spectrometry approach to analyze the PPP2R1A interaction network showed interaction of PPP2R1A with B regulatory subunits of PP2A that are involved in regulating Wnt and Nodal signaling, which further supports a function for PPP2R1A in the regulation of these signaling cascades.

2 Zusammenfassung

t-Haplotypen sind natürlich vorkommende Varianten einer ~40 Mb großen Region im proximalen Teil von Chromosom 17 der Hausmaus, die unter anderem die Embryonalentwicklung beeinflussen können. Der t^{w18}-Haplotyp trägt eine letale Mutation, die Defekte während der Gastrulation und Letalität zwischen Tag 8.5 und 10.5 während der Entwicklung hervorruft. Eine große Deletion wurde vorgeschlagen, das Gen zu enthalten, das den homozygoten t^{w18} Phänotyp verursacht. Durch Genomsequenzierung und PCR-Analysen konnten die Grenzen der Deletion präzise bestimmt werden. Dies zeigte eine 4.3 Mb große deletierte Region, die 74 Gene enthält. Unter diesen 74 Genen wurde *Ppp2r1a*, das für die Strukturuntereinheit Aα der Proteinphosphatase PP2A codiert, als Kandidatengen isoliert. Der Funktionsverlust des Gens erzeugt Embryonen, deren Phänotyp dem von t^{w18}-Homozygoten entspricht. Es ist außerdem möglich, den t^{w18}-Phänotyp durch Expression eines *Ppp2r1a*-BAC-Transgens zu komplementieren. Diese Ergebnisse bestätigen *Ppp2r1a* als das für den t^{w18}-Phänotypen verantwortliche Gen.

Transkriptomanalysen von mutanten Embryonen an Tag 6.5 zeigen, dass *Ppp2r1a* während der Gastrulation an der Regulierung wichtiger Signalwege, wie Wnt und Nodal beteiligt sein könnte. In Embryonen denen *Ppp2r1a* fehlt, führt die Deregulierung dieser Signalkaskaden dazu, dass einerseits mesendodermale Zelllinien nicht spezifiziert werden können und andererseits Zellen durch verstärkte Zelladhäsion, den Primitivstreifen nicht verlassen können. Dem Gegenüber konnte in *in vitro*-Massenspektrometrieversuche gezeigt werden, dass PPP2R1A mit PP2A B regulatorischen Untereinheiten interagiert, die an der Regulierung von Wnt- und Nodal-Signalwegen beteiligt sind. Dies bestätigt, dass PPP2R1A ebenfalls eine Funktion in der Regulierung dieser Signalkaskaden hat.

3 Introduction

An adult mammalian organism consists of more than 200 different cell types that all originate from a single cell: the zygote. Despite huge differences in morphology and function, all cell types of an organism contain the same genetic information. Meaning that, during development from the zygote to an adult organism, differentiation into many different cell types is almost never achieved by changes in the DNA sequence itself, but by highly controlled changes in gene expression. Thereby, every specialized, differentiated cell expresses a specific subset of genes that determines the cell's shape, size and function. This differential gene expression requires spatiotemporal information provided by gene regulatory networks that involve interactions of large numbers of genes and their regulators (Macneil and Walhout, 2011). Gene regulatory networks are influenced by the presence of signaling molecules and transcription factors. Internal or external signals influence complex pathways that control transcription, translation, mRNA or protein stability, and ultimately act on the activity of transcription factors that lead to changes in gene expression levels. To elucidate the function of genes within these complex networks, it is quit often helpful to analyze mutants in model organisms that show specific phenotypes.

In genetics, two approaches emerged to analyze gene functions. Reverse genetics, the more recent approach, explores the function of a gene by analyzing phenotypic effects based on a known genotype. In contrast, classical forward genetic approaches start from mutagenically induced or naturally occurring phenotypes to look for the genetic basis, particularly the gene that is affected. Despite all of the technical advances, the function of many genes have not yet been identified. It is therefore still in the interest of researchers to analyze gene function. The overarching Subject of the current project is an embryonic lethal phenotype in the house mouse. This phenotype is especially interesting since it involves disruption of a pro-

cess that controls the switch from a proliferative state towards differentiation during gastrulation. Isolation of the developmentally important gene that is responsible for this phenotype has thus provided insight into general processes that control the transition from proliferation to differentiation.

3.1 Mouse embryonic development

Preimplantation

Following fertilization, cleavage in the mouse zygote starts after around 24 h (Gilbert, 2014; Slack, 2009). These first mitotic cell divisions proceed very slowly, every 12-24 h, and often are asynchronous. In contrast to zebrafish and *Xenopus*, the zygotic genome is already activated at the two-cell stage. After the third cleavage, the eight blastomeres form a loose arrangement and initiate a process called compaction. The embryo acquires a nearly spherical shape, which is achieved through the expression of *E-cadherin* (Gilbert, 2014). This cell adhesion protein mediates flattening of the blastomeres and increases intercellular contacts. The compacted 16-cell embryo is called morula and consists of an outer layer of cells surrounding internal cells. At this stage, outer cells become polarized, displaying tight junctions at the outer surface, whereas gap junctions form between internal cells. Following further cell divisions, the first differentiation process during mouse embryogenesis becomes apparent: external cells form the trophoblast (trophectoderm), while internal cells give rise to the inner cell mass (ICM). Trophoblast cells do not contribute to the embryo proper, but form the tissue of the chorion, the extraembryonic membrane and part of the placenta. In contrast, the inner cell mass gives rise to the embryo proper and its associated yolk sac, allantois and amnion. Trophoblast cells secrete fluid into the morula to form the blastocoel. This cavitation process leads to positioning of the ICM at one side of the inside of the trophoblast layer, resulting in the formation of the blastocyst at around E3. Between E3.5 and E4.5, the primitive endoderm

delaminates from the ICM and the trophectoderm divides into a polar and a mural component (Fig. 1). The primitive endoderm surrounds the ICM at its blastocoelic surface. It will form the yolk sac and will be important during gastrulation for positioning and cell movements. The remaining ICM forms the epiblast that gives rise to all embryonic tissues, the amnion, and the allantois.

Implantation

When the embryo reaches the uterus at around E5.0, it hatches from the zona pellucida and attaches to the uterine epithelium. After implantation into the uterus, the embryo develops into a cylindrical structure, known as the egg cylinder (Fig. 1). At this stage, the epiblast surrounds the proamniotic cavity. While the epiblast remains visibly undifferentiated, the primitive endoderm divides into the visceral and the parietal endoderm. The visceral endoderm (VE), an important signaling center, forms a layer around the epiblast, whereas the parietal endoderm covers the whole inner surface of the mural trophectoderm and secretes Reichert's membrane. Pluripotency of the epiblast is maintained by the action of transcription factor complexes, involving POU5F1f1 (OCT4), SOX2, NANOG, and SALL4, and by suppression of differentiation-promoting genes by Polycomb proteins (reviewed in Tam and Loebel, 2007). In addition, Nodal signaling is required to avoid premature differentiation into the neuroectodermal lineage (Camus *et al.*, 2006).

Gastrulation

Prior to establishing the anteroposterior axis of the embryo, a proximodistal axis emerges. Breifly, NODAL which is expressed in the epiblast, induces activation of SMAD2 in the VE to form the distal VE (DVE) (Norris and Robertson, 1999; Brennan *et al.*, 2001). This important signaling center produces the Wnt and Nodal antagonists DKK1, CER1 and LEFTY1, that inhibit Wnt and Nodal signaling in the overlying distal epiblast. In addition, reciprocal interactions of the epiblast with the

extraembryonic ectoderm (ExE), that include BMP signals, are necessary to maintain and pattern the proximal epiblast. The proximodistal axis is then converted into a anteroposterior axis by migration of the DVE towards the prospective anterior end of the embryo and induction of the anterior VE (AVE) (Kondoh and Kuroiwa, 2014). Gastrulation is initiated at E6.25 with the formation of the primitive streak, and re-

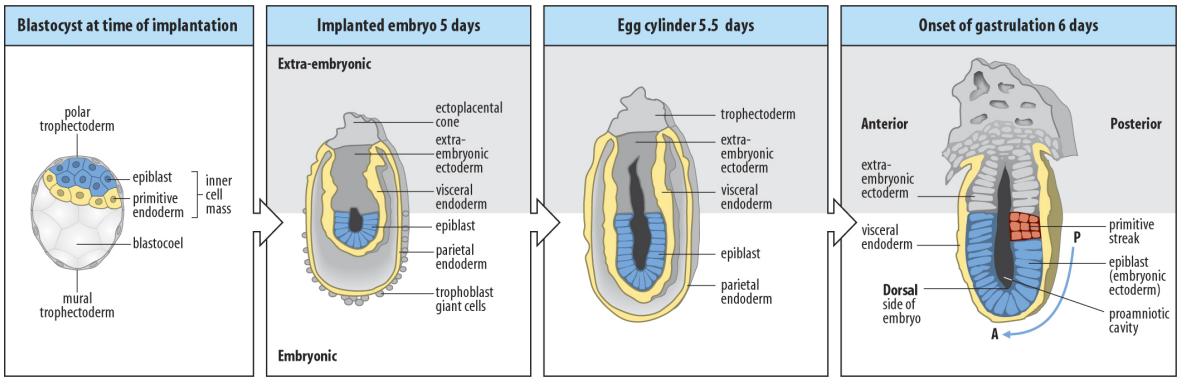

Figure 1. Early post-implantation development. The implanting blastocyst consists of the trophectoderm and the ICM, that will give rise to the embryo. The ICM separates into the primitive endoderm and the epiblast. After implantation, the cup-shaped embryo is called the egg cylinder. The epiblast elongates and forms an internal cavity, the proamniotic cavity. The primitive endoderm divides into the visceral and the parietal endoderm. Gastrulation is initiated with the formation of the primitive streak at the posterior end of the epiblast. Adopted from Wolpert (2007).

sults in formation of the three primary germ layers (Fig. 1). This process of extensive morphogenetic movements determines the anteroposterior axis of the embryo and establishes its basic body plan. Prior to formation of the primitive streak at the future posterior end of the embryo, an anteroposterior polarity has to be established in the epiblast and the visceral endoderm. This is achieved by a finely-tuned balance of Nodal signaling. Nodal and Wnt antagonists that are secreted by the AVE block signaling and induce neuroectodermal character. In contrast, signals on the prospective posterior side of the embryo allow mesendodermal characteristics (Arnold and Robertson, 2009). Thereby, Nodal induces expression of *Wnt3* that signals through the canonical pathway, involving β-catenin, Lrp5 and Lrp6 (Huelsken *et al.*, 2000; Kelly *et al.*, 2004; Liu *et al.*, 1999)

The formation of the primitive streak is initiated by the movement of epiblast cells

towards the posterior proximal pole of the embryo. The primitive streak extends across the ectoderm towards the distal tip of the embryo, where the node forms (Fig. 2). During this process, mesendodermal cells are being continuously specified. They originate from the epiblast, undergo epithelial-mesenchymal transition (EMT), loose *E-cadherin*, and ingress through the primitive streak. Mesoderm induction depends on BMP signaling from the ExE, Nodal and Wnt signaling from the epiblast and results in *Brachyury (T)* expression in nascent mesoderm. Depending on the time and site of ingression, mesodermal cells become allocated to distinct cell lineages in a posterior-anterior fashion (Lawson, 1999). The first cells that ingress through the primitive streak will give rise to extraembryonic mesoderm, which is followed by the specification of lateral plate, paraxial and cardiac mesoderm. Axial mesendodermal tissues emerge from epiblast cells that migrate through the most anterior part of the primitive streak. These form the prechordal plate, node, notochord and definitive endoderm (Gilbert, 2014).

EMT and cell movements through the primitive streak are regulated by FGF signaling. Mediated by Fgfr1, FGF signals induce the expression of *Snai1*. This transcriptional repressor directly downregulates *E-cadherin* expression (Cano *et al.*, 2000). In addition, the nodal target and T-box transcription factor Eomes is important for EMT and mesodermal cell migration. Although in *Eomes* mutant embryos, epiblast cells are specified towards mesoderm, cells fail to downregulate E-cadherin, to undergo EMT and to migrate towards the primitive streak (Russ *et al.*, 2000; Arnold *et al.*, 2008).

With induction of the notochord, the formation of the head is initiated. At E7.0, a head process forms anterior to the node. It consists of the notochordal plate flanked by definitive endoderm and neural plate. At this stage, the amnion and chorion begin to form as the amniotic fold emerges from the ectoderm and mesoderm at the junction of posterior primitive streak and ExE. This process also forms the amniotic cavity, the exocoelom and the ectoplacental cavity (Fig. 3). The node then

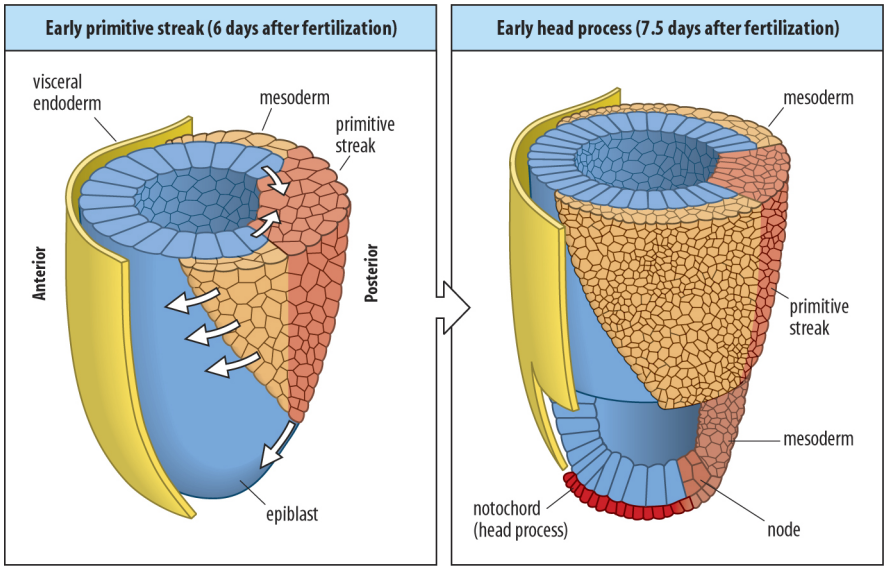

Figure 2. Mouse gastrulation. Epiblast cells ingress into the primitive streak and then spread out laterally between the epiblast surface and the visceral endoderm to form the mesodermal layer. The primitive streak elongates anteriorly and forms the node. The notochord emerges from the node and is essential for the formation of the head process. Adopted from Wolpert (2007).

regresses posteriorly, while mostly trunk mesoderm is allocated in an anteroposterior sequence. The posterior region of the embryo is patterned by FGF, Wnt and retinoic acid gradients. While *Fgf8* is expressed in the elongating posterior tip of the embryo, *Fgf8* mRNA is progressively degraded in more anterior tissue. This results in an *Fgf8* mRNA and protein gradient (Dubrulle and Pourquié, 2004). An opposing retinoic acid gradient is established by anteriorly expressed retinoic acid-synthesizing and posteriorly expressed degrading enzymes (Oosterveen *et al.*, 2004; Swindell *et al.*, 1999). These gradients act on *Cdx* genes that in turn regulate *Hox* gene expression, that specify anteroposterior positioning (Lohnes, 2003).

At around E8.5, the embryo starts the process of turning, during which it rotates along its own axis. Turning not only brings the dorsal surface to the outside and the ventral surface inwards (Fig. 3), it also results in the complete surrounding of the embryo by the amnion. Between E9.25-9.5 the primitive streak becomes incorporated in the caudal end forming the tailbud. For several more days the caudal end generates new mesoderm (Schoenwolf, 1977).

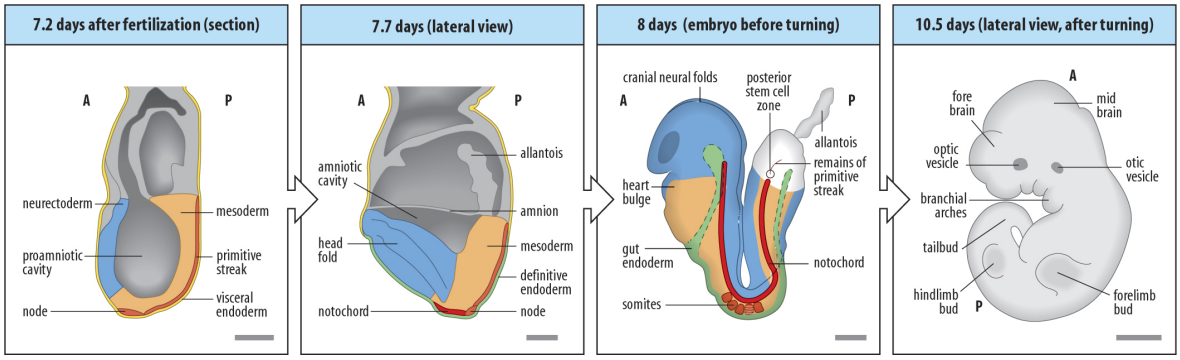

Figure 3. Generation of the basic body plan. During gastrulation the basic body plan of the embryo is established. Mesoderm and the definitive endoderm are allocated by migration through the primitive streak. The notochord serves as signaling center to guide the development of neural structures from anterior ectoderm. By E8 a distinctive head, neural folds, the heart, somites and the gut are visible. After turning the embryonic body plan is established. Adopted from Wolpert (2007).

Organogenesis

While during gastrulation the three germ layers and the embryonic body plan forms, organogenesis in parallel leads to the differentiation and development of the germ layers into individual organs, with the heart being the first organ formed. In the course of prenatal development in the mouse, the fetus grows and is born 18-21 days after fertilization, depending on the strain.

3.2 The *t* complex and *t* haplotypes

Up to 25% of wild house mice (*Mus musculus*)carry a variant form of the proximal region of chromosome 17, the so-called *t* haplotype (Lenington *et al.*, 1988). They were first discovered more than 90 years ago when heterozygous *T*/+ mutants that do not show any abnormalities except for a short tail, were crossed to wild house mice (Dobrovolskaia-Zavadskaia and Kobozieff, 1932). A certain percentage of the offspring of these matings were completely tailless. And due to their many fascinating features, including pleiotropic effects on tail length, embryonic development, fertility and genetic recombination, *t* haplotypes have long been viewed as mysterious elements that hide within the mouse genome. It was first suggested by Mary

Lyon that *t* haplotypes are related by forming an altered chromosomal structure of a large genetic locus (Lyon and Phillips, 1959). Her findings were long ignored by colleagues until the inversions were discovered: a variety of investigations including molecular marker and classic genetic analyses clarified that *t* haplotypes emerged during evolution of *Mus musculus* from a common ancestor by four subsequent inversions (*in(17)1-in(17)4*) in a region called the *t* complex (Silver *et al.*, 1992). These inversions greatly suppress homologous recombination with the wild-type chromosome, and the *t* haplotype is thus inherited by the offspring as if it was a single locus and is maintained as a well-defined genomic entity (Silver and Artzt, 1981). The *t* complex is contained within the proximal half of mouse chromosome 17 spanning over 20 cM (~ 40 Mbp). It includes the *Brachyury* (*T*) locus, as well as the major histocompatibility complex (*H-2*) and many other genes. In addition to many normally functioning genes, *t* haplotypes carry a number of independent mutant loci that are responsible for the various features of *t* haplotypes (Silver, 1985).

Although *t* haplotypes carry genes that cause embryonic lethality or male sterility in homozygotes, they have been maintained in mouse populations. This can be explained by altered transmission. *t* haplotypes are not transmitted in a Mendelian ratio, but promote their own transmission at the expense of the wild-type counterpart. Heterozygous *t*/+ males transmit the *t* chromosome to up to 99% of the offspring. This phenomenon is called transmission ratio distortion (TRD). Thereby, one can discriminate between complete and partial *t* haplotypes. While complete *t* haplotypes carry all four inversions, and with them all elements necessary for a high transmission, partial *t* haplotypes also contain wild-type sequences. They originate from rare recombination events between a complete *t* haplotype and the wild-type chromosome. Partial *t* haplotypes, therefore, do not carry all TRD elements and transmission ratios vary depending on the retained *t* DNA.

Evolution of *t* haplotypes

Various studies have aimed to analyze the relationship between *t* haplotypes. First attempts using monoclonal or polyclonal antibodies specific for the *H-2* complex were complemented by sequencing approaches (Nizetić *et al.*, 1984; Hammer and Silver, 1993; Morita *et al.*, 1992). Morita *et al.* (1992) sequenced an intron of the *Tcp-1* gene in the second inversion, *in(17)2*, in four different *t* haplotypes and Hammer and Silver (1993) sequenced the *Hba-ps4* locus located in the fourth inversion, *in(17)4*, in 19 *t* haplotypes. Both studies revealed a very low level of polymorphisms, showing that all *t* haplotypes are closely related and share a common ancestor that must have lived 100 000 years ago (reviewed in Silver, 1993). Surprisingly, *t* haplotypes are present in four different *Mus* subspecies (*domesticus*, *musculus*, *castaneus* and *bactrianus*), which evolutionarily separated around 1 million years ago (Bonhomme, 1986). This means that the descendants of the common ancestor of *t* haplotypes rapidly spread across large geographical distances and was distributed within different subspecies by introgression.

Evolution towards the present-day *t* haplotypes took a much longer period of time than the past 100 000 years since the common ancestor. Phylogenetic analyses showed that *in(17)2* was the first inversion, which happened ~3 million years ago before divergence of the *M. musculus* lineage from the *M. macedonicus* lineage, but after separation from the *M. spretus* lineage. Despite an enhanced transmission ratio, this inversion was not fixed in mouse populations, most likely due to negative effects on homozygous male fertility. Later, within a period of about one million years, three other inversions *in(17)1*, *in(17)3* and *in(17)4* accumulated in the *Mus musculus* lineage (Hammer *et al.*, 1989). It is speculated, that the most recent common ancestor arose in the *M. musculus domesticus* lineage and that this *t* haplotype replaced less effective descendants in other *M. musculus* subspecies, leading to present-day *t* haplotypes.

Transmission ratio distortion and male sterility

Transmission of the *t* chromosome from heterozygous *t*/+ males to their offspring differs from the expected Mendelian ratio of 50%. They instead transmit the *t* chromosome to up to 99% of their offspring (Chesley and Dunn, 1936). Males homozygous for one *t* haplotype, or that carry two different complementing *t* haplotypes, are sterile, while females show normal transmission and fertility (reviewed in Lyon, 2003). The fact that only males are affected hints towards a scenario that includes sperm function. Indeed, it has been shown that motility of wild-type sperm is impaired while *t* sperm retain normal fertilization ability (Katz *et al.*, 1979; Olds-Clarke and Johnson, 1993). TRD is, in this manner, caused by the action of several *t* haplotype-encoded *t* complex distorters (*Tcd1-4*) that act on the *t* complex responder (*Tcr*) locus (Lyon, 1984). The *t* haplotype-encoded *Tcds* are *trans*-acting factors that mediate a harmful effect during spermatogenesis. Since spermatogenesis occurs in a syncytium, the gene products of the distorters are equally distributed between wild-type and *t* sperm. The responder, *Tcr*, acts in *cis* to rescue this harmful effect only in *t* sperm which encode the *Tcr* gene. This leads to a normal motility in *t* sperm, while the motility of wild-type sperm is impaired. *Tcr* was identified as a fusion gene between the *Smok1* (Sperm motility kinase 1) at the N-Terminus and the 3' UTR of*Rsk3* (ribosomal protein S6 kinase) at the C-terminus (Herrmann *et al.*, 1999). The product of the fusion gene results in a dominant-negative Smok1 with reduced kinase acitivity. Two of the *Tcd* genes that were identified so far, encode mutant forms of regulators of Rho small G-proteins (Bauer *et al.*, 2005, 2007). In a TRD model, Bauer *et al.* suggest that the distorters additively act on Rho signaling pathways that regulate Smok1 leading to its hyperactivation in *t* and wildtype sperm and abnormal flagellar function. This hyperactivation is rescued in *t* sperm by the reduced activity of dominant-negative Smok1^{Tcr}, bringing *t* flagellar function back to normal levels.

In a homozygous *t* haplotype case, double the amount of *distorter* genes is expressed, which enhances their harmful effect (Lyon, 1986). This stronger effect can-

not be rescued by *Tcr*, and impaired sperm motility results in male sterility. Homozygous male sterility thus seems to be the cost of enhanced transmission ratio in *t* haplotypes. If this is the case, the introduction of homozygous lethal alleles in *t* hapotypes poses an evolutionary advantage that removes sterile males from mating competition with heterozygous *t*/+ males (Silver, 1993).

t lethal genes

A study on complete *t* haplotypes from mice trapped in Europe and the Middle East showed that 22 of the 30 recovered *t* haplotypes (73%) carried homozygous lethal alleles (Klein *et al.*, 1984). Whereas complete *t* haplotypes cannot be distinguished from one another in most of their properties, they can carry different lethal mutations that can be assigned to different complementation groups (Dunn, 1937). In genetic tests, heterozygous animals from different *t* haplotypes are crossed, and the progeny is analyzed for viability of animals carrying both *t* haplotypes. Lethal mutations from different complementation groups affect different developmental genes which result in viable compound heterozygous offspring. These types of experiments illustrated that these *t* lethal genes are non-allelic and map to different loci on the chromosome (Artzt *et al.*, 1982). *t* haplotype members from the same complementation group affect the same gene locus or developmental pathway, and concurrence of both *t* haplotypes results in embryonic lethality. In this manner, Klein *et al.* (1984) found eight new complementation groups that raised the number of presently known complementation groups to 16, meaning that at least 16 developmentally important genes are present in *t*-haplotypes.

Genetic analyses of the *t* lethals turned out to be very difficult, but lethal *t* haplotypes have been analyzed for their morphological effects on mouse embryogenesis. Bennett (1975) summarized defects of lethal *t* haplotypes from different complementation groups during early embryonic development (Fig. 4). This shows that genes are affected in *t* haplotypes that function during different stages of development.

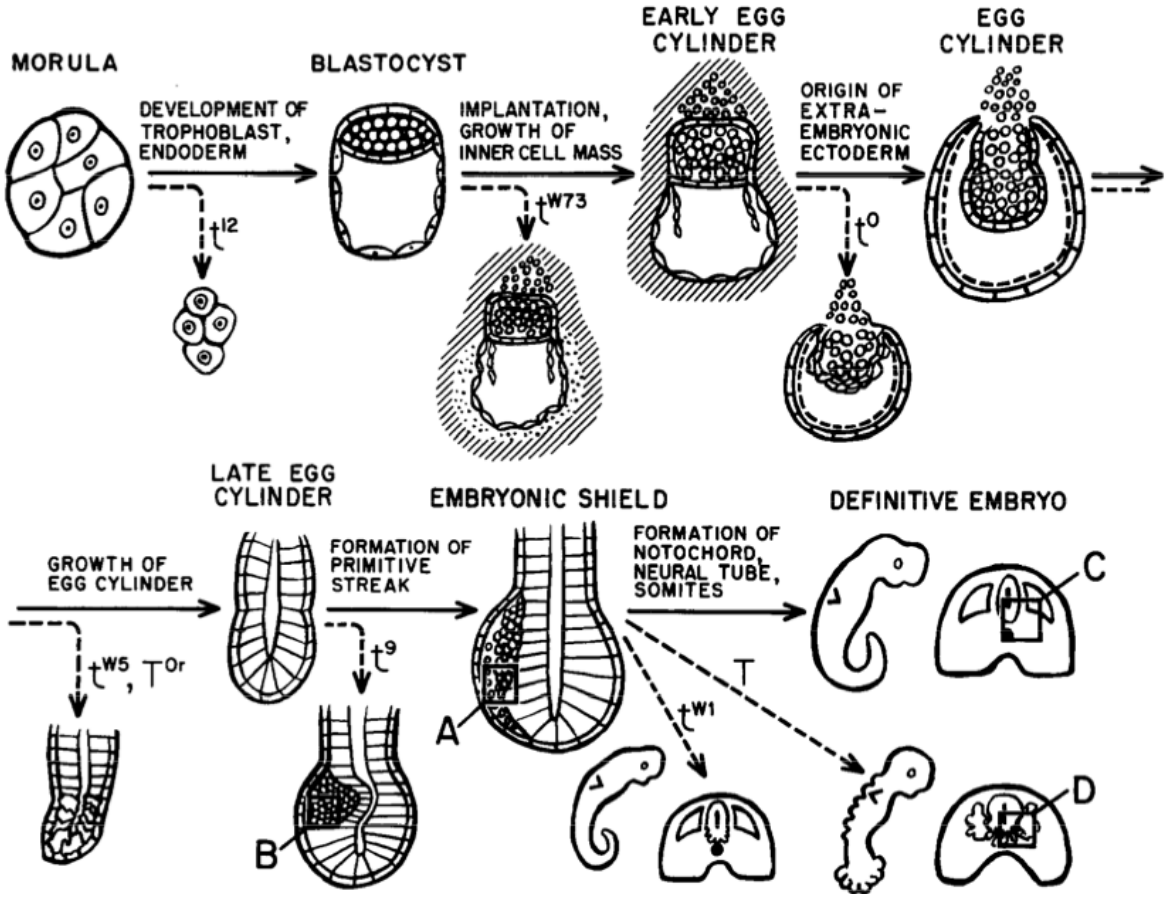

Figure 4. Schematic representation of *t* lethal phenotypes. Embryonic defects from various *t* haplotypes are depicted at different stages during early mouse development. Adopted from Bennett (1975).

While, for example, t^{12} homozygous embryos become arrested just prior to blastocyst stage and do not implant, defects in t^{9} homozygotes occur during initiation of primitive streak formation, resulting in abnormal or absent mesoderm formation (Smith, 1956; Bennett and Dunn, 1960; Moser and Gluecksohn-Waelsch, 1967).

Recombination suppression between wild-type and *t* DNA made gene mapping approaches and the isolation of mutated genes of lethal *t* haplotypes very difficult, and until very recently none of the genes that cause embryonic lethality in *t* haplotypes had been identified. In a recent study, the t^{w5} haplotype was isolated by Sugimoto *et al.* (2012). This *t* haplotype is characterized by a specific defect in embryonic ectoderm (epiblast) formation resulting in lethality at E6.5 (Bennett and Dunn, 1958). Immunofluorescence staining of homozygous t^{w5} embryos with antibodies

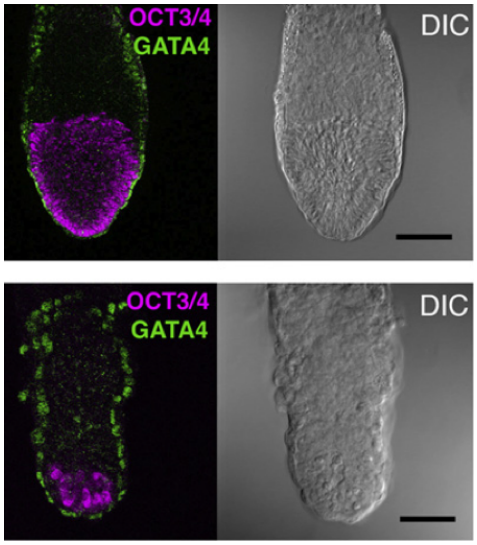

Figure 5. Growth defects in embryonic ectoderm of t^{w5}/t^{w5} embryos. Immunofluorescence staining of $t^{w5}/+$ (upper panel) and t^{w5}/t^{w5} (lower panel) embryos, showing severe defects in Oct3/4-positive embryonic ectoderm with normal VE (Gata4-positive) in t^{w5} homozygotes. Adopted from Sugimoto *et al.* (2012).

against Oct3/4, an embryonic ectoderm marker, and Gata4, a VE marker, shows that growth of the embryonic ectoderm is severely disrupted, while VE is normally formed (Fig. 5) (Sugimoto *et al.*, 2012). A very specific defect that affects growth and differentiation of the epiblast prior to initiation of gastrulation is observed, with extraembryonic tissues developing almost normally. To isolate the gene responsible for the t^{w5} phenotype, Sugimoto *et al.* (2012) followed a positional cloning approach by functional complementation through BAC transgenesis using a 750-kb critical region that was determined in previous studies (Abe *et al.*, 2004). Transgenic $t^{w5}/+$ mouse lines were established that expressed one of five BACs that spanned this region. Mice were crossed then to t^{w5} heterozygous animals. Indeed, one of the BACs rescued the lethal t^{w5} phenotype and pups were recovered that carried the t^{w5}/t^{w5} genotype in addition to the BAC transgene. To identify the responsible gene in this region, rescue experiments were repeated with transgenes consisting of restriction enzyme fragments from the identified BAC. This led to the isolation of the candidate gene *Vps52* (*vacuolar protein sorting 52*). Sequencing of the gene in the t^{w5} haplotype revealed a frameshift mutation resulting in a premature termination codon. The no-

tion that the absence of functional *Vps52* is responsible for the phenotype was further validated by targeted disruption of *Vps52*. In functional analyses that followed, Sugimoto *et al.* (2012) showed that *Vps52* is specifically expressed in the VE and that it supports growth and differentiation of the epiblast via cell-cell interactions. To date, *Vps52* is the only gene that has been isolated that is responsible for a classic *t* lethal recessive mutation belonging to one of the 16 complementation groups.

3.2.1 the t^{w18} haplotype

Recombination between wild-type and *t* DNA is largely suppressed due to chromatin mismatching that is caused by four inversions in *t* haplotypes (Silver and Artzt, 1981; Silver *et al.*, 1992). However, recombination of wild-type and *t* DNA can occur very infrequently. These events can cause deletion or duplication of DNA sequences due to imperfect pairing (Silver *et al.*, 1980). The t^{w18} haplotype originated from such a rare recombination event. It was found in the offspring of a female from a population trapped near Storrs, Connecticut (Dunn, 1957). In this population, the lethal t^{w11} haplotype was detected. In the offspring of one $t^{w11}/+$ female, one animal was discovered that produced viable t/t offspring after breeding with $t^{w11}/+$ animals. This means that a mutation occured in the t^{w11} haplotype that produced a new *t* haplotype, designated t^{w18} (Dunn, 1957). This new *t* haplotype proved to also carry a lethal allele, but which belonged to another complementation group than the t^{w11} lethal. The t^{w18} lethal phenotype was analyzed in detail between E6-10 by Bennett and Dunn (1960). At E6 t^{w18} mutants cannot be distinguished from wild-type or heterozygous littermates. The first abnormalities can be detected at E7.0, wheret^{w18} homozygotes remain at the egg cylinder stage and do not show axial structures other than the primitive streak. In the region of the primitive streak, an abnormal thickening of the wall of the egg cylinder becomes apparent. One day later, at E8 this thickening, produced by an overgrowth of the primitive streak, becomes a median bulge that projects dorsally into the amniotic cavity. Due to excessive amounts

of primitive streak tissue, neural epithelium that covers the primitive streak forms a duplicated neural groove which run parallel to eachother over the length of the overgrown primitive streak, and then gradually merge into one another. The neural groove is the only structure that is duplicated in these embryos. Other axial structures or derivates of the primitive streak do not show doubling or overgrowth, supporting the notion that duplication of the neural grooves results from mechanical reasons alone. In general, mutant embryos are growth retarded compared to normal littermates which becomes even more prominent by E9. Embryos are unturned and the two neural tubes are open. At this stage, t^{w18} homozygotes show definite signs of deterioration such as crumpling and pycnosis. By E10 most of the mutant embryos are dead and degenerating (Bennett and Dunn, 1960).

In summary, the most striking feature of t^{w18} mutant embryos is overgrowth of the primitive streak. During gastrulation, cells enter the primitive streak but are unable to switch towards differentiation of mesoderm, resulting in an accumulation of cells that bulge into the amniotic cavity. Further analyses by Snow and Bennett (1978) of pre-primitive streak embryos showed that mutant embryos also exhibit a smaller cell number but a higher mitotic activity, with disoriented planes of cleavage compared to normal embryos. Snow and Bennett (1978) explained this elevated mitotic index by a blockage in cell division that leads to a greater proportion of cells present in metaphase and/or anaphase.

Next to t^4 and t^9, t^{w18} belongs to the t^9 complementation group (Bennett and Dunn, 1964; Moser and Gluecksohn-Waelsch, 1967). Members of this group emerged from recombination events between wild-type and *t* haplotype DNA. The resulting partial *t* haplotypes consist of a proximal part derived from the donor *t* chromosome and a distal wild-type-derived portion (Dunn *et al.*, 1962; Bennett *et al.*, 1976; Artzt *et al.*, 1982). In addition, it has been shown by Búcan *et al.* (1987), that these recombination events close to the proximal breakpoint of *In(17)4* resulted in deletions and duplications. More precisely, relative to the wild-type, the proximal part of *In(17)4*

is deleted and the distal part is duplicated. It has been speculated that the gene responsible for the lethal phenotype of the t^9 group is encoded in the deleted region and that homozygous loss of this gene results in developmental abnormalities and embryonic lethality (Búcan *et al.*, 1987). In a detailed analysis of the t^{w18} deleted region by construction of a YAC contig and marker analyses, Barclay *et al.* (1996) were able to show that a region of at least 3.3 Mb is deleted in the t^{w18} haplotype.

This study aims to isolate the gene responsible for the t^{w18} homozygous phenotype. *Ppp2r1a* was extracted from the deleted region as a promising candidate to cause this phenotype when deleted.

3.3 *Ppp2r1a* - the candidate gene

Ppp2r1a encodes the scaffolding subunit of protein phosphatase 2A (PP2A), a diverse family of serine-threonine phosphatases implicated in many different cellular processes like regulation of signaling pathways, cell cycle, DNA replication and apoptosis (Virshup, 2000; Janssens and Goris, 2001). The PP2A core enzyme consists of a catalytic C subunit and a structural A subunit (Kremmer *et al.*, 1997). This core dimer interacts with an additional B subunit (Fig. 6A). To date, four different classes of B subunits have been identified, known as B, B′, B″, and B‴ families. Since each of the PP2A subunits exist in at least two isoforms and in different splice variants, a multitude of assembly combinations results in at least 96 holoenzymes exerting diverse cellular functions (Sents *et al.*, 2013). The combinatorial assembly of C, A and B subunits, plus the interaction with other regulators, provide the information essential for subcellular targeting, substrate specificity and regulation of phosphatase activity. The scaffolding subunit is encoded by two genes, *Ppp2r1a* and *Ppp2r1b*, whose encoded proteins are also known as PR65α and PR65β or Aα and Aβ (Hemmings *et al.*, 1990). Both isoforms share 87% sequence identity and are differentially expressed. Analyses performed in rabbit and *Xenopus* showed that most

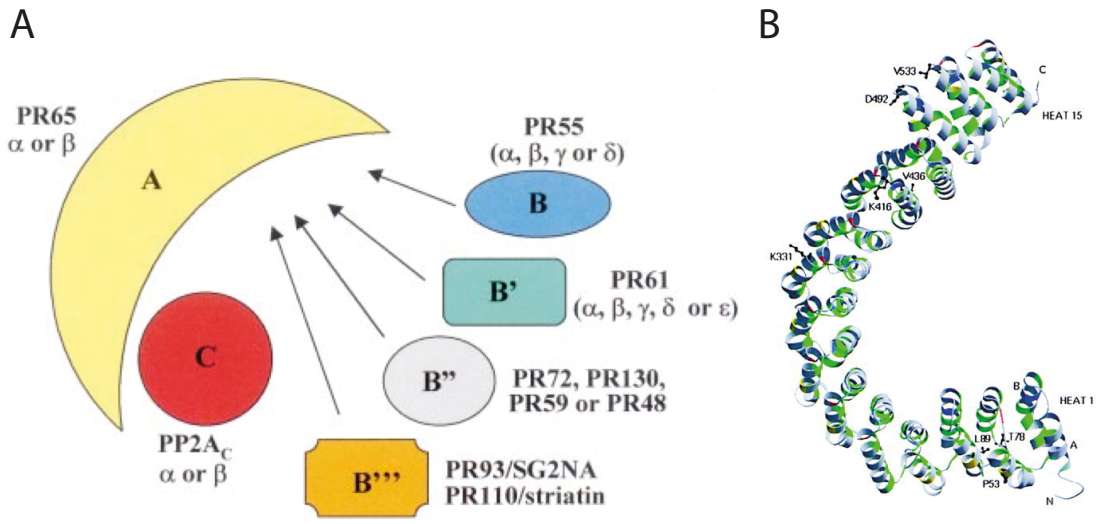

Figure 6. PP2A assembly. (A) The scaffolding subunit A interacts with the catalytic subunit C to form the PP2A core enzyme. Association of a regulatory B subunit completes the PP2A holoenzyme. The B subunits can be clustered in 3 families B, B′, B″, and B‴. Adopted from Janssens & Goris, 2001. (B) Ribbon diagram of the PR65/A subunit. The 15 HEAT motifs assemble to form a horseshoe-shaped structure consisting entirely of helices. Each HEAT motif forms a pair of antiparallel helices (Groves *et al.*, 1999).

PP2A holoenzymes in adult skeletal muscle contain the α-isoform while PR65β is the major isoform associated with PP2A in *Xenopus* oocytes and, early developmental stages (Hendrix *et al.*, 1993; Bosch *et al.*, 1995). Structurally, the scaffolding subunit consists of 15 tandem repeats of HEAT (huntingtin-elongation-A subunit-TOR) motifs (Hemmings *et al.*, 1990; Andrade and Bork, 1995). These conserved 39 amino acid repeats lead to an elongated, horseshoe-shaped structure defined by a double layer of antiparallel α helices (Fig. 6) (Groves *et al.*, 1999).

While kinases have been studied extensively, phosphatases have long been overlooked as simple housekeeping enzymes that are present only to reverse phosphorylation reactions. But a variety of recent studies have demonstrated that protein dephosphorylation is tightly regulated and, just like phosphorylation, plays a highly important role in many cellular processes. Regulation of PP2A occurs at different levels. Besides holoenzyme composition, PP2A is regulated by post-translational modifications like phosphorylation and methylation, or by interaction partners such as inhibitory proteins or second messengers (reviewed in Janssens & Goris, 2001).

Deregulation of PP2A is associated with a range of human diseases like Alzheimer's disease and different types of cancer (Eichhorn *et al.*, 2009; Vafai and Stock, 2002).

The biological role of PP2A has been analyzed in different *in vitro* and *in vivo* systems. Use of okadaic acid, a potent phosphatase inhibitor, has suggested a role for PP2A in regulation of mitosis and tumor growth (Goris *et al.*, 1989; Yamashita *et al.*, 1990; Fujiki and Suganuma, 1993; Suganuma *et al.*, 1988). In addition, mutant forms or knockouts of PP2A subunits have been established and analyzed in different model organisms, including yeast and *Drosophila*, supporting a role for PP2A in cell cycle, embryonic development and signaling pathways (Kinoshita *et al.*, 1990; Snaith *et al.*, 1996; Wassarman *et al.*, 1996; Yang *et al.*, 2003). In the mouse, a Cα homozygous-null mutant has been established (Götz *et al.*, 1998). Homozygous knockout of the α isoform of the PP2A catalytic subunit results in embryonic lethality around E6.5 and defects in mesoderm formation. Since even at E13.5 degenerated embryos can be recovered, it was suggested that while differentiation is significantly impaired, cell proliferation was not affected. This observation could also involve a role for PP2A in signal transduction pathways controlling apoptosis. Overall, these observations provided a good deal of evidence to support a role for PPP2R1A in embryogenesis, and thus made it an attractive candidate for the t^{w18} lethal gene.

4 Results

4.1 Analysis of the t^{w18} phenotype

The lethal t^{w18} allele was described by Bennett and Dunn (1960). The most striking feature of t^{w18} homozygotes involves excessive proliferation of primitive streak material leading to partial duplication of the neural tube. The overgrowth of the primitive streak first becomes apparent at day 7 post fertilization and the lethal period lies between 8 and 11 days post fertilization (Bennett and Dunn, 1960). To begin the task of isolating the t^{w18} lethal gene, the homozygous t^{w18} phenotype was reanalyzed. Heterozygous animals that were kept on a 129S2 or mixed 129S2/C57BL/6J background were mated, and embryos were analyzed between E6.5 and E8.5. To identify gastrulation defects, marker gene expression was visualized by *in situ* hybridization for probes specific to the mesoderm markers *T* and *Tbx6* (Fig. 7A). Embryos were genotyped for presence of the t^{w18} allele following *in situ* hybridization (Fig. 7B). The PCR genotyping strategy using *Vil2* primers (see section 6.2.4) had already been established in our laboratory and this strategy was used for genotyping both mouse and embryo material.

Heterozygous t^{w18} littermates developed completely normally, were viable and were therefore used as control (Fig. 7A, upper panel). At E6.5 t^{w18} homozygotes could not be morphologically distinguished from heterozygous littermates. On the gene expression level, however, the first differences already had become apparent. While t^{w18}/+ embryos expressed *T* along the primitive streak in nascent mesoderm, t^{w18} homozygotes did not or only faintly showed *T* expression. At E7.5, control embryos showed further signs of differentiation. The node and head process were visible and embryos showed a large domain of *Tbx6* expressing mesoderm. On

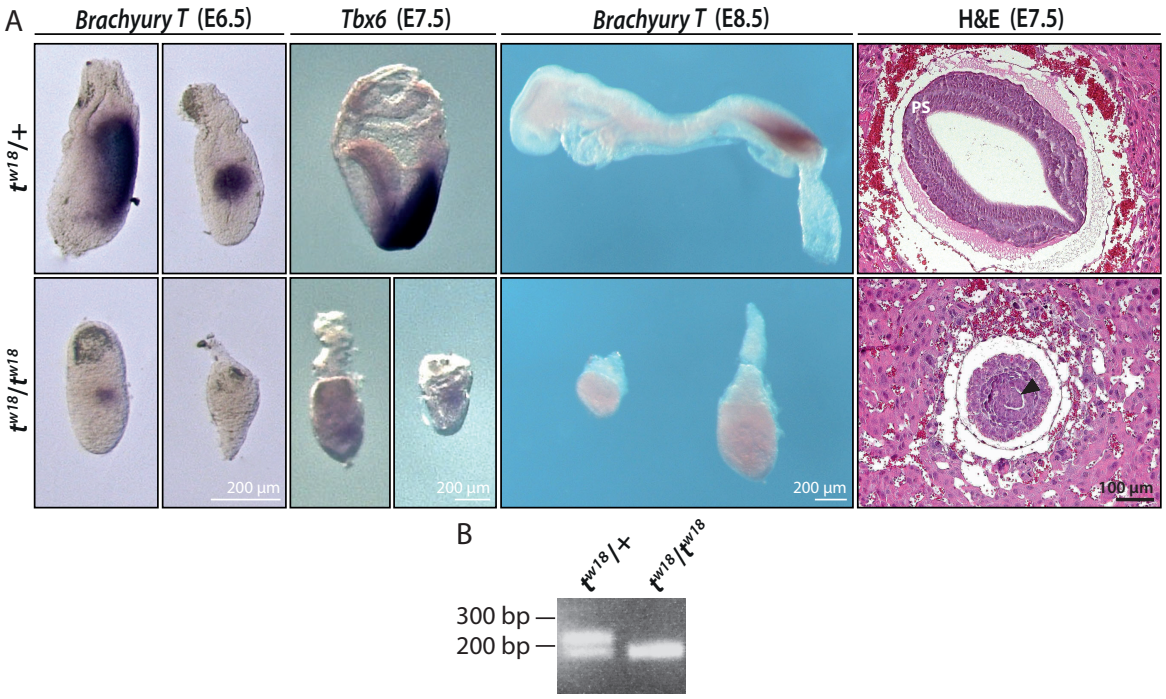

Figure 7. Phenotypic analysis of t^{w18} heterozygous and homozygous embryos. (A) Embryos from matings of heterozygous t^{w18} animals were analyzed by WISH with probes for *T* or *Tbx6* between E6.5 and E8.5. In addition, transvers sections of E7.5 embryos were H&E stained. Black arrowhead indicates overgrowth of the primitive streak in homozygotes. PS: primitive streak. (B) Example of PCR genotyping for the t^{w18} allele. PCR using *Vil2* primers (see section 6.2.4) produces fragments of 230 bp for wild-type and of 180 bp for t^{w18} alleles.

the other hand, in t^{w18}/t^{w18} embryos, no *Tbx6* expression was detectable at E7.5. In addition, embryos were growth retarded and also lacked other signs of differentiation. At E8.5, differences between normal and homozygous embryos became even more pronounced. $t^{w18}/+$ embryos formed somites, the head further differentiated and the heart was clearly visible. In contrast, t^{w18} homozygotes appeared as undifferentiated balls of cells that did not form mesoderm, since *T* expression was not detectable. In H&E stained sections from E7.5 embryos the prominent overgrowth of the primitive streak, described by Bennett and Dunn (1960) was clearly visible. Normal embryos showed a large amniotic cavity, a primitive streak and a head fold in transvers sections. In contrast, the amniotic cavity of t^{w18} homozygous embryos was filled with cells that bulged from the primitive streak.

In summary, there were differences between the t^{w18}/t^{w18} phenotype described by

Bennett & Dunn in 1960 and the phenotype I observed in t^{w18} homozygotes. In particular, partial duplication of the neural tube was not observed since embryos differentiated to a much lesser degree than the ones described earlier. For this reason the t^{w18} phenotype I describe here appears more severe, with the most striking feature, the overgrowth of the primitive streak, also being present. This variable degree of severeness is likely due to the different backgrounds between the t^{w18} heterozygous animals that were mated. In our laboratory t^{w18} animals are kept on a 129S2 background, while t^{w18} animals from Bennett & Dunn originated from offspring of a wild female carrying the t^{w18} haplotype (Dunn, 1957).

4.2 Analysis of the region deleted in the t^{w18} genotype

A previous study suggested a deletion of at least 3.3 Mb of the *t* complex on chromosome 17 in the t^{w18} haplotype (Barclay *et al.*, 1996). Since the breakpoints and the overall extent of the deletion were not identified in this study, a NGS approach was followed. By sequencing the genomes of t^{w18}/+ ESCs and t^{w18} homozygous embryos we aimed at defining the borders of the deletion. Genomic DNA was genotyped for presence of the t^{w18} allele using the genotyping strategy described in section 6.2.4 and depicted in Fig. 7B. The sequencing was performed by the NGS core facility of our institute (Dr. Bernd Timmermann, MPIMG) using the Illumina HiSeq 2000 system creating 36 bp single reads by shotgun sequencing. Analyses of the NGS data was performed by Dr. Martin Werber. Analyses followed the assumption that the number of mapped reads is directly correlated to zygosity. The number of reads that mapped to chromosome 17 following NGS of t^{w18}/+ DNA were plotted to their location on chromsome 17. The diagram in Fig. 8 depicts the read number mapping to the critical region between 17.0-25.0 Mb. The distal, telomere-close breakpoint of the deletion was precisely mapped to position chr 17:23600000 (Fig. 8, asterisk).

The proximal centromere-close breakpoint could roughly be demarcated between chr 17:18.0-19.7 Mb (Fig. 8, red line).

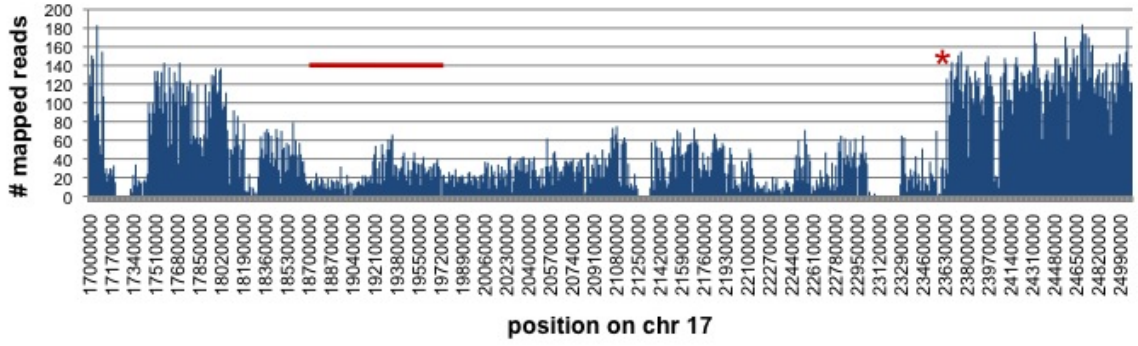

Figure 8. Mapping of the t^{w18} deletion by NGS t^{w18}/+ DNA. The number of reads that mapped to position chr 17:17000000-25090000. The 3′ end of the deletion is found at position chr 17:23600000 (asterisk) whereas the 5′ end could not be clearly defined (red line).

Analyses of homozygous t^{w18} NGS data did not provide further results that narrowed down the 5′ breakpoint due low sequencing coverage (data not shown). To isolate the proximal border of the deletion, PCR analyses were performed. DNA fragments were analyzed for their presence in heterozygous and homozygous t^{w18} genomic DNA following PCR amplification. Amplicons were detected until chr 17:19190492 in both DNA samples (Fig. 9, 18.48-19.19 Mb), whereas fragments from chr 17:19330513 on were absent from the t^{w18}/t^{w18} sample (Fig. 9, 19.33 and 19.41 Mb, lower panel). The PCR analysis thus defined a region located between chr 17:19190492-19330513 that contains the proximal breakpoint. A further narrowing of the region was not possible due to repetitive DNA that disturbs PCR amplification. In summary, a region of around 4.3 Mb between 19.3-23.6 Mb defines the deletion in the t^{w18} haplotype. Accordingly, all genes within this region are missing in t^{w18} homozygous embryos.

Analysis of genes located within the deleted region showed that the specified region between 19.19-19.33 Mb containing the proximal breakpoint does not contain any genes. Thus, the gene closest to the centromere which was found to be deleted is identified to be *Vmn2r99* at position chr 17:19362134. A complete list of genes

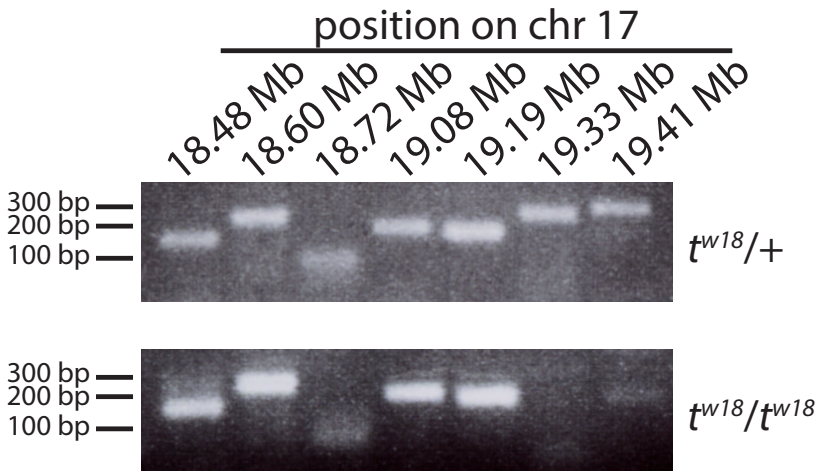

Figure 9. Mapping of the t^{w18} deletion by PCR. The presence of DNA elements around the region determined to contain the proximal breakpoint were analyzed by PCR in heterozygous (upper panel) and homozygous (lower panel) t^{w18} genomic DNA. DNA fragments were amplified up to position chr 17:19.19 Mb in both samples. In homozygous t^{w18} DNA amplicons were absent from position chr 17:19.33 Mb on.

deleted in the t^{w18} haplotype is available in the supplementary information (Table S1). The region contains 74 genes: 20 Zinc finger proteins, 34 vomeronasal receptors, 12 non-coding RNAs, 2 formyl peptide receptor related sequences, 1 PP2A subunit, 2 RIKEN clones and 3 other predicted genes. Acting on the assumption that the loss of one of those genes within this region would cause the early developmental defects in t^{w18} homozygotes, those genes were analyzed by literature mining.

The gene encoding the PP2A scaffolding subunit Aα , *Ppp2r1a* was selected as the most promising candidate. It has been shown that homozygous loss of another permanent subunit of PP2A, the catalytic subunit Cα (*Ppp2ca*) results in embryonic lethality and defects in mesoderm formation (Götz *et al.*, 1998). The Cα loss-of-function phenotype is not completely similar, but comparable to the t^{w18} homozygous phenotype. Both mutants show early embryonic lethality and severe gastrulation defects with failure in mesoderm formation. The PPP2R1A protein represents an important component of the PP2A heterotrimer mediating the interaction of the catalytic subunit with additional regulatory B subunits. It is conceivable that loss of the A subunit disturbs PP2A holoenzyme assembly, and consequently PP2A ac-

tivity and function, resulting in a phenotype comparable to the one described for loss of *Ppp2ca* (Götz *et al.*, 1998). To test this hypothesis a knockout approach was followed, where *Ppp2r1a*$^{-/-}$ embryos were expected to show a similar phenotype as t^{w18} homozygotes if the hypothesis was correct.

4.3 Knockout of *Ppp2r1a* reconstitutes the t^{w18} phenotype

To investigate whether loss of *Ppp2r1a* causes the t^{w18} homozygous phenotype, the establishment of a *Ppp2r1a*$^{+/-}$ mouse line was pursued. Therefore, classical gene targeting was performed in ES cells that, via homologous recombination, replaced the wild-type allele with a transgenic version provided by a targeting vector. To target the *Ppp2r1a* locus a targeting vector (PRPGS00108_A_B03) was obtained from the KOMP repository (University of California, Davis) (Fig 10A). This construct provides the possibility to create a knockout first allele (*Ppp2r1a*$^{tm2a(KOMP)Mbp}$) by inserting a stop cassette into the second intron of the *Ppp2r1a* gene which abrogates transcription. The *Ppp2r1a*$^{tm2a(KOMP)Mbp}$ allele will in the following be designated as *Ppp2r1a*$^{-}$ allele for simplification reasons. The FRT flanked stop cassette contains a LacZ expression unit followed by a neomycin resistance cassette. The LacZ cassette consists of a splice acceptor site (En2 SA) followed by an internal ribosomal entry site (IRES) and a LacZ gene with polyA signal. The promoter driven neomycin resistance cassette is in addition flanked by loxP recombination sites. Moreover, to provide the potential to generate a conditional knockout allele, the third exon of *Ppp2r1a* is flanked by loxP sites. Flp recombinase mediated recombination thereby deletes the stop cassette creating a conditional *Ppp2r1a* knockout allele that can be converted into a *Ppp2r1a*$^{\Delta ex3}$ allele via Cre-mediated recombination (Fig 10A).

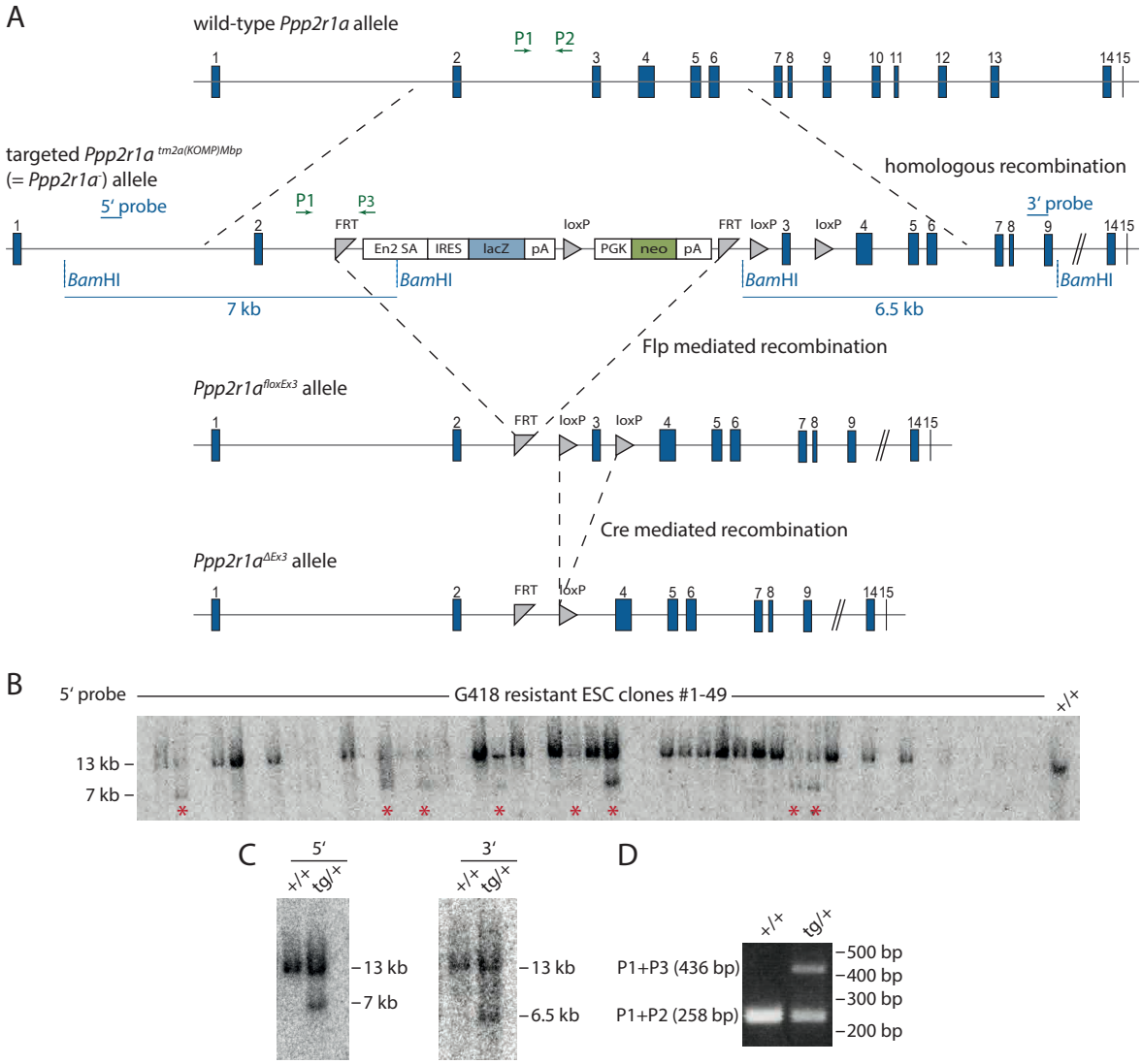

Figure 10. Targeting of the *Ppp2r1a* locus. (A) A *Ppp2r1a* targeting construct was integrated into the wild-type *Ppp2r1a* locus by homologous recombination. The integrated Stop cassette provides the possibility to generate a conditional knockout allele ($Ppp2r1a^{floxEx3}$) after *Flp* recombinase expression. This conditional allele can produce the $Ppp2r1a^{\Delta Ex3}$ allele that, due to deletion of exon 3, results in a premature Stop codon leading to premature termination of translation. (B) G418 resistant clones were screened for positive homologous recombination by Southern blot. Following *Bam*HI digest fragment sizes of 13 kb for the wt allele and 7 kb for the targeted allele can be detected with the 5′ external Southern probe. Clones positive for the targeted allele are highlighted with red asterisks. (C) The genotype of mice generated from a positively targeted ESC clone (tg/+) was confirmed by Southern blot with 5′ and 3′ external probes (D) A multiplex PCR genotyping strategy using 3 different primers (P1, P2, P3) distinguished between wt and transgene (tg) containing mice.

4.3.1 Generation of a *Ppp2r1a* knockout ESC line

In order to generate a *Ppp2r1a* knockout ESC line, G4 cells were electroporated with the KOMP construct. Transfected cells were selected for G418 resistance and screened for homologous recombination by Southern blot (Fig 10B). *Bam*HI restriction enzyme-digested genomic DNA created different fragment sizes in the wild-type and targeted *Ppp2r1a* alleles that were detected by hybridization with specific radiolabeled probes. Two external Southern probes were established that hybridize to the *Ppp2r1a* locus 5′ upstream or 3′ downstream relative to the targeting vector. These probes detected a fragment of 13 kb in the wild-type allele and 7 kb or 6.5 kb fragments in the targeted knockout allele. At least eight of 48 picked clones (17%) showed the correct restriction enzyme pattern after Southern blot analyses with 5′ and 3′ external probes, verifying a positive targeting of the *Ppp2r1a* locus (Fig 10B and data not shown). Any of these clones could thus be used to establish a mouse line.

To later facilitate genotyping of mice or embryos, a PCR strategy was established (Fig. 10D). This multiplex PCR approach used 3 primers that produced PCR fragments of 258 bp for the wild-type and 436 bp for the targeted allele by using the same forward primer, but two different reverse primers.

4.3.2 Generation of a *Ppp2r1a* knockout mouse line and phenotypic analyses

Four of the positively targeted *Ppp2r1a*$^{+/-}$ ESC clones were used to generate chimeric mice by diploid complementation (Eakin and Hadjantonakis, 2006). One of these ESC clones produced viable offspring. These F0 founder males showed, as estimated by the animals' coat chimerism, a high degree of ESC contribution. In addition, they were found to transmit the *Ppp2r1a* transgene through the germ line, since matings with C57BL/6 females produced heterozygous *Ppp2r1a*$^{+/-}$ offspring.

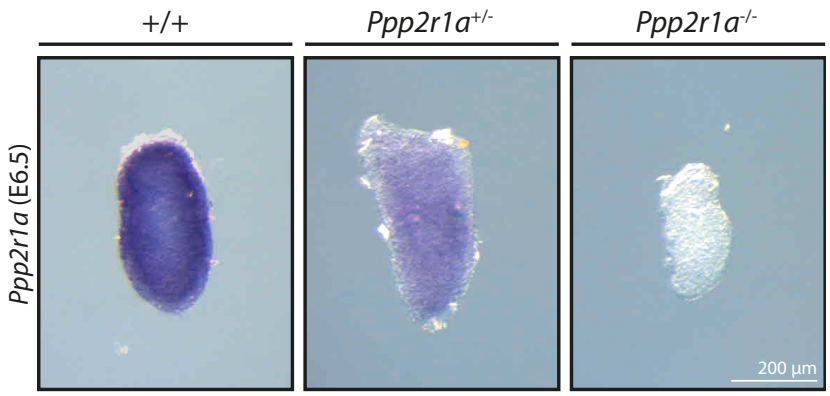

Figure 11. *Ppp2r1a* expression in *Ppp2r1a*-deficient embryos. WISH analysis of embryos at E6.5 resulting from *Ppp2r1a*$^{+/-}$ intercrosses showed absence of *Ppp2r1a* expression in homozygous *Ppp2r1a*$^{-/-}$ embryos.

Ppp2r1a$^{+/-}$ animals developed completely normally, similar to t^{w18}/+ mice. To establish and maintain a mouse line, the F0 animals were mated with C57BL/6 females and the produced F1 animals were again mated with C57BL/6 mice. It was verified by Southern blot as well as PCR that the genotypes of individuals of this newly established mouse line were positive for the *Ppp2r1a*$^{-}$ allele (Fig. 10C, D). To analyze the phenotype of *Ppp2r1a*$^{-/-}$ embryos and look for reconstitution of the t^{w18} homozygous phenotype, *Ppp2r1a*$^{+/-}$ mice were intercrossed or mated with t^{w18}/+ mice. Embryos were dissected between E6.5 and E8.5.

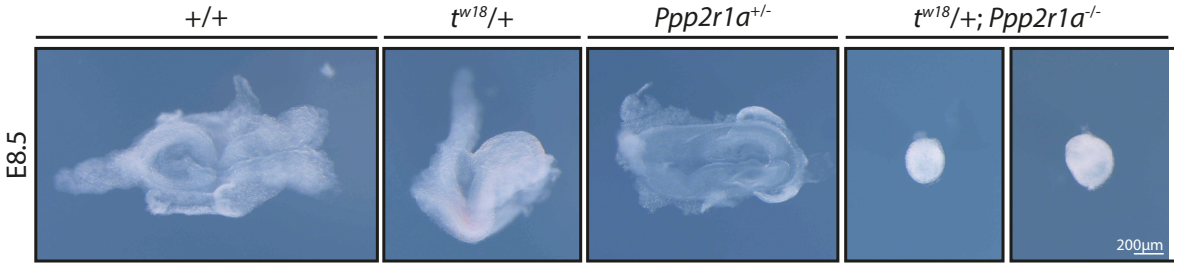

Figure 12. Morphology of embryos from t^{w18}/+ and *Ppp2r1a*$^{+/-}$ matings. E8.5 littermates were PCR genotyped, for presence of t^{w18} and *Ppp2r1a*$^{-}$ alleles, following imaging. t^{w18}/+;*Ppp2r1a*$^{-/-}$ embryos failed to gastrulate and resembled t^{w18} homozygotes.

Importantly, to show that the targeting of the *Ppp2r1a* locus with the KOMP construct resulted in complete abrogation of transcription, WISH was performed. E6.5 embryos from *Ppp2r1a*$^{+/-}$ intercrosses were hybridized with a *Ppp2r1a* specific probe covering nucleotides 930-1858 of the *Ppp2r1a* transcript (NCBI: NM_016891.3). Fig.

11 clearly shows that no *Ppp2r1a* mRNA was detectable in homozygous embryos compared to wild-type and heterozygous littermates, which verified that the transgenic allele resulted in a *Ppp2r1a*-null allele. The morphology of embryos from matings of $Ppp2r1a^{+/-}$ with $t^{w18}/+$ mice was further analyzed at E8.5 (Fig. 12). Following imaging and morphological analysis, genomic DNA was extracted from embryos used for PCR genotyping for presence of the t^{w18} and $Ppp2r1a^{-}$ alleles. As expected wild-type and heterozygous littermates did not show any developmental defects. Whereas, embryos that carried the t^{w18} allele in addition to the $Ppp2r1a^{-}$ allele, resulting in homozygous loss of *Ppp2r1a* expression, strongly resembled t^{w18} homozygous embryos (compare with Fig. 7).

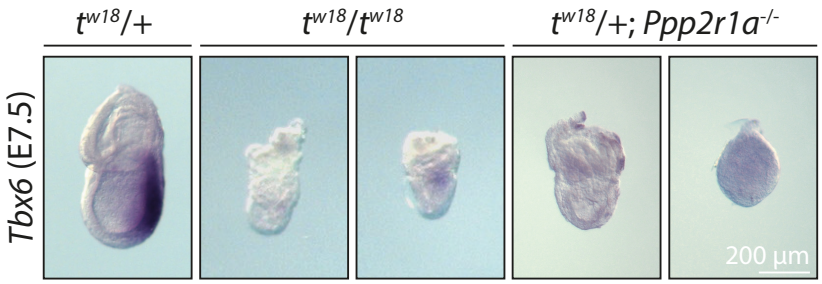

Figure 13. WISH analysis of *Tbx6* expression in t^{w18}/t^{w18} and $t^{w18}/+;Ppp2r1a^{-/-}$ embryos. E7.5 embryos with homozygous loss of *Ppp2r1a* failed to express *Tbx6*.

These embryos failed to gastrulate and did not show differentiation at E8.5, suggesting that loss of *Ppp2r1a* reconstituted the t^{w18} homozygous phenotype. In addition, mesoderm marker genes like *Tbx6* were not expressed in $t^{w18}/+;Ppp2r1a^{-/-}$ embryos at E7.5 (Fig. 13). To further confirm that $Ppp2r1a^{-/-}$ showed the same phenotype as t^{w18} homozygotes, embryos in deciduae were paraffin-embedded, sectioned and H&E stained. For genotyping, embryonic material was scraped off of the slides after H&E staining with a tungsten needle. Comparison with t^{w18}/t^{w18} embryos indeed showed that both homozygotes were very similar. As observed for the t^{w18}/t^{w18} embryos, the amniotic cavity of $Ppp2r1a^{-/-}$ embryos was filled with cells at E7.5 (Fig. 14).

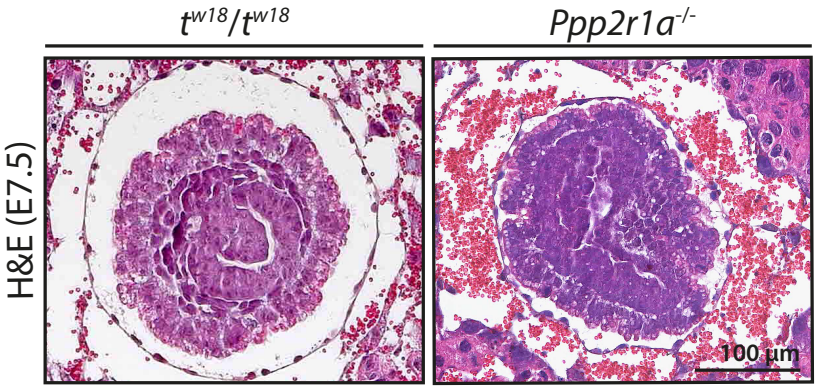

Figure 14. Histological analysis of *Ppp2r1a* knockout embryos. HE stained paraffin sections of E7.5 t^{w18}/t^{w18} and $Ppp2r1a^{-/-}$ embryos. The amniotic cavities of both embryos were filled with cells.

4.4 *Ppp2r1a* expression rescues t^{w18} homozygous phenotype

Ppp2r1a is located within the region deleted in the t^{w18} haplotype and knockout experiments suggested that the t^{w18}/t^{w18} and $Ppp2r1a^{-/-}$ embryos showed the same phenotype. This greatly supports the assumption that it is loss of *Ppp2r1a* causing the t^{w18} homozygous phenotype. To finally validate this notion, it had to be shown that *Ppp2r1a* expression is able to complement the t^{w18} phenotype. Therefore, a rescue experiment was performed. A transgenic *Ppp2r1a* BAC construct was expressed in t^{w18} mice and after breeding experiments, embryos were analyzed for rescue of developmental defects and embryonic lethality.

4.4.1 Generation of the *Ppp2r1a* rescue construct

In order to ensure endogenous *Ppp2r1a* expression levels, a BAC transgene was generated that contained the *Ppp2r1a* locus including the gene's endogenous promoter and polyA signal. Most often BACs do not only contain the gene of interest, but many other genes. In this case other genes that were encoded by the BAC (RPCI-23-209P21) and that were deleted in the t^{w18} genotype might be able to compensate

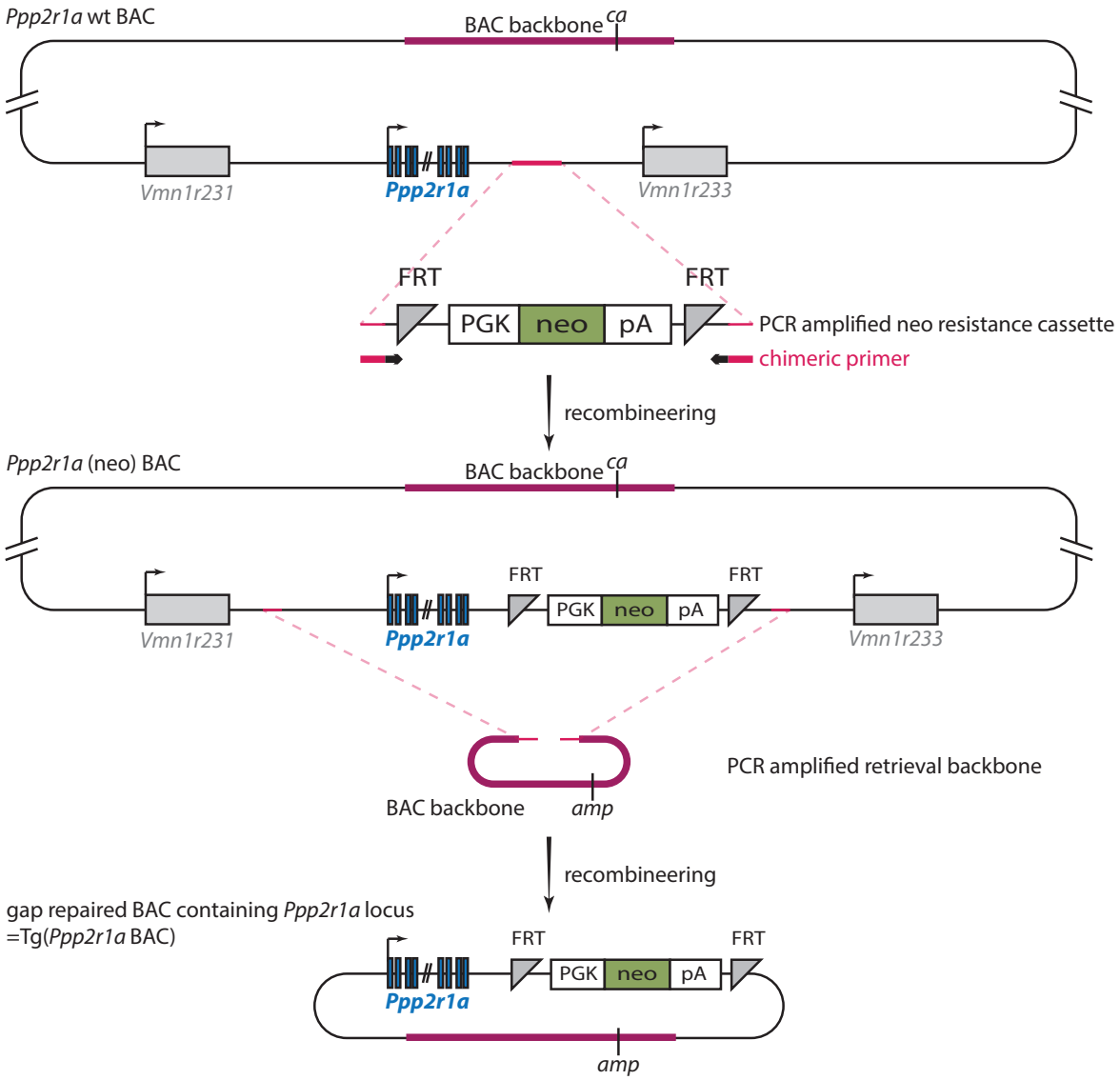

Figure 15. Two-step cloning strategy to generate the *Ppp2r1a* rescue construct (Tg(*Ppp2r1a* BAC)). A neo resistance cassette was inserted in the *Ppp2r1a* wt BAC by homologous recombination. Bacteria that positively generated the *Ppp2r1a* (neo) BAC were selected for chloramphenicol and neomycin resistances. In a second step an ampicillin resistant retrieval BAC backbone was recombined with the *Ppp2r1a* (neo) BAC to create the Tg(*Ppp2r1a* BAC) through a gap repair mechanism.

for the t^{w18} phenotype. To definitely show that it is loss of *Ppp2r1a* that caused the t^{w18} phenotype, a cloning strategy was designed that created a BAC construct containing the *Ppp2r1a* genomic locus only with its regulatory sequences but no other genes (Fig. 15). For a first recombineering step a neomycin resistance cassette was amplified with chimeric primers. These contained sequences homologous to the target recombination site on the BAC and to the R6K vector carrying the neomycin resistance cassette. The gel purified PCR product was electroplated in *Ppp2r1a* wt BAC containing bacteria that transiently expressed Red/ET recombination enzymes. Homologous recombination created a *Ppp2r1a* BAC that encoded a neomycin resistance cassette 3' of the *Ppp2r1a* gene. Positive BAC clones were selected for chloramphenicol and kanamycin resistance, were verified by PCR and integrity of the BAC was determined by *Hind*III digestion. In a second rebombineering step a BAC backbone encoding an ampicillin resistance gene was amplified with chimeric primers. This linear retrieval backbone was used to subclone a region containing the *Ppp2r1a* locus and the neomycin resistance cassette from the previously generated transgenic BAC via a mechanism called gap repair (Liu *et al.*, 2003). Clones were screened for successful homologous recombination events by PCR as well as restriction enzyme digestion (data not shown). The complete construct (Fig. 15, Tg(*Ppp2r1a* BAC)) was linearized and used for establishing a transgenic ESC line.

4.4.2 Testing the expression of the *Ppp2r1a* BAC rescue construct in ESCs

The *Ppp2r1a* rescue construct was randomly integrated into the genome of t^{w18}/+ ESCs by electroporation, followed by G418 selection. Antibiotic resistant clones were screened for successful integration by PCR analysis. Three positive ESC clones (#5, 8, 12) were expanded and further tested for expression of the transgene. Since *Ppp2r1a* is expressed in ESCs, these cells could directly be tested, prior to establishing a mouse line. *Ppp2r1a* mRNA levels were analyzed by qPCR following RNA

extraction and cDNA synthesis and compared to control samples. Since transgenic *Ppp2r1a* expression could not be distinguished from endogenous *Ppp2r1a* expression levels, on the one hand t^{w18}/+ ESCs carrying one *Ppp2r1a* allele and on the other hand G4 ESCs with two *Ppp2r1a* alleles were used as controls to estimate transgene expression and analyze whether *Ppp2r1a* wild-type expression levels were restored. As expected, *Ppp2r1a* expression was around twofold higher in G4 cells compared to t^{w18}/+ cells (Fig 16A). qPCR analyses of the transgenic clones showed that the transgene was expressed in all three clones, but with varying strength. While clone 5 and 8 showed *Ppp2r1a* expression levels comparable to or even higher than G4 cells, clone 12 did not reach G4 levels. In addition to mRNA, Ppp2r1a protein levels were analyzed by Western blot and band intensities were quantified with the Fusion software (Peqlab) (Fig. 16B). Ppp2r1a protein levels were normalized to histone H3 protein. Consistent with the qPCR analyses, clone 5 showed the highest transgene expression and even more Ppp2r1a protein than G4 cells. In contrast, Ppp2r1a protein levels in clone 8 were only 1.3-fold higher compared to t^{w18}/+ cells. Although clone 12 showed the weakest transgene expression in qPCR, detected Ppp2r1a protein levels were comparable to clone 5 and G4.

4.4.3 Generation of a *Ppp2r1a* rescue mouse line and phenotypic analyses

To actually analyze complementation of the t^{w18} phenotype by *Ppp2r1a* expression from the generated transgene, a mouse line had to be established from transgenic ESC clones. Since the *Ppp2r1a* rescue construct could only be tested *in vitro* and expression levels of the transgene might be different in embryos, two clones (clone 5 and 12) of the three previously tested clones were used to generate mouse lines by diploid aggregation. Both ESC clones were of good quality and gave viable offspring. These F0 founder males with a t^{w18}/+ background carrying the *Ppp2r1a* rescue transgene did not show any developmental abnormalities, were fertile and

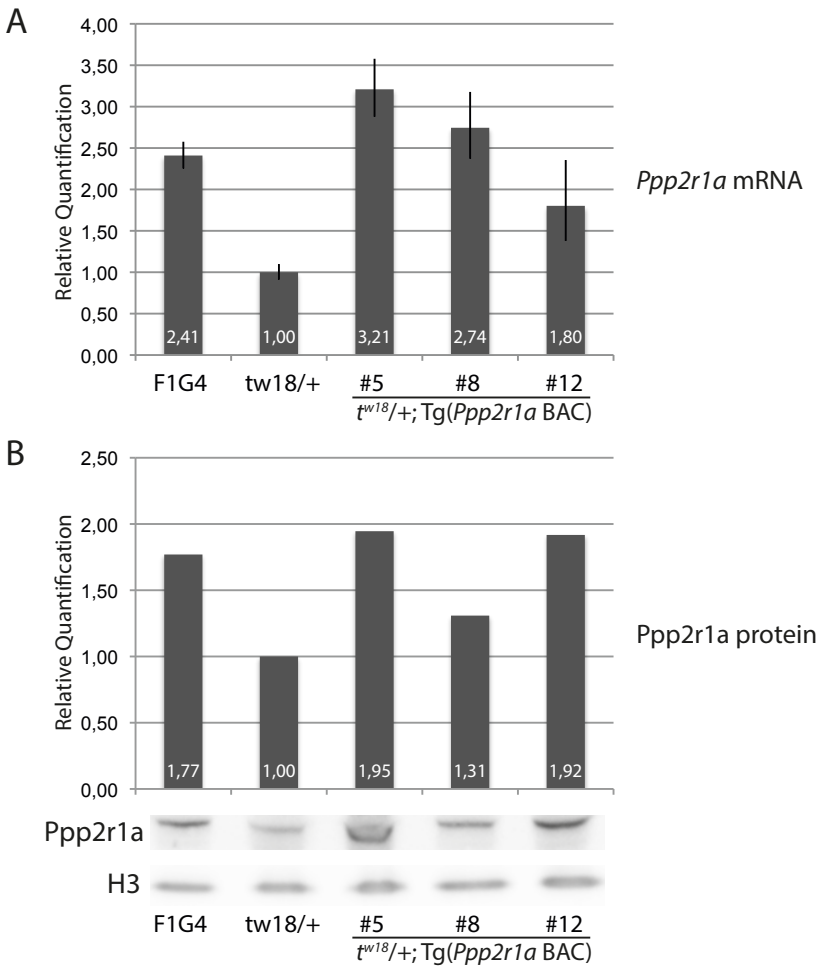

Figure 16. Testing the *Ppp2r1a* rescue construct in three ESC clones. Control G4 and t^{w18}/+ cells carried two or one *Ppp2r1a* allele, respectively. Consequently, *Ppp2r1a* expression was approximately two-fold higher in G4 cells as shown for mRNA levels analyzed by qPCR and normalized to *Pmm2* and *Hmbs* (A) and protein levels analyzed by Western blot followed by quantification relative to H3 protein (B). Expression of the rescue transgene increased *Ppp2r1a* mRNA and protein levels in the transgenic ESC clones #5, 8, 12.

mated with heterozygous t^{w18}/+ females. From these breedings embryos were dissected at E10.5, morphologically analyzed and genotyped for the t^{w18} allele and the presence of the transgene (Tg(*Ppp2r1a* BAC)). Indeed, t^{w18} homozygous embryos that were positively genotyped for the transgene (t^{w18}/t^{w18}; Tg(*Ppp2r1a* BAC)) did not show any morphological abnormalities at E10.5 or later stages of development (Fig 17A). These embryos could morphologically not be distinguished from wild-type or *tw18* heterozygous littermates, showing that the transgene rescued defects caused by the t^{w18} haplotype. As expected, t^{w18} homozygous littermates without the

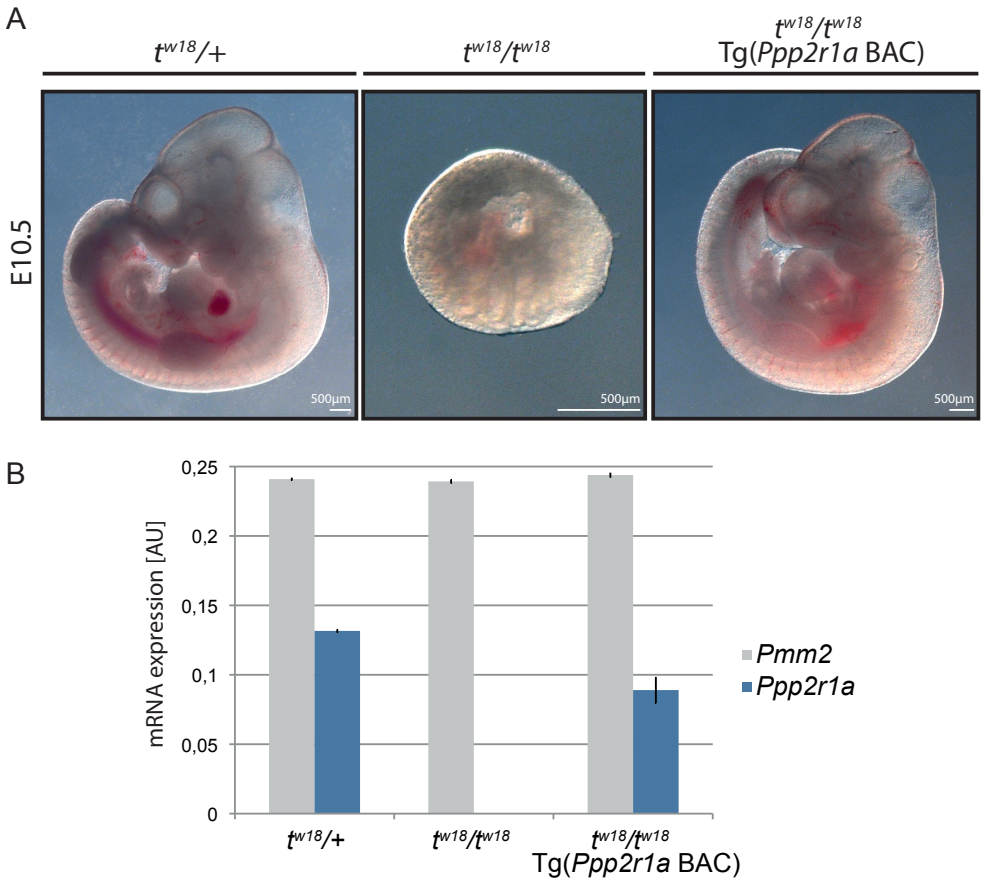

Figure 17. *Ppp2r1a* expression rescued t^{w18} homozygous phenotype. (A) Embryos from breedings of $t^{w18}/+$ females with $t^{w18}/+$, Tg(*Ppp2r1a* BAC) males (clone 5) were analyzed at E10.5. Embryos homozygous for t^{w18} that in addition carried the Tg(*Ppp2r1a* BAC) developed normally and did not show any abnormalities typical for t^{w18} homozygotes. (B) *Ppp2r1a* expression levels were restored to 67 % of the wt allele of t^{w18} heterozygotes by expression of the rescue construct.

transgene showed strong developmental defects and failed to gastrulate. To validate that in t^{w18} homozygotes *Ppp2r1a* expression is restored and that it really is expression from the transgene rescuing the t^{w18} phenotype, *Ppp2r1a* expression levels were analyzed in these embryos in addition to morphology (Fig. 17B). qPCR data showed that *Ppp2r1a* expression from the transgene restored expression to 67 % of t^{w18} of one *Ppp2r1a* wild-type allele. These experiments clearly showed that *Ppp2r1a* expression rescues the t^{w18} homozygous phenotype and, thereby, proves that *Ppp2r1a* is its causative gene.

4.5 Analyzing Ppp2r1a function

Ppp2r1a was identified as the gene causing the t^{w18} homozygous phenotype, but its function during early embryogenesis remained to be elucidated. To address this issue, different approaches were followed. First, analyzing the PPP2R1A interactome would allow the identification of specific B regulatory subunits that are associated with PPP2R1A during this process. In addition, it would be highly interesting to unravel possible PP2A targets that cannot be dephosphorylated in the mutant. This failure in dephosphorylation could affect the proteins' function, thereby contributing to the mutant phenotype. To analyze PPP2R1A interacting proteins, a mass spectrometry approach using mouse ESC was followed (see below). Second, analyzing the transcriptome of mutant and normal embryos would show consequences of loss of *Ppp2r1a* on gene expression level. The analysis of dysregulated genes can reveal pathways that are regulated by PP2A and probably are disturbed in the mutant. Especially in combination with the PPP2R1A interactome this could clarify the function of *Ppp2r1a* during early embryogenesis.

4.5.1 The PPP2R1A interaction network

The function of most proteins is mediated or specified by the association with other proteins in large protein complexes. In order to analyze Ppp2r1a interacting proteins I took advantage of a previously established affinity purification coupled with mass spectrometry (AP-MS) protocol (Glatter *et al.*, 2009). This method uses a small double-affinity tag to purify protein complexes in combination with a direct liquid chromatography tandem mass spectrometry (LC-MS/MS) approach in collaboration with Matthias Gstaiger in the group of Rudi Aebersold (ETH Zurich, Institute of Molecular Systems Biology, Switzerland) that performed the LC-MS/MS. The affinity tag used consists of a combination of a Strep-tag II and a HA epitope and is henceforth referred to as the SH-tag. The Strep-tag II was developed by the IBA

GmbH and binds to a modified streptavidin called streptactin. This principle was utilized to purify SH-tagged PPP2R1A with a single-step affinity purification protocol (see 6.3.1). Since, we assumed that *Ppp2r1a* functions during embryogenesis in the switch from a proliferative state towards differentiation, an *in vitro* assay that reflects this process was used. In our laboratory Dr. Eun-ha Shin previously established a protocol to *in vitro* differentiate mouse ESCs towards the mesodermal cell lineage under BMP4 treatment (see section 6.5.4)(Shin, 2011). This differentiation protocol was combined with AP-MS to unravel and compare PPP2R1A complexes in differentiated and undifferentiated cells. It was therefore necessary to establish an ESC line that expresses a *Ppp2r1a* with an SH-tag.

Generation of a ESC line expressing SH-tagged *Ppp2r1a*

In order to eliminate effects of overexpressing *Ppp2r1a* in ESCs, I aimed at tagging the endogenous wild-type *Ppp2r1a* allele present in t^{w18}/+ ESCs by homologous recombination. But since targeting of the *Ppp2r1a* allele was not successfull in this case (data not shown), an alternative strategy had to be applied to obtain tagged PPP2R1A. Therefore, a BAC transgene was cloned expressing SH-tagged *Ppp2r1a* at endogenous levels. This transgene was randomly integrated in the genome of t^{w18}/+ ESC in addition to the one *Ppp2r1a* copy present in the wild-type allele of the cells. It has to be considered that untagged wild-type PPP2R1A protein is present in these cells that might compete with SH-tagged PPP2R1A for binding partners and this approach of integrating a BAC transgene was therefore perhaps not the optimal strategy. The transgene was generated by BAC recombineering resulting in C-terminal tagging of the *Ppp2r1a* coding sequence. Therefore, an R6K vector was cloned containing the SH-tag with a stop codon followed by a neomycin resistance cassette. This vector was used to amplify the PCR product containing the SH-tag and the neomycin resistance cassette with the necessary 50 nucleotides homology region for BAC recombineering (Fig. 18). Therefore, the oligonucleotides for ampli-

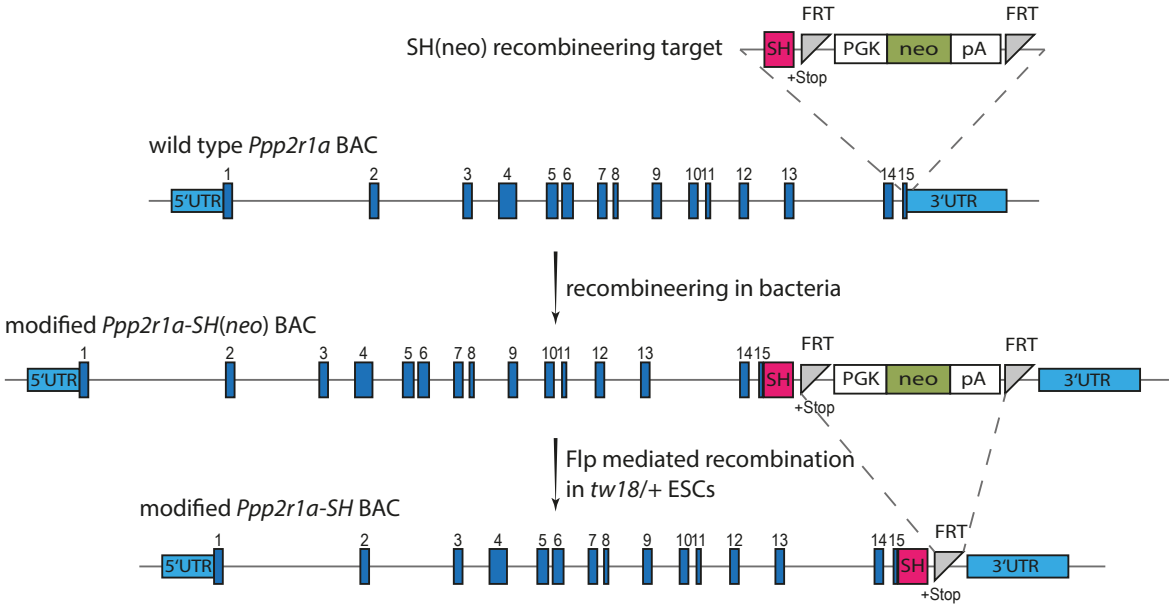

Figure 18. Recombineering strategy to generate SH-tagged Ppp2r1a.A cassette containing SH-tag (with stop codon) in combination with *FRT*-flanked neomycin resistance gene was PCR amplified and recombined at the 3′ end of the *Ppp2r1a* gene in the wild-type BAC. The resulting *Ppp2r1a-SH*(*neo*) BAC was randomly integrated in t^{w18}/+ ESC. To enable efficient expression of the transgene the neomycin resistance cassette was removed by Flp mediated recombination of the flanking *FRT* sites.

fication were selected in a way that the tag sequence replaced the endogenous stop codon and was inserted directly after the last amino acid codon of *Ppp2r1a* and in front of the endogenous 3′ UTR. The resulting *Ppp2r1a-SH(neo)* BAC was randomly integrated in t^{w18}/+ ESC. Since presence of the neomycin resistance cassette in the transgene can disturb transcription of *Ppp2r1a-SH*, this cassette had to be removed. This was possible due to *Frt* sites that flanked the neomycin resistance gene. Transient *Flp* recombinase expression enabled by Lipofectamine transfection of a *FlpO* expression plasmid led to recombination of the *Frt* sites resulting in deletion of the neomycin resistance cassette (Fig. 18). This recombination left a *FRT* site, which did not interfere with expression of the transgene. A positive, neomycin sensitive clone was tested for PPP2R1A-SH expression directly by Strep pull-down to enrich the tagged protein and overcome low levels of expression followed by Western blot (Fig. 19). Protein samples of wild-type t^{w18}/+ and *Ppp2r1a-SH* expressing cells were analyzed by Western blot with a PPP2R1A antibody. This antibody detected

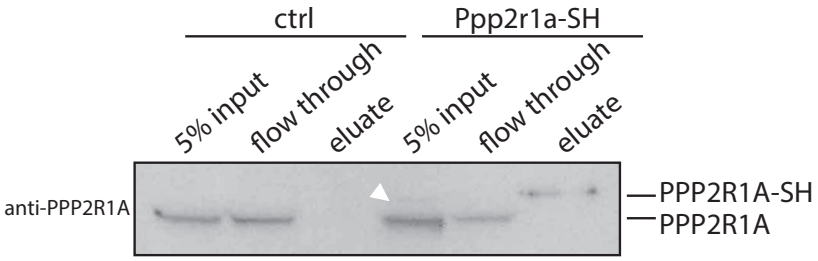

Figure 19. Western blot analysis to test *Ppp2r1a-SH* expression and Strep-PD efficiency. The used PPP2R1A antibody detected endogenous PPP2R1A (lower band) as well as the tagged version (upper band). In contrast to the endogenous protein that was detected in input and flowthrough of both the wild-type t^{w18}/+ ESC (crtl) and in the transgenic cell line, the PPP2R1A-SH protein was only detectable in the transgenic cell line. Thereby, only a faint band of PPP2R1A-SH was visible in the input sample (arrowhead) that was enriched in the eluate sample. No PPP2R1A-SH was detectable in the flowthrough indicating high binding efficiency of PPP2R1A-SH to the streptactin beads.

endogenous PPP2R1A as well as the tagged protein. Discrimination between both proteins is possible due to increased size of the tagged PPP2R1A (Fig. 19, upper band). PPP2R1A-SH was not detectable in the control samples, as expected, but in input and eluate of PPP2R1A-SH samples. The input only showed a faint band of PPP2R1A-SH compared to endogenous PPP2R1A indicating low levels of transgene expression. A stronger band was visible in the eluate sample confirming enrichment of the tagged protein by this affinity purification method. In addition, no PPP2R1A-SH was detectable in the flowthrough showing that the tagged protein efficiently bound to the streptactin beads. In summary, the transgenic cell line was suitable to affinity purify SH-tagged PPP2R1A which could then be used for mass spectrometry analysis. Since, we wanted to combine AP-MS with differentiation of ESC, the potential to differentiate t^{w18}/+ ESCs, the parental cell line of the PPP2R1A-SH expressing cells had to be tested.

Testing the differentiation potential of t^{w18}/+ ESCs towards the mesodermal cell lineage

The t^{w18}/+ ESC line was established in our laboratory by Dr. Hermann Bauer and it had not been previously tested how efficiently t^{w18}/+ ESC can be differentiated into the mesodermal cell lineage. The differentiation efficiency can be estimated by measuring *T* induction which is a marker gene for nascent mesoderm. To be able to directly observe *T* induction, a reporter BAC expressing *H2BmCherry* under the *T* promoter (provided by Dr. Frederic Koch) was randomly integrated in t^{w18}/+ ESCs (Fig. 20). This *T::H2BmCherry* BAC enables that cells that induce *T* expression become fluorescent and can be counted by FACS analysis. Thereby, up to 90% T^+ cells can be achieved by this differentiation protocol (Shin, 2011). The workflow to differentiate ESCs into the mesodermal cell lineage is depicted in Fig. 20. Feeder-

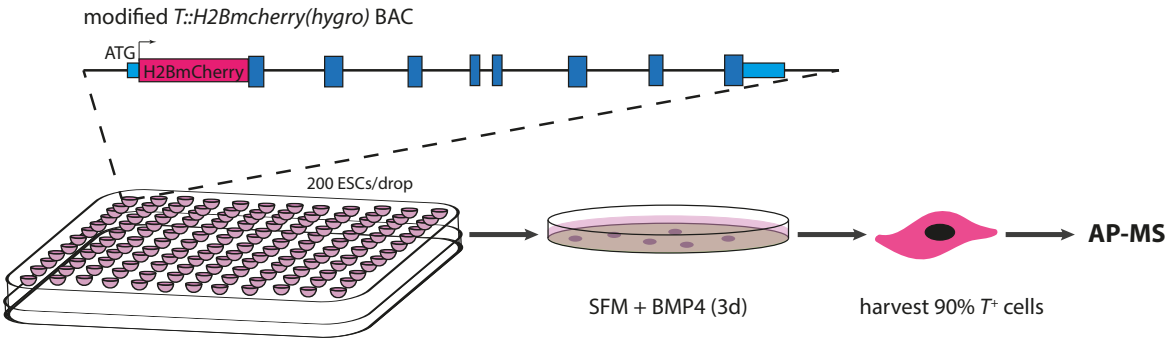

Figure 20. Workflow to differentiate ESCs into the mesodermal cell lineage. Feeder-free ESCs that contained a *T* reporter BAC were cultured in hanging drops with 200 cells/drop for 24 h. Aggregates were plated on fibronectin-coated dishes and cultured in serum free medium with BMP4. After 3 days of culture around 90% fluorescent T^+ cells can be harvested and used for AP-MS.

depleted ESCs that carried the *T* reporter BAC were cultured in hanging drops for 24 h. This was necessary to form aggregates of a fixed number of 200 cells, which was the optimized aggregate size for this differentiation protocol. Cell aggregates were then plated on fibronectin-coated culture dishes with serum free medium containing BMP4. After 3 days of BMP4 treatment 90% of the cells induced *T* expression which was observed by H2BmCherry fluorescence. These mesodermal cells could

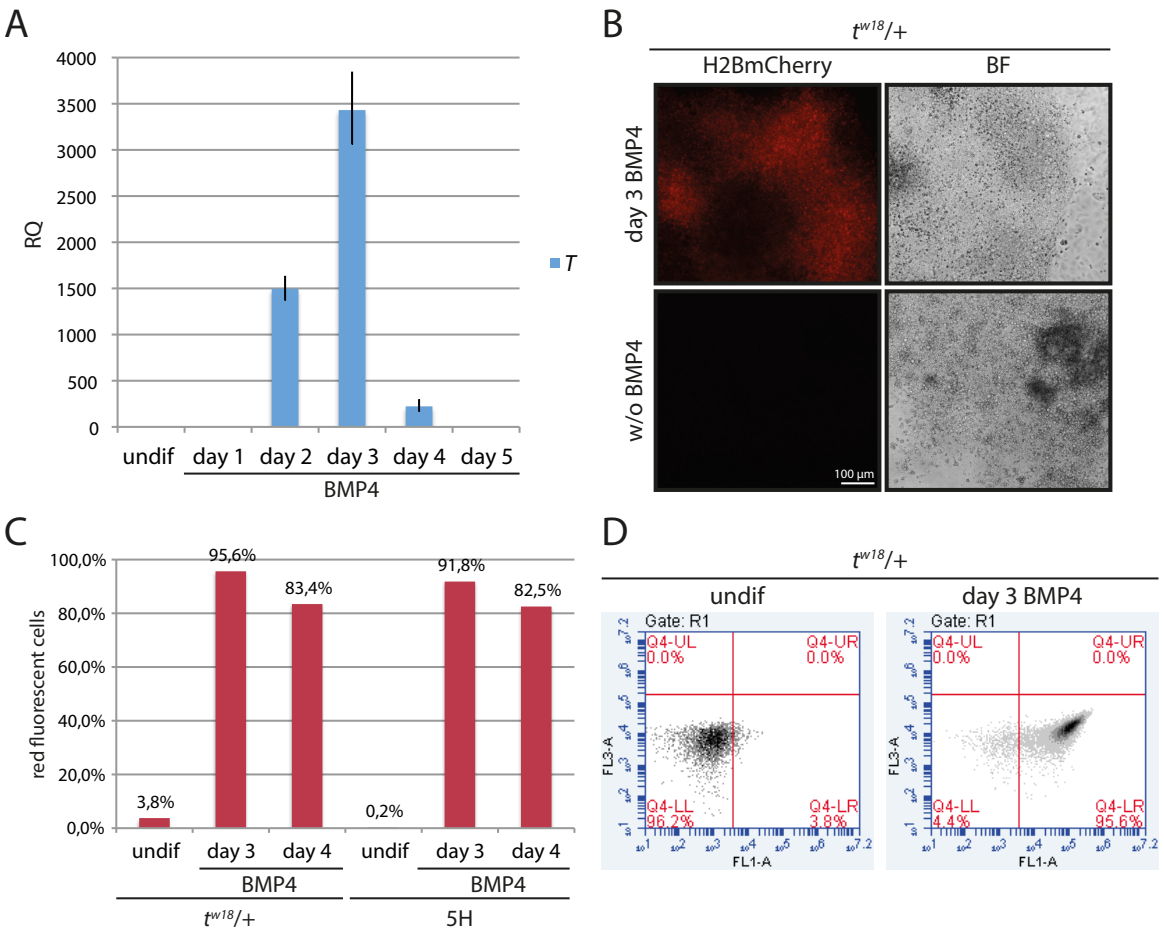

Figure 21. Differentiation of t^{w18}/+ ESCs into the mesodermal lineage. (A) t^{w18}/+ ESCs induced the mesoderm marker *T* under BMP4 treatment. *T* expression peaked on day 3 in qPCR. (B) The *T* reporter is strongly expressed on day 3 of BMP4 treatment shown by H2BmCherry fluorescence. (C) Fraction of T^+ cells measured by FACS for H2BmCherry fluorescence. t^{w18}/+ ESCs were compared to previously established wt ESC containing a *T::mCherry* reporter BAC. (D) Representative fluorescence scatter blots of differentiated and undifferentiated t^{w18}/+ cells showing increased Cherry fluorescence.

then be used for AP-MS analysis. This protocol was followed to test the differentiation potential of t^{w18}/+ ESCs. t^{w18}/+ ESCs were cultured under BMP4 treatment over the course of 5 days and RNA samples were collected every 24 h. Thereby, *T* expression was strongly induced on day 2 and peaked on day 3 of BMP4 treatment (Fig. 21A). H2BmCherry under the *T* promoter was strongly detectable on day 3 (Fig. 21B, D). To quantify the number of red fluorescent cells that represented T^+ cells, FACS analysis was performed. t^{w18}/+ ESCs were compared to previously established wild-type ESCs containing a *T::mCherry* BAC, designated as 5H cells (es-

tablished by Shin (2011)). Fig 21C shows that more than 90% of the cells were T^+ on day 3 of BMP4 treatment in both cell lines. On day 4 still more than 80% were red fluorescent. This differed from the qPCR data where *T* expression was strongly reduced compared to day 3, since the fluorescent reporter is more stable than the endogenous *T* mRNA.

In summary, the differentiation data showed that t^{w18}/+ ECSs could be efficiently differentiated into the mesodermal lineage just like other cell lines, leading to a very high percentage of cells that express the mesoderm marker *T*. This means that t^{w18}/+ ECSs could be used to express SH-tagged PPP2R1A and to produce large quantities of mesodermal cells for AP-MS.

AP-MS analyses of PPP2R1A complexes in undifferentiated ESCs and cells differentiated towards mesoderm

The workflow to affinity purify SH-tagged PPP2R1A is illustrated in Fig. 22. Ppp2r1a-SH expressing cells were cultured until a minimum of 10^7 cells was reached. The cell lysate was then loaded to streptactin sepharose containing columns. The flowthrough of this step contained unbound protein that did not bind to PPP2R1A complex on the beads. In addition, this sample was analyzed for binding efficiency of PPP2R1A-SH to the beads. The beads with bound proteins were then washed on the column. Afterwards, purified proteins were eluted from the beads by competitive elution with biotin that shows a higher binding affinity to streptactin than the Strep-tag. After confirming successful purification, the eluate samples were used for mass spectrometry analyses.

The previously described ESC line expressing PPP2R1A-SH was differentiated into the mesodermal lineage in large-scale experiments to produce 30 million differentiated cells. These cells were used to purify PPP2R1A-SH complexes via streptactin beads. Wild-type t^{w18}/+ ECSs served as negative control to be able to exclude unspecific binding to the beads. Prior to performing mass spectrometry analyses,

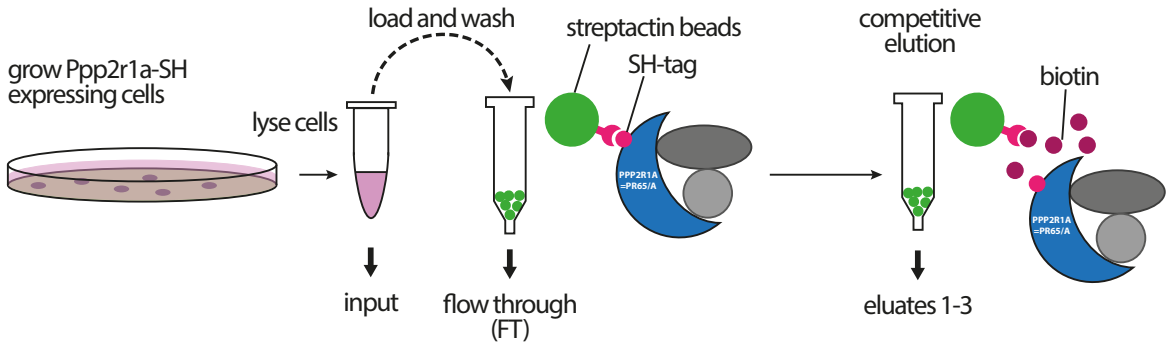

Figure 22. Workflow to affinity purify SH-tagged PPP2R1A. Cells that expressed *Ppp2r1a-SH* were grown under necessary culture conditions to the desired cell density, harvested and lysed. An input sample was taken from the lysate for Western blot analysis before loading to streptactin sepharose containing columns. The flowthrough of this step was also collected for Western blot analysis. After washing the beads the bound proteins were eluted from streptactin with biotin. A sample of the eluate was analyzed by Western blot prior to mass spectrometry.

purified protein samples were analyzed by Western blot and compared to input samples for successful purification (Fig. 23). PPP2R1A-SH was specifically highly enriched in eluate samples from undifferentiated and differentiated transgenic cells compared to the input lysate where no tagged protein could be detected (Fig. 23A). Endogenous PPP2R1A was only detectable in input samples. Fig. 23B confirms differentiation of both cell lines. T protein was detectable in input lysates from BMP4 treated cells, but not in undifferentiated cells. These Western blot data showed that PPP2R1A-SH was successfully purified from differentiated and undifferentiated cells. Direct LC/MS-MS was performed in collaboration with Dr. Matthias Gstaiger. His group was provided with the eluate samples and performed the sample preparation, as well as LC/MS-MS and analysis of the raw data. Data from three independent experiments that were performed with the same cell number and protocol were pooled.

A set of 49 proteins that were specifically co-purified in the PPP2R1A-SH sample in both states, differentiated and undifferentiated, in at least two of the three replicates was identified (Table 1). These proteins were assigned to different groups of related complexes that have been described previously: PP2A subunits, integrator

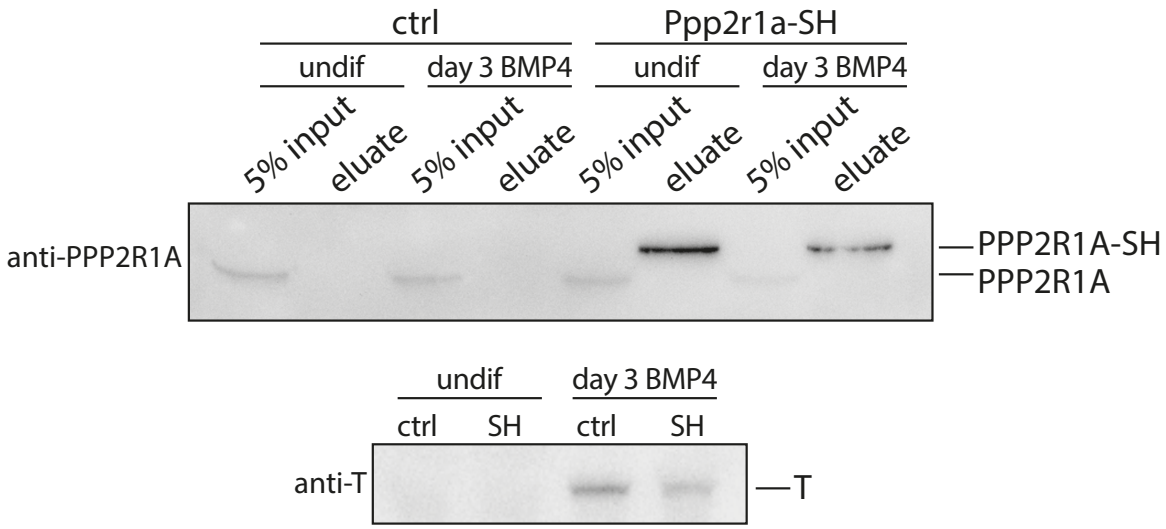

Figure 23. Affinity purification of SH-tagged PPP2R1A. (A) Western blot analyses of input and eluate samples from t^{w18}/+ (ctrl) and PPP2R1A-SH expressing (SH) ESCs with PPP2R1A antibody. (B) Western blot of input lysates with T antibody.

subunits, STRIPAK, methylesterase module and other proteins (Glatter *et al.*, 2009; Herzog *et al.*, 2012). This data set recapitulated many PPP2R1A interaction partners that have previously been identified. As expected, other PP2A subunits were found. In addition to the PP2A catalytic subunits Cα (PPP2CA) and Cβ (PPP2CB), the B regulatory subunits Bα/PR55α (PPP2R2A), Bδ/PR55δ (PPP2R2D), B′α/PR61α (PPP2R5A), B′γ/PR61γ (PPP2R5C) and B′ϵ/PR61ϵ (PPP2R5E) were detected. This supports that the PP2A scaffolding subunit Aα (PPP2R1A) is present in many different PP2A heterotrimeric holoenzymes and mediates the interaction of catalytic subunits with B regulatory subunits.

Striatins are commonly also known as PP2A regulatory B‴ subunits. They are found in the so-called STRIPAK (striatin-interacting phosphatase and kinase) complex and are therefore designated as distinct group in Table 1 (Goudreault *et al.*, 2009). This complex consists of PP2A scaffolding and catalytic subunit, members of the striatin family and striatin interactors. These include MOB4 (phocein, MOBKL3), STRIP1 (striatin interacting protein 1, FAM40A), members of the GCKIII (germinal center kinase III) subfamily, as well as CCM3 (cerebral cavernous malformation 3, PDCD10). MOB4 and STRIP1 were reliably found in all three of our mass

spec experiments. In addition, mutually exclusive interactions of STRIPAK with CTTNBP2 (cortactin binding protein 2) and CTTNBP2NL (CTTNBP2 N-terminal like) or with SLMAP (sarcolemmal membrane-associated protein, SLAP) have been reported (Goudreault *et al.*, 2009). In our experiments the interactions with CTTNBP2NL and SLMAP were recapitulated, suggesting that PPP2R1A is found in both STRIPAK complexes in mouse ESCs.

Table 1. PPP2R1A interaction partners identified by AP-MS with SH-tagged Ppp2r1a.

Modules	Gene name
PP2A subunits	Ppp2r1a, Ppp2r1b, Ppp2ca, Ppp2cb, Ppp2r2a, Ppp2r2d, Ppp2r5a, Ppp2r5c, Ppp2r5e,
Integrator complex	Ints1, Ints2, Ints3, Ints4, Ints5, Ints6, Ints7, Ints8, Ints9, Ints10, Cpsf3l (Ints11), Ints12, Asun (Ints13), Polr2a, Polr2b,
STRIPAK	Strn, Strn3, Strn4, Mob4, Strip1, Cttnbp2nl, Slmap
Methylesterase module	Ppme1
SOSS complex	Nabp2, Inip
Others	Ankle2, Ccdc6, Espl1, Fech, Ppfia2, Ppfia3, Rbm7, Skiv2l2, Sptbn1, Soga2, Soga3, Sgol2, Skt, Tbccd1, Vwa9, Zcchc8

The interaction of PP2A with the integrator complex has been previously described (Herzog *et al.*, 2012). This large protein complex consists of at least 13 integrator subunits (INTS1-12, ASUN) and associates with the C-terminal repeat of RNA polymerase II (Baillat *et al.*, 2005; Chen *et al.*, 2012). Next to its role in 3′-end processing of small nuclear RNAs (snRNAs), integrator proteins are implicated to function in other cellular processes. In our experiments, the 13 integrator subunits were co-purified with PPP2R1A. In addition, we found POLR2A and POLR2B in the mass spec data.

PPME1 has been found to regulate PP2A activity by demethylation of the PP2A catalytic subunit. Thereby, it is mostly associated with an inactive population of PP2A (Longin *et al.*, 2004; Hombauer *et al.*, 2007). A PPME1 module has been sug-

gested by Glatter *et al.* (2009), where PPME1 interacts with PPP2R1A and the PP2A catalytic subunits. We confirmed the interaction of PPP2R1A and PPME1 in our screen.

We found the proteins NABP2 (nucleic acid binding protein; human synonym: hSSB1) and INIP (INTS3 and NABP2 interacting protein; human synonym: hSSBIP1) to co-purify with tagged PPP2R1A. It has been shown that these proteins interact with INTS3 in the SOSS (sensor of ssDNA) complex that is important for DNA repair and G2/M checkpoint (Skaar *et al.*, 2009; Huang *et al.*, 2009).

Next to these interaction partners that were grouped together we found other proteins in association with PPP2R1A (Table 1). For some of the proteins an interaction with PP2A has already been shown, but we also found new interaction partners. Glatter *et al.* (2009) showed that the human homologues of ANKLE2, CCDC6, FECH, RBM7, SKIV2L2, and SOGA2 interact in HEK293 cells. The association of PPP2R1A with the liprins PPFIA2 and PPFIA3 has also been shown in HEK293 cells (Goudreault *et al.*, 2009). ESPL1 (separase) is important for chromosome segregation during transition from metaphase to anaphase. Studies showed that ESPL1 interacts with PP2A via the B′γ regulatory subunit (PPP2R5C) (Holland *et al.*, 2007). In our data set we found ESPL1 as well as PPP2R5C co-purified with PPP2R1A. Another protein involved in chromosome segregation is SGOL2 (shugoshin-like 2). It interacts with the PP2A core dimer as well as with different PP2A holoenzymes (Xu *et al.*, 2009; Rattani *et al.*, 2013). The interaction of another shugoshin protein, SGOL1, with PP2A in human and yeast cells has been shown before (Kitajima *et al.*, 2006). Glatter *et al.* (2009) confirmed this interaction in a mass spec approach similar to our experiments, where we found an association of Sgol2 with PP2A.

In our data set we found SPTBN1, SOGA3, SKT, TBCCD1 and VWA9 to co-purify with PPP2R1A. An interaction of these with PP2A has not yet been published and the function and relevance of these interactions remains to be elucidated.

Since AP-MS was performed with undifferentiated and differentiated cells one

can look for changes in the Ppp2r1a interaction network between these two states. The second of the three replicates was excluded from this analysis, since much lower peptides were retrieved in the differentiated compared to the undifferentiated sample. These peptide counts strongly differed also from the other experiments. Thus, involving these data would have distorted the results. Peptide counts from differentiated and undifferentiated samples from the other replicates were set relative to one another and normalized to the Ppp2r1a value. Only seven of the 49 proteins showed a difference by at least a factor of two between the two states (Table S2). All of these proteins showed a stronger interaction with Ppp2r1a in undifferentiated than in differentiated cells. Notably, these seven proteins were represented by only a few peptide counts or strongly differed between the two replicates. Differences are therefore likely due to technical variation.

4.5.2 Analyzing the Transcriptome of t^{w18} homozygous, heterozygous and wild-type embryos at E6.5

The t^{w18} homozygous phenotype first becomes morphologically apparent by E7.5. Before the phenotype is morphologically visible, changes in gene expression levels are already manifested. At E6.5 a severe reduction of mesodermal marker gene expression is detectable (Fig. 7). To further analyze global changes in gene expression levels and to further analyze the function of *Ppp2r1a* during early embryogenesis a RNA-seq approach was followed. The transcriptome of t^{w18} homozygous, heterozygous and wild-type embryos was analyzed at E6.5.

It was necessary to obtain RNA as well as DNA from these embryos, because the genotype could not be determined by the morphology of the embryos. Therefore, embryos were dissected into an embryonic part, consisting of epiblast, and surrounding VE that was used for RNA-seq, and the extraembryonic tissue that was used for genotyping. Around ten embryo samples (11x +/+, 9x t^{w18}/t^{w18}, 10x $t^{w18}/+$) with the same genotype were then pooled for each of the RNA-seq experi-

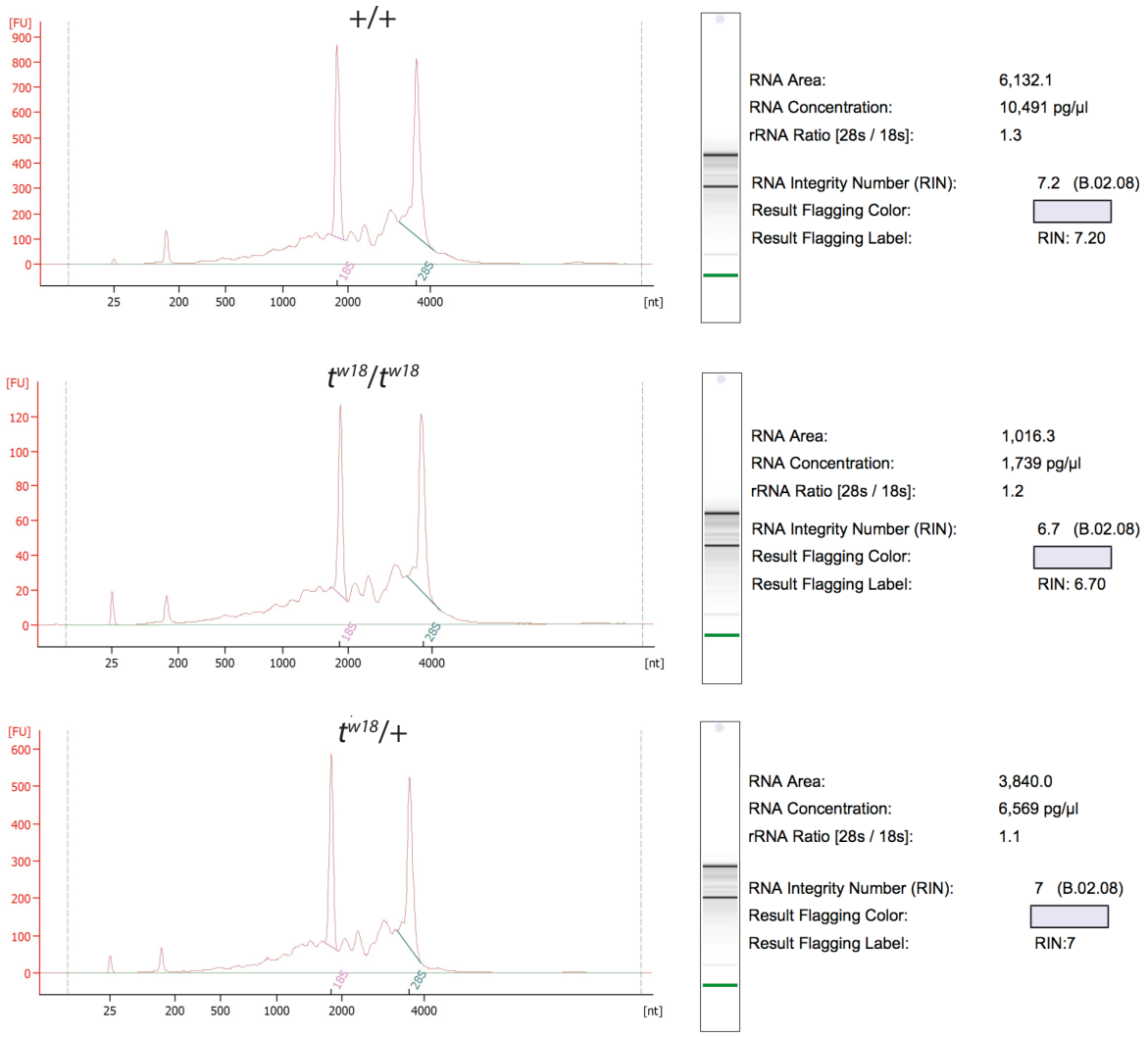

Figure 24. RNA quality assessment using the Bioanalyzer system. Electropherograms, gel-like images and RNA results of the wild-type, homozygous and heterozygous t^{w18} samples.

ments. The quality of extracted RNA was estimated using the Bioanalyzer system (Agilent) (Fig. 24). The RIN (RNA integrity number) gives information about RNA quality. For the three RNA samples isolated from E6.5 epiblasts a RIN around 7 was determined with most of the RNA being intact, although some degradation had already occurred. According to experiences in our laboratory samples with a RIN around 7 provided sufficient RNA quality to continue with cDNA synthesis and library preparation for RNA-seq as downstream experiment. The TotalScript™ RNA-Seq KIT (epicenter) was used for cDNA synthesis from 5 ng RNA and library

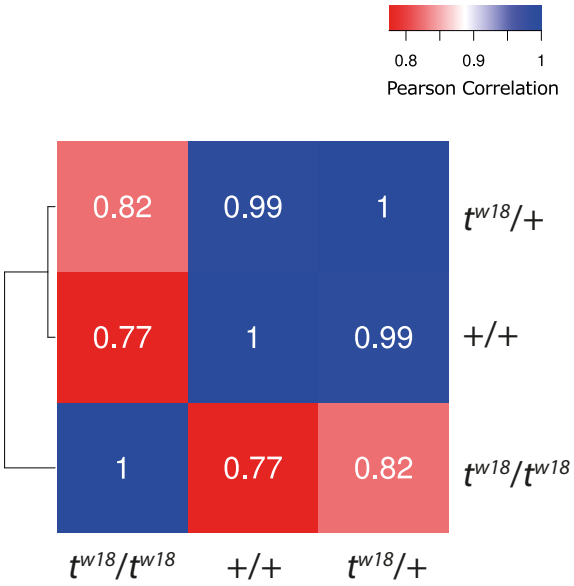

Figure 25. Pearson correlation coefficient of NGS data from wild-type, homozygous and heterozygous t^{w18} samples.

preparation. The sequencing was performed by the NGS core facility (Bernd Timmermann, MPIMG) using the Illumina HiSeq 2500 (High Output) system for 50 bp paired end reads. Bioinformatic raw data analyses were performed by Jinhua Liu.

The sequencing reads were mapped to the mouse genome mm10 (GRCm38) using TopHat v2.0.8b and Cuffdiff was used to calculate normalized FPKM (fragments per kilobase of transcript per million mapped reads) (Table S3). To get a first overview of the data the Pearson correlation coefficient (PCC) was calculated (Fig. 25). The wild-type and the heterozygous t^{w18} sample were very similar, showing a PCC of 0.99, while the t^{w18}/t^{w18} sample greatly differed from the wild-type (PCC 0.77) and the heterozygous sample (PCC 0.82). From the NGS data, lists of genes that were differentially expressed between the three samples were extracted (Tables S4, S5, S6). Since the PCC showed that the wild-type and heterozygous sample were very similar, first analyses were constrained to comparing the wild-type and homozygous mutant datasets. Differentially expressed genes between the +/+ and t^{w18}/t^{w18} sample were selected based on different threshold levels of the fold change of the FPKM. For a fold change (FC) of $\log_2 \geq 2$ (FC ≥ 4) a set of 190 genes were found to

be differentially expressed, whereas 543 and 1759 genes were dysregulated for fold changes of $\log_2 \geq 1.5$ (FC ≥ 2.8) and $\log_2 \geq 1$ (FC ≥ 2), respectively.

Prior to further analyses I checked for genes that are located in the t^{w18} deleted region and that are not expected to contribute to the t^{w18} phenotype. Most of the 74 genes that are deleted were not expressed in the epiblast at E6.5. In contrast, 19 of the 20 zinc finger protein genes within the t^{w18} region were expressed in wild-type embryos and were downregulated in homozygous mutants. Unexpectedly, some expression was still detectable in the t^{w18}/t^{w18} sample although these genes are deleted in the t^{w18} genotype. The same tendency was observed for *Ppp2r1a*. Most likely this expression is due to contamination of the samples with maternal material during the dissection process. Since *Ppp2r1a* expression alone rescued the t^{w18} homozygous phenotype, these other genes within the deleted region were excluded from further analyses.

Visualization of genes dysregulated with an arbitrary cutoff of $\log_2(\text{FC}) \geq 1.5$ in a heatmap revealed that more than two-thirds of the genes were upregulated (416 genes) in t^{w18}/t^{w18} compared to the wild-type, whereas 127 genes were downregulated (Fig. 26). *T* was one of the genes most strongly downregulated ($\log_2$(FC) = -4.3) with expression being absent in t^{w18} homozygotes. The absence of *T* expression showed that the RNA-seq experiment as well as specific genotyping of embryos were successful since downregulation of *T* expression in t^{w18}/t^{w18} embryos was previously observed by *in situ* hybridization. In order to investigate the dataset of dysregulated genes for enrichment of biological functions, gene ontology (GO) term enrichment analysis was performed using the Ontologizer tool. Relevant and significantly enriched GO terms are depicted in Figure 27 (A complete list of GO terms is available in Table S7). This showed that genes functioning in developmental processes, organ morphogenesis, differentiation and proliferation were enriched among genes more than twofold dysregulated in t^{w18} homozygotes (Fig. 27, upper panel). For a better interpretation, enriched GO terms were separately analyzed for

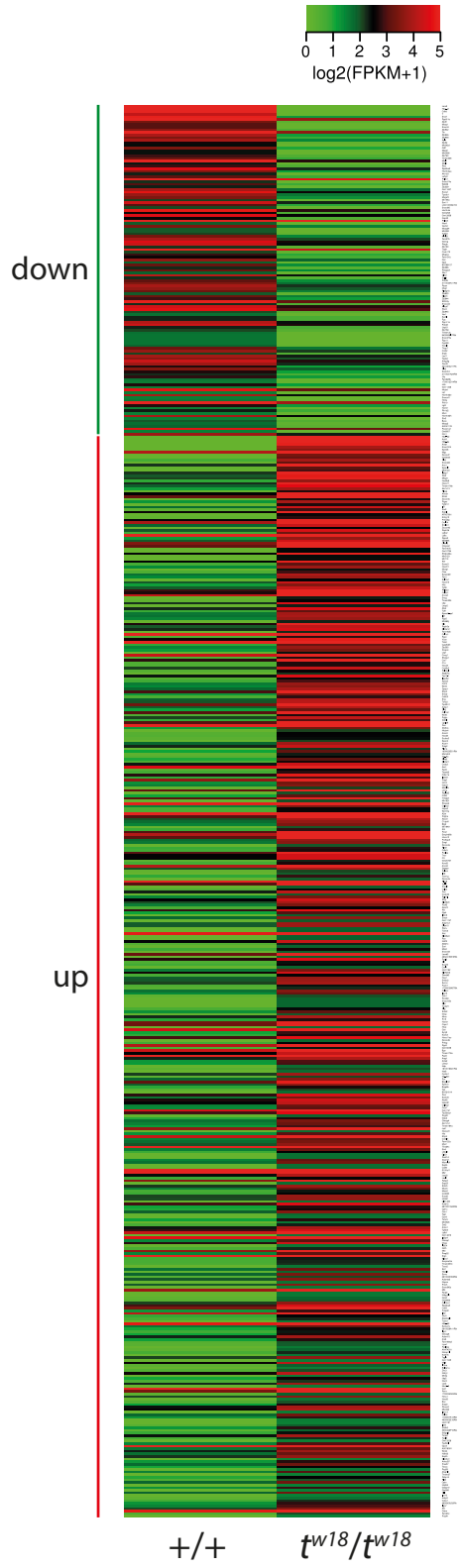

Figure 26. Dysregulated genes in the t^{w18} homozygous compared to the wild-type sample. Heatmap of 543 differentially expressed genes between wild-type and homozygous t^{w18} with $\log_2(\text{FC}) \geq 1.5$. 416 genes were upregulated, while 127 genes were downregulated.

up- and downregulated genes. Genes downregulated in t^{w18} showed enrichment for GO terms that relate to gastrulation and mesoderm formation (Fig. 27, middle panel). These included genes like *Fgf8*, *Mesp1*, *Mesp2*, *T*, *Mixl1*, *Eomes*, *Nanog*, *Pou5f1* (*Oct4*) and others. The downregulation of genes functioning in gastrulation is consistent with the observed phenotype of t^{w18} homozygous embryos showing large gastrulation defects. More general GO terms like regulation of differentiation and proliferation that included large groups of genes were enriched for genes upregulated in t^{w18}/t^{w18} (Fig. 27, lower panel). In addition, the GO term biological adhesion was significantly enriched. For example, cell adhesion is regulated during gastrulation when epiblast cells lose their epithelial and switch towards a mesenchymal morphology. Adhesion molecules function, in addition to their roles in cell-cell or cell-ECM interactions, also in modulating signal transduction processes that influence cell motility, proliferation, survival and differentiation. The group of upregulated genes annotated with the GO term biological adhesion contains genes that encode adhesion receptors like integrins (*Itga1*, *Itga7*, *Itga8*), cadherins and protocadherins (*Cdh13* (*T-cadherin*), *Cdhr5*, *Pcdhgc3* (μ-*protocadherin*)), members of the Ig-CAM superfamily (*Icam1*, *Mcam*, *Ceacam1*) and ECM components like laminins (*Lama1*, *Lamb2*, *Lamc1*, *Lamc2*), collagens (*Col1a1*, *Col3a1*, *Col6a1*, *Col6a2*, *Col14a1*, *Col15a1*) and a nidogen (*Nid1*). The upregulation of these genes suggests a stronger adhesion between cells and with the ECM that could disturb the gastrulation process.

It is remarkable that developmentally important genes expressed in ICM-derived extraembryonic tissue, namely the VE, were not affected or were only slightly upregulated in t^{w18}, whereas genes expressed in embryonic tissues, namely epiblast or primitive streak were more strongly affected and downregulated (Table 2). The difference in dysregulation between genes expressed in VE and embryonic tissue might indicate that the epiblast is more strongly affected by the mutation than extraembryonic tissues. Since trophectoderm-derived extraembryonic tissue was re-

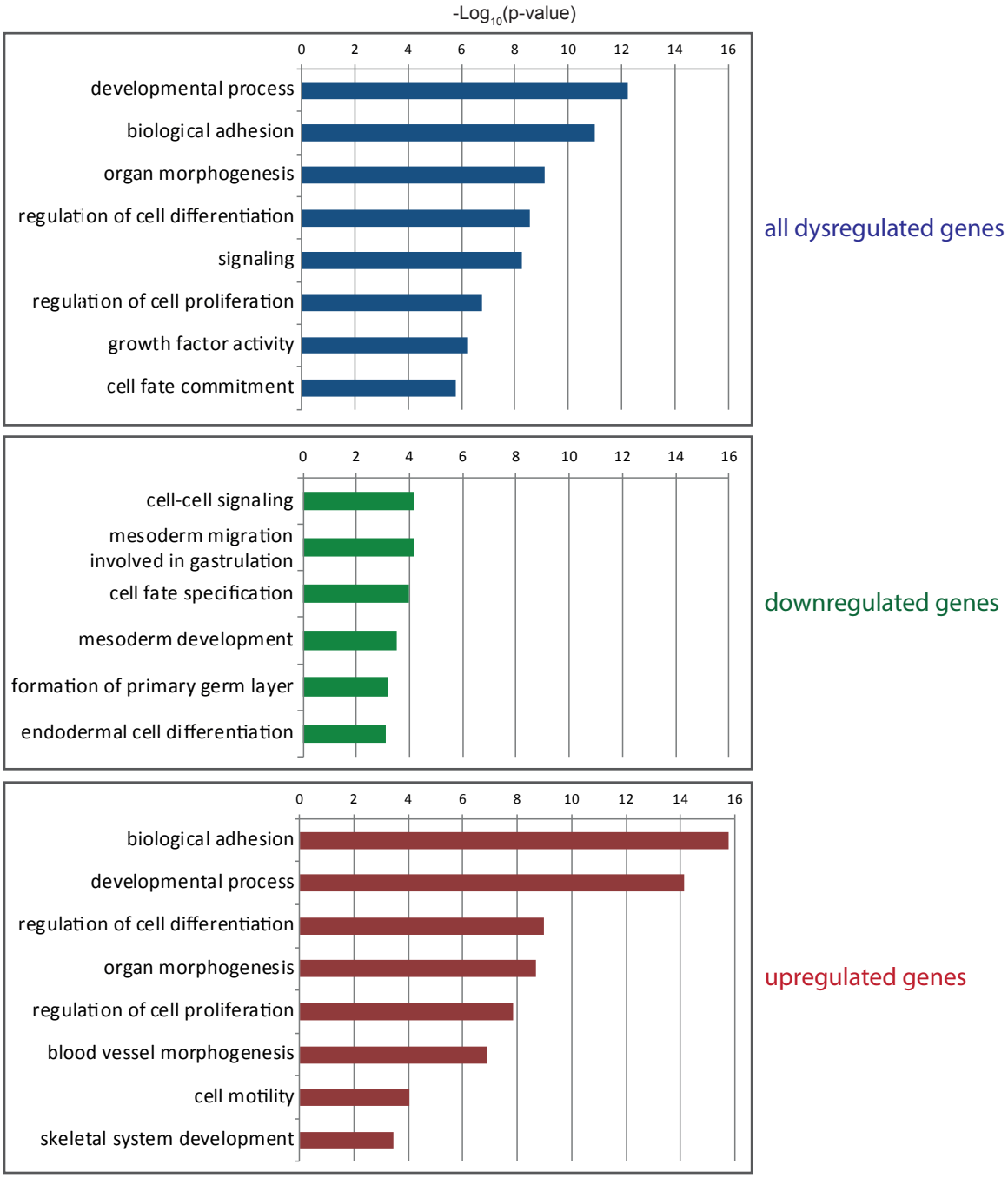

Figure 27. GO term enrichment analyses of dysregulated genes (FC $\geq$ 2). GO terms were individually analyzed for all dysregulated genes (upper panel), for downregulated genes (middle panel) and for upregulated genes (lower panel). The diagrams shows selected GO term with corresponding -Log_{10} of the P-value that were given by the Ontologizer tool. A background of genes expressed in the dataset with FPKM $\geq$ 2 was used.

Table 2. Expression domains of selected genes at E6.5 in visceral endoderm or embryonic tissue with corresponding $\log_2$ fold change.

Gene symbol	Expression domain (E6.5)	$\log_2$(FC)
Hesx1	AVE (Hermesz *et al.*, 1996)	1.6
Hhex	AVE, definitive endoderm (Thomas *et al.*, 1998)	1.3
Bmp2	EmVE (Coucouvanis and Martin, 1999)	1.1
Foxa2	AVE, PS (Norris *et al.*, 2002)	n.a.
Lhx1	AVE, PS (Norris *et al.*, 2002)	n.a.
Cited2	AVE (Dunwoodie *et al.*, 1998)	n.a.
Amot	AVE (Shimono and Behringer, 2003)	n.a.
Wnt3	PS and overlaying VE (Rivera-Pérez and Magnuson, 2005)	n.a.
Dkk1	AVE (Kimura-Yoshida *et al.*, 2005)	n.a.
T	PS (Rivera-Pérez and Magnuson, 2005)	-4.3
Mixl1	posterior epiblast, PS (Robb *et al.*, 2000)	-2.4
Tdgf1 (*Cripto*)	posterior epiblast (Norris *et al.*, 2002)	-1.9
Nanog	posterior epiblast (Hart *et al.*, 2004)	-1.9
Fgf8	PS (Crossley and Martin, 1995)	-1.4
Pou5f1 (*Oct4*)	epiblast (Beck *et al.*, 2002)	-1.2
Sox2	epiblast (Avilion *et al.*, 2003a)	-1.2
Eomes	PS (Ciruna and Rossant, 1999)	-1.0
Evx1	PS (Dush and Martin, 1992)	n.a.

Abbreviations: AVE, anterior visceral endoderm; EmVE, embryonic visceral endoderm; n.a., not affected; PS, primtive streak; VE, visceral endoderm.

moved from the RNA sample for genotyping, it cannot be stated how genes would be affected that are expressed in the extraembryonic ectoderm. A stronger effect on genes expressed in the epiblast suggests that the epiblast has a stronger requirement for *Ppp2r1a*. Additionally, it is striking that pluripotency markers like *Nanog*, *Oct4* or *Sox2* that are required for maintenance of pluripotency in the epiblast (Nichols *et al.*, 1998; Avilion *et al.*, 2003b; Mitsui *et al.*, 2003) were downregulated.

Dysregulated genes were further analyzed to find developmentally important signaling pathways that might be affected in t^{w18} homozygozes. A finely-tuned balance of Nodal and WNT signaling is required for positioning of the anteroposterior axis, formation of the primitive streak and mesoderm formation (Schier and Shen, 2000).

In t^{w18}/t^{w18} embryos, targets of Nodal signaling were dysregulated: *Tdgf1* (*Cripto*), *Gsc*, and *Lefty1/2* were downregulated showing that Nodal signaling is disturbed in t^{w18} homozygotes (Table 3).

Table 3. Nodal and Wnt targets dysregulated in t^{w18} homozygotes.

Nodal targets	$\log_2$(FC)
Tdgf1 (*Cripto*) (Brennan *et al.*, 2001; Beck *et al.*, 2002)	-1.9
Gsc (Toyama *et al.*, 1995; Jones *et al.*, 1995)	-1.9
Lefty1 (Schier and Shen, 2000)	-1.0
Lefty2 (Schier and Shen, 2000)	-2.3
Wnt targets	**$\log_2$(FC)**
T (Arnold *et al.*, 2000)	-4.3
SP5 (Weidinger *et al.*, 2005; Fujimura *et al.*, 2007)	-1.4
Axin2 (Jho *et al.*, 2002; Lustig *et al.*, 2002)	-1.3

In addition, expression of *T* and *Fgf8* were downregulated in t^{w18}, which is also lost in *Nodal*-deficient embryos (Brennan *et al.*, 2001). The *Nodal* ligand itself controls its own expression in an autoregulatory loop (Norris *et al.*, 2002). *Nodal* expression levels were not affected, suggesting defects in the signaling pathway downstream of the ligand during transduction of the signal to the nucleus. Expression of Nodal convertases, *Furin* (*Spc1*) and *Pcsk6* (*Spc4*) (Beck *et al.*, 2002), and intracellular transmitters of Nodal signaling, Smads (Kumar *et al.*, 2001), were also not affected in t^{w18}. However, the Nodal feedback inhibitor *Cer1* (Piccolo *et al.*, 1999), *Hesx1* and *Hhex1*, markers of the anterior visceral endoderm (AVE) were upregulated which indicates that an anteroposterior polarity is established with a possibly extended anterior domain. In addition, WNT antagonists like *Sfrp1* and *Sfrp5* (Pfister *et al.*, 2007) expressed in the AVE were upregulated. However, *Wnt3* expressed in the posterior epiblast and VE (Rivera-Pérez and Magnuson, 2005) was not affected, indicating that the anteroposterior axis was properly established. The primitive streak is marked by expression of genes including *T* (Rivera-Pérez and Magnuson, 2005),

Fgf8 (Crossley and Martin, 1995) and *Mixl1* (Pearce and Evans, 1999), all of which were downregulated in t^{w18}. It has been shown that *T* is a direct target of Wnt signaling (Arnold *et al.*, 2000). The lack of *T* expression in t^{w18} while *Wnt3* expression is maintained, suggests that *Ppp2r1a* functions in Wnt signaling downstream of the ligand. Other Wnt target genes like *Sp5* (Weidinger *et al.*, 2005; Fujimura *et al.*, 2007) or *Axin2* (Jho *et al.*, 2002; Lustig *et al.*, 2002) that are induced upon Wnt signaling, were downregulated.

In summary, analyses of dysregulated genes showed that the t^{w18} mutation is characterized by (1) a stronger effect on the epiblast than on the VE, as seen by downregulation of pluripotency markers and developmentally important genes expressed in the epiblast, (2) disturbed Nodal and Wnt signaling downstream of the ligands, and (3) an upregulation of cell adhesion molecules.

5 Discussion

Embryos homozygous for the t^{w18} haplotype show severe gastrulation defects and early embryonic lethality. The genotype of t^{w18} is characterized by a large deletion on mouse chromosome 17 containing the causative gene. By next generation sequencing in combination with PCR analyses, I was able to define the overall extent of the deletion and the gene content of this region. One of the 74 genes deleted, *Ppp2r1a* was extracted as a prime candidate. I showed that knockout of *Ppp2r1a* resulted in an embryonic lethal phenotype similar to the t^{w18} homozygous phenotype. Expression of *Ppp2r1a* from a BAC transgene that contained the *Ppp2r1a* locus alone in t^{w18}/t^{w18} embryos was able to rescue the mutant phenotype. These results demonstrate that *Ppp2r1a* is responsible for the defects observed in the t^{w18} haplotype containing mouse strain.

Towards functional analysis of *Ppp2r1a* during early embryogenesis, the transcriptome of t^{w18} homozygous embryos compared to wild-type littermates was investigated by RNA-seq, to unravel gene expression profiles dependent on *Ppp2r1a* function. Analysis of genes dysregulated in t^{w18} embryos showed that the Wnt and Nodal signaling cascades were disturbed, leading to downregulation of their target genes. In addition, mesendodermal as well as pluripotency markers were downregulated, whereas genes mediating cell adhesion were upregulated. Transcriptome analyses were combined with an *in vitro* pull-down system to identify interacting proteins including other PP2A regulatory subunits, as well as possible dephosphorylation targets. PPP2R1A interacting proteins included PP2A subunits that regulate signaling cascades and function during embryogenesis. Moreover, proteins functioning in cell cycle were found in complex with PPP2R1A.

5.1 *Ppp2r1a* exerts specific functions during gastrulation

5.1.1 *Ppp2r1a* function in Wnt and Nodal signaling

The phenotypes of t^{w18} and *Ppp2r1a* loss-of-function embryos demonstrate a role for *Ppp2r1a* during gastrulation. Gene expression data from t^{w18} embryos reinforce a specific function in cell lineage specification in the epiblast and in gastrulation. PP2A is thought to function in a variety of cellular processes, including the cell cycle (Janssens and Goris, 2001). It is therefore surprising to find that loss of *Ppp2r1a* results in specific gastrulation defects.

The Wnt and Nodal signaling pathways play essential roles in initiating gastrulation and cell lineage differentiation. Although expression levels of the morphogens *Nodal* and *Wnt3* were unaffected in t^{w18} embryos, their target genes were downregulated (Table 3), suggesting defects in these pathways. It is therefore likely that *Ppp2r1a* functions at some level by regulating these signaling cascades.

Concerning canonical Wnt signaling, complete abrogation of the cascade is not indicated. Otherwise t^{w18} embryos would greatly resemble mutants lacking the Wnt downstream effector *β-catenin*. Huelsken *et al.* (2000) showed that *β-catenin*$^{-/-}$ mutants fail to develop an anteroposterior axis by loss of *Hhex*, *Hesx1* and *Otx2* expression. These anterior marker genes are expressed in t^{w18} embryos and therefore the anteroposterior axis of the embryo is established. Moreover the phenotype of t^{w18} embryos greatly differs from *Wnt3* loss-of-function embryos which do not form a primitive streak, while the single-layered epiblast continues to proliferate (Liu *et al.*, 1999). Morphological observations of t^{w18} embryos show a bulge of cells emanating from the epiblast at a specific restricted site where the primitive streak is supposed to form (Fig. 7, arrowhead). A structure like this is not observed in *Wnt3*$^{-/-}$ embryos. In contrast to *Wnt3*$^{-/-}$ embryos, a primitive streak is therefore initiated in both t^{w18}

and embryos lacking *Ppp2r1a*.

Several studies provide evidence for a role of PP2A in Wnt signaling, with negative as well as positive regulation being suggested. In our current understanding of PP2A phosphatase activity, substrate specificity is mediated by assembly of the core enzyme consisting of the structural A subunit (PPP2R1A or PPP2R1B) and catalytic C subunit (PPP2CA, PPP2CB) with a variable regulatory B subunit (Sents *et al.*, 2013).

The roles of PP2A containing specific B subunits in signaling cascades has been investigated in different systems. A report by Bajpai *et al.* (2004) showed that in *Drosophila*, loss of the homologue of a B (PR55) subunit of PP2A results in downregulation of Wnt targets, suggesting a positive role for PP2A:PR55α in Wnt signaling by stabilizing cytoplasmic β-catenin. Overexpression of this B subunit leads to a dominant-negative phenotype that was interpreted by Bajpai *et al.* (2004) as an imbalance in the relative amounts of the three subunits in the heterotrimeric PP2A complex. In addition, work by Zhang *et al.* (2009) demonstrates that PP2A is required for Wnt signaling in *Drosophila in vivo*. The group identified the B regulatory subunit PR55α to directly interact with β-catenin and to mediate its dephosphorylation thereby inhibiting its degradation.

A negative role in Wnt signaling has been shown by Seeling (1999), Li *et al.* (2001) and Yamamoto *et al.* (2001). These studies are based on overexpression of PP2A subunits in *Xenopus* and mainly focus on B′ (PR61) regulatory subunits. However, it should be noted that a general negative role for *Ppp2r1a* in Wnt signaling is not supported by gene expression data in embryos lacking *Ppp2r1a*, which showed downregulation of Wnt target genes (Table 3).

Thus, there are two possibilities for PP2A function in Wnt signaling: (1) Different B regulatory subunits exert opposing functions. PR61 subunits might play a negative role as indicated by overexpression studies, while PR55α has a positive impact on the Wnt signaling cascade. (2) The negative role of PR61 subunits suggested from

overexpression studies results from a dominant-negative effect that masks the actual function in Wnt signaling. Therefore, experiments investigating loss-of-function of PR61 subunits are necessary to clearify their function in regulating Wnt signaling.

PR55α (PPP2R2A) was found to interact with PPP2R1A by mass spectrometry experiments within this thesis. I aimed at functionally analyzing *Ppp2r1a* by identifying interacting proteins. An SH-tagged version of *Ppp2r1a* was expressed in t^{w18}/+ ESCs from a BAC transgene. These transgenic ESCs were either used in an undifferentiated state or differentiated towards the mesodermal cell lineage by BMP4 treatment. Protein complexes containing tagged PPP2R1A were affinity-purified and interacting proteins were identified by mass spectrometry. Within the set of interacting proteins several PP2A B regulatory subunits were identified (Table 1). PPP2R1A was found in undifferentiated and differentiated cells to interact with PR55α (PPP2R2A) the B regulatory subunit that in *Drosophila* directly interacts with β-catenin (Zhang *et al.*, 2009). These data infer that also in mice PPP2R1A might be required to assemble the PP2A holoenzyme containing PR55α to regulate β-catenin dephosphorylation and stability. To test this hypothesis, it would be necessary to analyze β-catenin protein levels in *Ppp2r1a* loss-of-function embryos to show whether increased β-catenin phosphorylation and degradation cause the reduction in Wnt target gene expression observed.

The interactome data also identified the B regulatory subunit PR61α (PPP2R5a) to interact with tagged PPP2R1A. As discussed above, overexpression of this subunit in *Xenopus* suggested a negative role for PP2A:PR61α in Wnt signaling, acting in various components, such as APC (Seeling, 1999) and Axin (Li *et al.*, 2001). Future experiments are necessary to identify the dephosphorylation targets of PP2A:PR61α and whether it exerts a negative role in Wnt signaling.

Other direct elements of the Wnt signaling pathway have not been identified by the mass spectrometry approach, and thus should be investigated by other methods in order to determine whether PPP2R1A is found in a complex with β-catenin or

other Wnt components. It would also be interesting to look at Wnt signaling by integrating a Wnt reporter system in t^{w18} or *Ppp2r1a* knockout embryos. It is possible that PP2A does not play a positive role in Wnt signaling in general, but depending on the B regulatory subunit, could also have negative impact. A detailed analysis of expression patterns of PP2A subunits in mouse embryos is not presently available. If B subunits are differentially expressed during embryogenesis, then lack of *Ppp2r1a*-mediated phosphatase activity could suppress or increase Wnt signaling differently in distinct tissues. Such a scenario might explain a stronger effect of *Ppp2r1a* loss-of-function within the epiblast. In an epiblast-specific knockout of *Wnt3*, it has been shown that Wnt3 signaling from the posterior VE is required to establish the anteroposterior axis and initiate gastrulation (Tortelote *et al.*, 2013).

The second developmentally important signaling cascade that was found to be dysregulated in t^{w18} homozygous embryos was the Nodal pathway. Expression profiles showed that while expression of the Nodal ligand itself was not affected, its target genes were downregulated (Table 3). These resulted suggest PPP2R1A to function in the signaling cascade downstream of the ligand. To date, not much is known about how PP2A regulates TGFβ/Activin/Nodal signaling, but a first report showed that PR55α interacts with type I TGFβ receptors (Griswold-Prenner *et al.*, 1998). Moreover, a later study showed that the closely related B regulatory subunits PR55α (PPP2R2A) and PR55δ (PPP2R2D) exert opposing effects on the TGFβ/Activin/Nodal pathway (Batut *et al.*, 2008). Knockdown of PR55α or overexpression of PR55δ in *Xenopus* embryos resulted in embryos with a truncated anteroposterior axis, resembling phenotypes of mutants with reduced Nodal signaling. Indeed, expression levels of the Activin/Nodal target genes *Gsc* (*Goosecoid*) and *Xbra* (*Xenopus Brachyury*) were strongly reduced in these embryos. In addition, knockdown of PR55δ leads to *Xenopus* embryos resembling embryos with increased Activin/Nodal signaling. Batut *et al.* (2008) further suggested that PR55α enhances TGFβ/Activin/Nodal signaling by stabilizing the basal level of the type I receptors,

ALK4 and ALK5, whereas PR55δ played a negative role in these pathways by restricting receptor activity. However, the mechanisms behind these effects have not been elucidated.

Since a reduction of Nodal targets in mouse embryos lacking *Ppp2r1a* was observed, it is possible that PPP2R1A is required for positive regulation of Nodal signaling mediated by PR55α by stabilizing basal levels of type I TGFβ receptors, as has been shown in *Xenopus*. An interaction of PPP2R1A (PR65α) has been shown for both PR55α (PPP2R2A) and PR55δ (PPP2R2D) in the mass spectrometry approach (Table 1). The spatiotemporal expression of these subunits during early embryogenesis and whether type I receptors are destabilized or their receptor activities affected in t^{w18} embryos requires further investigation.

As discussed above, the PR55α subunit has been shown to positively regulate, Wnt and Nodal signaling pathways that both are dysregulated in loss of *Ppp2r1a* embryos. Therefore, it is tempting to speculate that disruption of assembly of a PP2A holoenzyme containing the Aα scaffolding subunit (PPP2R1A) and the B PR55α subunit might be the cause for defects in these embryos.

For evaluation of the mass spectrometry data, it has to be considered that this *in vitro* system might not be the optimal approach for analyzing *Ppp2r1a* function during embryogenesis. The tagged protein is expressed from a BAC transgene, while another untagged, endogenous copy of *Ppp2r1a* is still present in t^{w18}/+ ESCs. The endogenous protein is therefore able to compete with the SH-tagged PPP2R1A for interacting proteins. This might reduce the probability of detecting low-frequency interactions. It cannot be ruled out that the tag might also alter the binding affinities for certain interactors. Thus, the mass spectrometry data do not necessarily reflect the full set of proteins that PPP2R1A interacts with *in vivo*. It is also surprising that no differences between differentiated and undifferentiated cells were observed. We expected to find changes in the PPP2R1A interaction network that might reflect specific functions during the differentiation process and that correspond to functions

during embryogenesis. It is therefore not clear whether the findings from the *in vitro* approach can be used to fully interpret PPP2R1A's *in vivo* function.

In the mass spectrometry experiments, different protein classes were revealed to be in complex with tagged PPP2R1A (Table 1). As expected, different PP2A subunits were co-purified, including catalytic and B regulatory subunits. As discussed above, some of these subunits have been shown to regulate developmentally important signaling cascades. Apart from PP2A subunits, the only other interaction partner uncovered that is potentially relevant during embryogenesis, was Integrator subunit 6 (INTS6). INTS6 is part of the integrator complex and has been shown to be required for dorsoventral patterning in zebrafish embryos by restricting dorsal organizer gene expression (Kapp *et al.*, 2013). The Integrator complex consists of 13 subunits and is associates with the C-terminal repeat of the largest subunit of RNA polymerase II. It is implicated to function in 3'-end processing of small nuclear RNAs (snRNAs), which are components of the spliceosome functioning in pre-mRNA processing (reviewed in Jurica and Moore, 2003). Neither the specific role of INTS6 in the integrator complex, nor the impact of its loss-of-function on snRNA biogenesis and on splicing, are yet known. Dorsoventral patterning defects in the *Ints6* mutant can be rescued by suppression of Nodal signaling or activation of BMP signaling, ruling out global defects in snRNA processing and in splicing (Kapp *et al.*, 2013). It seems more likely that splicing of single developmentally important genes is affected in mutant embryos. The underlying molecular mechanism, genes affected, as well as PP2A function in this process are, however, unclear.

The reduction of mesendodermal marker gene expression observed in t^{w18} is most likely caused by dysregulation of Wnt and Nodal signaling. In addition, the mutants showed a downregulation of genes like *Nanog*, *Oct4* or *Sox2*, suggesting a loss of pluripotency in the epiblast. In $Nodal^{-/-}$ embryos the expression of *Sox1* and *Six3* is upregulated indicating a precocious neural differentiation (Camus *et al.*, 2006). These early, general neural markers were unaffected in t^{w18} embryos, though *Emx2*,

a dorsal forebrain marker, that is not expressed in *Nodal*$^{-/-}$ mutant, was upregulated. It remains to be investigated what identity epiblast cells that lack *Ppp2r1a* adopt and how exactly their lineage differentiation is affected.

5.1.2 Lack of *Ppp2r1a* might cause increased cell adhesion in the early streak

Besides dysregulation of Wnt and Nodal signaling cascades, the gene expression profile of t^{w18} embryos showed an upregulation of genes involved in regulation of cell adhesion. As discussed above, an early primitive streak is most likely initiated, but cells then fail to delaminate and become and thus stalled in that region. Under wild-type conditions, cells ingressing through the primitive streak undergo EMT mediated by downregulation of *E-cadherin* expression. EMT during gastrulation is mediated by *Snai1*, a direct repressor of *E-cadherin* (Carver *et al.*, 2001).

RNAseq data showed that *Snai1* is normally expressed in t^{w18} embryos, arguing against defective EMT. In contrast, *Eomes* is downregulated in the t^{w18} mutants. Arnold *et al.* (2008) showed that mutant lacking *Eomes* specifically in the epiblast display defects in EMT and maintenance of *E-cadherin* expression, although *Snai1* is normally expressed in these mutants. Whether *E-cadherin* is specifically downregulated in the primitive streak of t^{w18} embryos cannot be assessed from the transcriptome data of whole embryos. The gene is widely expressed in all epithelial tissues, which might mask expression changes within a small subgroup of cells. This might explain comparable expression levels in wild-type and mutant embryos. Thus, suppression of *E-cadherin* in the primitive streak should be investigated in t^{w18} embryos by other methods, such as *in situ* hybridization or immunohistochemistry.

It is conceivable that EMT does not occur in t^{w18} embryos, since *Eomes* is downregulated and, in addition, several adhesion molecules are upregulated. Stronger cell-cell adhesion would probably hinder cells from becoming mesenchymal. *Cdh13* (*T-cadherin*), a nonclassical cadherin, functions in cell adhesion by engaging in in-

tercellular recognition through a homophilic interface (Ciatto *et al.*, 2010). Indeed, it has been shown in various cancer cell lines and in mouse models that overexpression of *Cdh13* inhibits invasiveness by enhancing cell-cell association (Lee, 1998; Kuphal *et al.*, 2009), whereas *Cdh13* downregulation increases cancer invasive potential (Adachi *et al.*, 2009). Two other members of the cadherin superfamily, *Cdhr5* (*μ-protocadherin*) and *Pcdhgc3* (*Pcdhγc3*) that also were upregulated in t^{w18} embryos, have been found to induce aggregation in classical cell aggregation assays (Obata *et al.*, 1995; Goldberg *et al.*, 2000). Notably, both molecules play roles in negative regulation of canonical Wnt signaling. Overexpression of *Pcdhgc3* was able to markedly suppress Wnt reporter activity in a colon cancer cell line (Dallosso *et al.*, 2012). And CDHR5 directly interacts with β-catenin to reduce its transcriptional activity probably by preventing its nuclear translocation in colon cancer cells (Hinkel *et al.*, 2012).

Cell adhesion is mediated by interaction of cells with the extracellular matrix. The first recognizable step during EMT in gastrulation is breakdown of the basement membrane (Nakaya *et al.*, 2008). The basement membrane underlying all epithelia is primarily composed of laminins. Upregulation of several laminins and other components of the basement membrane, like *Nid1* therefore suggests that basement membrane disassembly does not occur in t^{w18}.

Both loosening of cell-cell contacts, along with breakdown of the basement membrane, are required for cells to become mesenchymal. Defects in EMT are in line with the observed phenotype of loss of *Ppp2r1a* embryos where ingressing cells become stalled in the early primitive streak. In contrast to other mutants showing defects in EMT during gastrulation, like in *Snai1*- or epiblast-specific *Eomes*-loss-of-function (Carver *et al.*, 2001; Arnold *et al.*, 2008), the embryos lacking *Ppp2r1a* fail to induce mesodermal and endodemal marker genes, like *T*, *Mixl1*, *Mesp1* and *Mesp2*. This supports the notion that the t^{w18} and *Ppp2r1a*$^{-/-}$ phenotype cannot only be due to defective EMT. Rather it is more likely to be caused by a lack of differentiation into the mesendodermal lineage combined with the persisting epithelial character

of the primitive streak cells that causes the phenotype.

5.1.3 Is *Ppp2r1a* involved in cell cycle and proliferation *in vitro* and *in vivo*?

In our laboratory we were neither able to establish a t^{w18} homozygous nor a compound t^{w18}/+;*Ppp2r1a*$^{-/-}$ ESC line. Several attempts to do so led to the conclusion that cells isolated from the ICM of homozygous mutant embryos are not able to proliferate *in vitro*. Another group was able to establish t^{w18}/t^{w18} ESC lines from preimplantation mouse embryos, but with an unexpectedly low frequency (Martin *et al.*, 1987). These results further support an impairment of *in vitro* cell proliferation.

A function of *Ppp2r1a* in cell cycle or proliferation in ESCs has also been inferred from interactome data. Mass spectrometry revealed interactions of PPP2R1A with several proteins that support a function of PP2A during the cell cycle in cultured cells. ESPL1 (Separase) and SGOL2 are involved in chromosome segregation and it has been shown that PP2A prevents precocious activation of separase and sister chromatid separation (Clift *et al.*, 2009; Hellmuth *et al.*, 2014). An *in vivo* function of *Ppp2r1a* in the cell cycle has also been demonstrated in a recent study by Hu *et al.* (2014). They showed that oocyte-specific loss of *Ppp2r1a* causes severe defects in oocyte meiotic maturation, leading to defective embryonic development. In mutant oocytes, precocious separation of sister chromatids results in aneuploidy and disturbed pronuclear formation in zygotes. Mutant embryos arrest before blastocyst stage and undergo apoptosis by E4.0, suggesting that cleavage is indepent of *Ppp2r1a*. These data demonstrate that lack of a maternal pool of *Ppp2r1a* results in cell cycle defects already before fertilization. However, t^{w18}/t^{w18} and *Ppp2r1a*$^{-/-}$ embryos develop until E6.5 without obvious morphological defects.

A phenotype comparable to t^{w18} was described for embryos lacking the PP2A catalytic subunit Cα (Götz *et al.*, 1998). The authors argued that loss of *Ppp2ca* is partially rescued by the catalytic β-subunit. The same concept is conceivable for the A

regulatory subunit. In embryos lacking *Ppp2r1a*, some aspects of its function might be fulfilled by *Ppp2r1b*. It is possible that in these mutants, maternal *Ppp2r1a* mRNA in combination with *Ppp2r1b*, ensure oocyte maturation and early embryonic development, while later embryonic *Ppp2r1a* is required for cell lineage commitment in the epiblast during gastrulation.

Snow and Bennett (1978) observed a blockage of cell division in t^{w18} homozygous embryos, further supporting that *Ppp2r1a* is required for proliferation, in addition to its role in lineage differentiation. It is thus unlikely that overgrowth of the primitive streak is caused by enhanced or maintained proliferation of primitive streak cells. Cells rather bulge into the amniotic cavity, since epiblast cells keep on ingressing into the primitive streak where they become stalled. It is therefore unlikely that a direct function of *Ppp2r1a* in proliferation is primarily causing the t^{w18} phenotype.

5.2 Severity of the t^{w18} phenotype is amplified in the 129S2/C57BL/6J background

Within the scope of this project the t^{w18} homozygous phenotype that was first described by Bennett and Dunn (1960) was reanalyzed. Bennett and Dunn report a prominent overgrowth of the primitive streak resulting in duplication of the neural tube due to excessive primitive streak material. In general, t^{w18} embryos are described as growth retarded. They fail to turn, and lethality occurs between E8.5-10.5. t^{w18} embryos generated in our laboratory were subsequently analyzed from E6.5 onwards and showed a more severe phenotype. They developmentally arrested at the egg cylinder stage without forming a head process or any mesodermal structures. Consistent with the study from 1960, a prominent overgrowth of the primitive streak was detected at E7.5 that produced a bulge of cells extending into the amniotic cavity. A gastrulation failure was further supported by the absence of mesodermal marker gene expression, like *T* or *Tbx6*. Mutant embryos could be

recovered until E10.5 as undifferentiated and degenerating balls of cells. Contrary to Bennett and Dunn, t^{w18} homozygous embryos never reached the morphology of E8.5 in our hands.

These differences can most likely be explained by different genetic backgrounds of t^{w18}/+ mice used for breedings. In our laboratory, t^{w18}/+ animals were kept on a 129S2-background. The embryos described in this study were either obtained from breedings between t^{w18} heterozygotes with a pure 129S2-background or a mixed 129S2/C57BL/6J-background. Heterozygous t^{w18} mice with a mixed 129S2/C57BL/6J-background were produced by mating t^{w18}/+ animals with wild-type C57BL/6J animals. Heterozygous offspring from these breedings were then intercrossed to obtain homozygous embryos. In contrast, the animals analyzed by Bennett and Dunn (1960) were obtained from the offspring of a wild animal. The genetic backgrounds of the animals analyzed are therefore not entirely comparable.

It is well-established that phenotypic variability in the mouse is influenced by the genetic background of mutant animals. Several studies have showed that different mouse strains can produce completely distinct phenotypes, variable penetrance or severity of a phenotype. For example, it has been reported that keratin 8-deficiency results in different phenotypes ranging from mid-gestational lethality or colorectal hyperplasia and inflammation, depending on the genetic background (Baribault *et al.*, 1993, 1994). Furthermore, Threadgill *et al.* (1995) showed that phenotypes caused by disruption of the *Egfr* (epidermal growth factor receptor) locus range from peri-implantation to mid-gestation or postnatal lethality. These examples support the idea that variability in the t^{w18} phenotype might be caused by differences in genetic background of mouse strains.

6 Material and Methods

6.1 Standard molecular biology methods

If not mentioned differently, molecular standard procedures were carried out according to established protocols Sambrook and Russel (2001).

6.2 Nucleic acid methods

6.2.1 DNA sequences

Plasmids and BACs

Plasmids and BACs used for this work are listed in Table 4.

Table 4. DNA constructs.

Construct	Function/Purpose	Source/Reference
RPCI-23-209P21	*Ppp2r1a* BAC	Osoegawa *et al.*, 2000
PRPGS00108_A_B03	*Ppp2r1a* knockout targeting vector	KOMP Repository Austin *et al.*, 2004
T::H2BmCherry BAC	*T* reporter BAC	Dr. Frederic Koch
pTO-SH-GW	cloning of SH-tag	Dr. Matthias Gstaiger
pR6K(neo)	cloning of SH-tag with *neo* into *Ppp2r1a* BAC	Dr. Phillip Grote

Oligonucleotides

Primer sequences used for cloning, genotyping or qPCR are listed in Table 5. Oligonucleotides were synthesized by LifeTechnology or Sigma-Aldrich. Lyophilized primers were resuspended in water to a concentration of 100 µM and stored at -20°C.

In situ hybridization probes

T and *Tbx6 in situ* hybridization probes were provided by the MAMEP database. Sequence information can be obtained from http://mamep.molgen.mpg.de. *Ppp2r1a* probe was synthesized as described in section 6.2.5 with primers listed in Table 5.

Southern probes

Southern probes were generated with primers listed in Table 5 from genomic DNA. Genome sequence information were extracted from the *Mus musculus* genome assembly mm10 (GRCm38).

Table 5. Primer sequences

Primer Name	Sequence	Function/Purpose
Vil2s	TCATGGACCAACACAAGCTC	t^{w18} genotyping
Vil2as	CACAAAACTGAAATCTCCCTC	
genoPpp2r1a_F1	GCAGGAGCTGGAGCATGCCA	*Ppp2r1a*$^{-}$ genotyping
genoPpp2r1a_R1	TGCAGCACAGGATGTTCAGTGGA	
genoPpp2r1a_R2	GGAGAGGGACCTGGCTCCTATG	
geno_Rescue-Ppp2r1a_F1	TTTTGCTGCTGTAATGGGGACC	Tg(*Ppp2r1a* BAC) genotyping
geno_Rescue-Ppp2r1a_R1	GCTAAAGCGCATGCTCCAGA	
18.5Mb_F1	AGTCCGAGGCCACGTCCTTGA	t^{w18} deletion mapping
18.5Mb_R1	GCTGCAGTTGCTGTGCTGGC	
18.6Mb_F1	GGCCTTCCATTCGGTCCTGGG	
18.6Mb_R1	AGGAGTGCTGTGCTGGACGC	
18.7Mb_F1	TCTTCCCCAGAGGACCCGGC	
18.7Mb_R1	GCAGCTGCAGTGGTGGGCAG	
19.1Mb_F1	GCCAACCTGAGAACGCGCTG	
19.1Mb_R1	AGGGAAATGCCTGGGGCAGGA	

Primer Name	Sequence	Function/Purpose
19.2Mb_F1	GCCGGCCAGCAGCTCACATA	
19.2Mb_R1	GGCAGCGTGCCCCACTGAAT	
19.3Mb_F1	CCCCGGCATATCCTGCGTAGATGA	
19.3Mb_R1	GGGTGATGGGCGAGCAACAAATCA	
19.4Mb_F1	AGCCCCATGCCCAGCGACTA	
19.4Mb_R1	AGTGGCTGTCTGGCCCACCA	
Ppp2r1a_3′Sonde_F	GCAGCCCTGAGATGCCCTGC	*Ppp2r1a* Southern probes
Ppp2r1a_3′Sonde_R	TGGCGCACTTCTCCCAGTACCT	
Ppp2r1a_5′Sonde_F	AGGGCTGCTGCTCACTGCTC	
Ppp2r1a_5′Sonde_R	ACGCTCTCCCCACCCCTAAGC	
Ppp2r1a_ISH_F1	ACTGTGAGGCCGAGGTGAGGG	*Ppp2r1a* antisense WISH probe
Ppp2r1a+T7_ISH_R1	TAATACGACTCACTATAGGGTGGACACCAGAGGCC GGCAA	
Ppp2r1a_qPCR_F1	CCACCAAGCACATGCTGCCC	*Ppp2r1a* qPCR
Ppp2r1a_qPCR_R1	TCCACATCCTGGTCCTGGGTCA	
T_qPCR_F	CAATGGAGGGGGACAGATCAT	*T* qPCR

Primer Name	Sequence	Function/Purpose
T_qPCR_R	CTGGTGATCATGCGTTGCG	
Pmm2 qPCR fwd	agggaaaggcctcacgttct	*Pmm2* qPCR
Pmm2 qPCR rev	aataccgcttatcccatccttca	
Hmbs_qPCR_F		*Hmbs* qPCR
Hmbs_qPCR_R		
rec pBAC.Ppp2r1a+neo_F1	TTTATTCCTTTCCCTACTGTACACGGAGAAATAAA	
	GGTGTAGAAATACTTGAAGTTCCTATTCTCTAGAA	recombineering neo
rec BAC.Ppp2r1a+neo_R1	AAGCCACAAGGCAGTGGGCTTTCCTCCATTCCGAT	*Ppp2r1a* BAC
	TACTAAGACTAGAGAATTATGTACCTGACTGATGA	
rec pBAC+Ppp2r1a(neo first)_F2	ATGTAAACATGGCTACAGGATTGGGTCGTGTTACC	
	ATGGGGGTCAAAGCTATCCTTCTATAGTGTCACCT	recombineering *Ppp2r1a(neo)*
rec-pBAC-Ppp2r1a_R1	GAGAGGGTGACCCCCAGTGATCCTTTCCCACTGAG	locus in BAC backbone
	GCCAGACAAGGCATCCTCTCCCTATAGTGAGTCGT	
NotI-SH_F	aaaaaGCGGCCGCatgtacccatacgatgttcc	cloning SH-tag in pR6K(neo)
SH+Stop-MluI_R	tttttACGCGTAAGtcaatcggccgctttttcgaact	

Primer Name	Sequence	Function/Purpose
Rec_P21+SH(neo)_F1	GTGTGGTTCTGAGGCGTATTGTTCTTGTTTCCCCAG TTCTCTCTCTTGCCatgtacccatacgatgttcc	recombineering SH(neo) in
Rec_P21+SH(neo)_R1	CAAGGCAGTGGGCTTTCCTCCATTCCGATTACTAA GACTAGAGAACCAAGATTATGTACCTGACTGATGA	*Ppp2r1a* BAC

6.2.2 Molecular cloning

Polymerase chain reaction (PCR)

The amplification of DNA fragments for cloning or recombineering was performed using the PrimeSTAR® HS DNA polymerase kit (Takara Bio Inc.) or the Expand Long Template PCR system (Roche) according to the manufacturer's instructions in a thermal cycler (Mastercycler®, Eppendorf). If necessary 1 M Betaine (Sigma-Aldrich) or 5% DMSO (v/v) were added to the reaction to improve the amplification result.

Agarose gel electrophoresis

DNA or RNA fragments were size separated by agarose gel electrophoresis. 0.6-2% agarose (w/v) were dissolved in TEA buffer (Table 19) by heating, EtBr (0.2-0.5 µg/ml, Sigma-Aldrich) was added and the agarose was poured into a cast, where polymerization occurred. Electrophoresis was performed in TEA buffer at 70-120 V.

DNA extraction from agarose gels

DNA bands were cut out of the gel and fragments were purified using the Wizard® SV Gel and PCR Clean-Up system (Promega) according to the manufacturer's protocol.

DNA Quantification

DNA was quantified using the NanoPhotometer® (Implen). If lower DNA concentrations had to bee meassured the Qubit® dsDNA BR assay kit (Life Technologies) in combination with the Qubit® 1.0 fluorometer (Life Technologies) was used according to the manufacturer's instructions.

Ligation of DNA fragment

DNA fragments were ligated using the Quick Ligation™ Kit (NEB) or T4 DNA ligase (Promega) according to the to the manufacturer's instructions.

Cultivation and chemical transformation of *E. coli*

Bacteria were cultured depending on the required conditions in liquid LB medium (1% Bacto-tryptone, 0.5% Yeast extract, 1% NaCl; pH 7.0) or low-salt LB medium (1% Bacto-tryptone, 0.5% Yeast extract, 0.5% NaCl; pH 8.0) or on (low-salt) LB agar plates ((low-salt) LB, 1.5% agar) with the required antibiotic(s) (Table 6). For chemical

Table 6. Used concentrations of antibiotics in LB (liquid) or LB agar.

Antibiotic	Concentration
Ampicillin	100 µg/ml
Kanamycin	30 µg/ml
Chloramphenicol	30 µg/ml
Tetracycline	10 µg/ml

transformation competent bacteria were thawed on ice, carefully combined with the DNA construct, incubated on ice for 10 min and 45 s at 42°C. After the heat shock bacteria were incubated on ice for 1 min, 500 µl LB medium were added and the transformation was agitated at 37°C (or 30°C if necessary) for 20-60 min and plated on (low-salt) LB agar plates with the required antibiotic and cultured overnight at 37°C or 30°C.

Small-scale plasmid and BAC preparation

For analytical purposes plasmid or BAC DNA were isolated from 2 ml bacterial overnight cultures using buffers of QIAprep Miniprep Kit (Qiagen) with the following modifications of the protocol. The bacteria pellet was resuspended in 250 µl P1 buffer and cells were lysed by the addition of 250 µl P2 buffer. The lysis was neutral-

ized with 350 µl N3 buffer. To remove cell debris the lysate was centrifuged for 10 min at 16.000 x g. The supernatant was transferred into a new 1.5 ml tube and DNA was precipitated by the addition of 600 µl Isopropanol followed by 10 min incubation at RT and 10 min centrifugation at 16.000 x g. The DNA pellet was washed with 70% EtOH. Afterwards the dried pellet was resuspended in 50 µl EB (Qiagen). To screen plasmids for correct cloning events DNA samples were digested with restriction enzymes and DNA fragments were separated by agarose gel electrophoresis and analyzed for correct sizes.

Large-scale plasmid and BAC preparation

To obtain large amounts of high quality plasmid DNA the Qiagen Plasmid Midi or Maxi Kits were used according to the supplied protocols. For the preparation of large quantities of BAC DNA the NucleoBond BAC100 Kit (Macherey-Nagel) was used according to the manufacturer's instructions with the following modifications of the protocol. After DNA precipitation with isopropanol as much isopropanol as possible was removed from the DNA pellet. The pellet was carefully resuspended with 270 µl H_2O and transferred in a 1.5 ml tube with a wide bore pipette tip. The DNA was the precipitated again with 700 µl EtOH and 30 µl 3 M sodium acetate (pH 5.2). After centrifugation for 30 min at 4°C, 16.000 x g the DNA pellet was washed with 70 % EtOH, dried and dissolved in 100 µl TE.

Red/ET recombineering

To recombine PCR products with BACs or plasmids bacteria containing the recombination target and the pSC101-BAD-gbaA(tet) plasmid were grown in the appropriate LB medium overnight at 30°C. On the next day 1.4 ml medium were inoculated with 30 µl of the bacteria culture and cultured for 2 h at 30°C. Expression of enzymes necessary for recombineering was induced by adding 30 µl of 10 % L-arabinose and agitation for 1 h at 37°C. Induced and control Bacteria were made

electrocompetent by washing with ice-cold water. Therefore, cells were centrifuged for 30 s at 9.300 x g and 4°C, the supernatant was discarded and bacteria were carefully resuspended in 1 ml ice-cold cell culture-grade H_2O. Washing was repeated twice and the pelleted bacteria were resuspended in the remaining fluid after discarding the supernatant from the last centrifugation step. Then gel purified PCR product (300-600 ng) was added to the bacteria and the mixture was transferred in a pre-cooled electroporation cuvette (Gene Pulser Cuvette, 0.1 cm gap, Bio-Rad). Electroporation was performed under the following conditions: 200 Ω, 1800 V, 250 µF. After electroporation 500 µl fresh medium were added and the bacteria were cultured for 1 h at 37°C. Afterwards the bacteria were plated on (low-salt) LB-agar plates containing the minimal concentration of the required selection marker (Table 7).

Table 7. Minimal concentrations of antibiotics in (low-salt) LB-agar plates.

Antibiotic	Concentration
Ampicillin	50 µg/ml
Kanamycin	10µg/ml

Sequencing

Plasmids or purified PCR products were sequenced by the Eurofins Genomics DNA sequencing service in value read tube format. Samples were prepared according to the specified requirements.

6.2.3 Southern blot analysis of ES cell clones

In order to screen ES cell clones for successful integration of electroplated constructs (see section 6.5.3) Southern analysis was performed. ES cells were grown in 96-well plates. When colonies grew to near confluence cells were washed twice with PBS and 50 µl Laird's buffer (100 mM Tris pH 8.3, 5 mM EDTA, 0.20% SDS,

200 mM NaCl) with 1:100 freshly added Proteinase K (> 800 U/ml, Sigma-Aldrich) were added to each well. The cell lysis occurred during overnight incubation of the plates at 37°C in a humid chamber. For DNA precipitation 100 µl ice-cold 75 mM NaCl/100% EtOH was added to the lysate and incubated at RT for 30 min. The DNA will precipitate as a filamentous network on the bottom of the wells. To discard the solution the plates were carefully inverted and remaining fluid on the edges of the plate were blotted onto paper towels. Then the plates were washed with 200 µl 70% EtOH per well which again was discarded by inverting the plates. After the last wash the DNA dried on the bench with removing the lid from the plates. It was important not to let over dry the DNA to be able to again get it in solution. When DNA was dried 25 µl 0.1 x TE buffer were added and the DNA was dissolved overnight at 37°C in a humid chamber. For each 96-well plate of ES cell clones two replica plates for DNA isolation were prepared. One of these DNA plates was used for restriction digest followed by Southern blot whereas the second replica plate was stored either already after cell lysis at -20°C or after DNA preparation at 4°C.

For the Southern blot analyses the DNA was digested with restriction enzymes that are suitable for cleaving genomic DNA. The restriction digest occurred in the 96-well plates in an end volume of 30 µl per well containing 25 µl DNA and 5 µl of a master mix that was added to each well. The master mix comprised the components listed in Table 8. The plates were incubated overnight at 37°C in a humid chamber. Digested DNA was separated by agarose gel electrophoresis in a 0.6% agarose/TAE

Table 8. Restriction digest for Southern blot analysis.

Master mix components	Supplier
1 x restriction buffer	Promega/NEB
1 mM spermidine	
100 µg/ml RNaseA	Thermo Scientific
100 µg/ml BSA	Promega/NEB
30-50 U restriction enzyme	Promega/NEB
H_2O	

(40 mM Tris-acetate, 1 mM EDTA, pH 8.2-8.4) (w/v) gel containing EtBr (0.2-0.5 µg/ml, Sigma-Aldrich). 6 µl 6 x orange G loading dye (Table 19) were added to the restriction digest per well and the samples loaded on the gel. Electrophoresis was performed at 60-80 V for 3-5 h until DNA fragments were sufficiently separated. The the gel was documented with the GelDoc™ (Bio-Rad). For transfer of the DNA to a membrane the gel was incubated in 0.25 N HCl twice for 10 min, in H_2O for 5 min and in 0.5 N NaOH for 40 min. During the incubation the gel was gently shaken. The DNA was then blotted overnight onto a pre-equilibrated nylon Zeta-Probe® membrane (Bio-Rad) by capillary transfer. On the next day, the DNA was UV-crosslinked to the membrane using a Stratalinker 2400 (Stratagene) with 5000 µJ/cm^2 radiation. The membrane was then washed twice with 2 x SSC and either dried and stored at RT or directly used for hybridization. To hybridize the membrane with a radioactively labeled probe the membrane was pre-hybridized with ExpressHyb™ hybridization buffer (Clontech) for at least 30 min at 65-68°C. Meanwhile the DNA probe was radioactively labeled with [α-^{32}P]dCTP (3000 Ci/mmol, Hartmann Analytic) using the Rediprime II DNA labeling system (Amersham) according to the manufacturer's instructions. After the labeling the probe was purified using illustra™ ProbeQuant G-50 micro columns (GE Healthcare) according to the manufacturer's protocol. The purified probe was added to ExpressHyb solution and the membrane was hybridized overnight at 65-68°C. On the next day, the membrane washed twice for 20 min with 2 x SSC/0.1% SDS and with 0.2 x SSC/0.1% SDS and the bound probe was visualized by autoradiography on X-ray films (BioMax MS, Kodak). If necessary the membrane was stripped by heating at 95°C in 0.1 x SSC/0.1% SDS for 20 min.

6.2.4 Genotyping of mouse material or ES cell lines

Mice were genotyped from tail or ear biopsy material. Therefore, the tissue was lysed in 300 µl Laird's buffer (100 mM Tris pH 8.3, 5 mM EDTA, 0.20% SDS, 200 mM

NaCl) with 1:100 freshly added Proteinase K (> 800 U/ml, Sigma-Aldrich) at 56°C. The lysate was centrifuged for 5 min at 16.000 x g to remove hair. The supernatant of the lysate was transferred into a new 1.5 ml tube and the DNA was precipitated with 1 ml EtOH. After centrifugation (5 min, 16.000 x g) the pelleted DNA was washed with 70% EtOH. The dried DNA pellet was resuspended in 200 µl TE (Table 19).

Cells were lysed for genotyping in an appropriate of volume Laird's buffer (see above, 500 µl for 1 well of 48 well plate or 500 µl for 1 x 6 cm dish). DNA was extracted as described above. The purified DNA was used for PCR analysis. Therefore, the GoTaq® Flexi DNA polymerase (Promega) was used with the following reaction (Table 9). The following standard PCR program was applied: 94°C for 2 min; 35x 94°C for 30s, 60°C for 35s, 72°C for 30s; 72°C for 2min.

Table 9. Genotyping PCR

Component	Final Volume	Final Concentration
DNA	2 µl	<250 ng
5 x Green GoTaq® Flexi buffer	5 µl	1 x
$MgCl_2$ (25 mM)	3 µl	3 mM
dNTP (10 mM each)	0.5 µl	0.2 mM each
Primer mix 10 µM each)	0.5 µl	0.2 µM each
GoTaq® DNA polymerase (5 U/µl)	0.13 µl	0.65 U
H_2O	13.87 µl	

Material from mouse embryos was either lysed with Laird's buffer as described above or using the REDExtract-N-Amp™ Tissue PCR Kit (Sigma-Aldrich) according to the supplied manual. Primers used for genotyping different mouse lines, embryos or cells are depicted in Table 5.

6.2.5 RNA probe synthesis for WISH

To synthesize RNA probes for *in situ* hybridization (section 6.4.1) template DNA was amplified with primers containing RNA polymerase specific promotor sequences

(Table 5). PCR products are directly used for the *in vitro* transcription reaction depicted in Table 10.

Table 10. *In vitro* transcription reaction

Component	Final Volume	Final Concentration
PCR product	9 µl	
10 x transcription buffer TRB	3 µl	1 x
ACG nucleotides (4 mM each) (Roche)	3 µl	0.4 mM each
digUTP-UTP mix (4 mM) (Roche)	0.75 µl	0.1 mM
200 mM DTT	1.5 µl	10 mM
RNA polymerase (20 U/µl) (Promega)	1.5 µl	30 U
RNase inhibitor (30 U/µl) (Peqlab)	1 µl	30 U
RNase-free H_2O	10.25 µl	

The reaction was incubated at 37°C for T7 and T3 polymerases and at 40°C for SP6 polymerase. After 2.5 h 3 µl of RNaes-free DNaseI (10 U/µl, Roche) were added and the reaction was incuated for another 15 min at 37°C. Then 1.2 µl glycogen (Peqlab) and 12 µl 10M ammonium acetate were added and the reaction was mixed. Tp precipitate the RNA 150 µl ice-cold EtOH were added, the tubes were inverted and centrifuged for 30 min (4°C, 16.000 x g). The supernatant was discarded, 150 µl ice-cold 70% EtOH were added and the tube was centrifuged for 10 min (4°C, 16.000 x g). The supernatant was discarded and the air-dried pellet was resuspended in 100 µl RNase-free H_2O. To estimate the amount of probe necessary for WISH and the RNA quality, 5 µl of the probe were separated by agarose gel electrophoresis.

6.2.6 RNA extraction

RNA was extracted from cells or embryo tissues using the RNeasy Mini or Micro Kits (Qiagen) depending on the amount of starting material. If purification of RNA and DNA from the same sample was necessary the AllPrep Mini Kit (Qiagen) was used. The starting material was lysed in 350 µl RLT (Plus) containing 143 mM β-mercaptoethanol. The sample was homogenized by either vortexing or by pass-

ing through a needle attached to a syringe. RNA (and DNA) was then extracted following the kits protocol.

6.2.7 cDNA synthesis and quantitative realtime PCR (qPCR)

cDNA was synthesized from total RNA using the QuantiTect® Reverse Transcription Kit (Qiagen) according to the supplied protocol. qPCR was performed using the GoTaq® qPCR Master Mix (Promega) according to the manufacturer's protocol. qPCR oligonucleotides are listed in Table 5.

6.2.8 Gene expression profiling

Embryo dissection

Embryos from t^{w18}/+ intercrosses were dissected at E6.5 in cold PBS. Using a tungsten needle embryos were separated in an embryonic part (epiblast and overlying VE) for RNA-seq and an extraembryonic part for genotyping. Embryonic parts were separately transferred in 350 µl RLT buffer (+β-me, Qaigen) and stored at -80°C until RNA was isolated. Extraembryonic parts kept separately for t^{w18} genotyping using the REDExtract-N-Amp™ Tissue PCR Kit (Sigma-Aldrich). Volumes of the buffers were scaled down to 10% of the volumes indicated in the manufacturer's specification, otherwise the provided protocol was followed for DNA extraction. Following genotyping epiblast samples were combined according to their genotypes (11 x +/+, 9 x t^{w18}/t^{w18}, 10 x t^{w18}/+).

RNA isolation and library preparation

Total RNA was isolated from pooled samples as indicated in section 6.2.6 and quantified using the Qubit® RNA HS assay kit (Life Technologies) in combination with the Qubit® 1.0 fluorometer (Life Technologies). RNA quality was estimated using the Bioanalyzer 2001system (Agilent) according to the manufacturer's proto-

col. The TotalScript^{TM} RNA-Seq KIT (epicenter) was used for cDNA synthesis and library preparation. Reaction volumes indicated in the manual were adjusted to avoid waste of excessive cDNA sample synthesized. Therefore, the cDNA synthesis protocol was modified as follows. Steps not described were executed following the provided manual.

11.3 µl total RNA (5 ng)

1.95 µl TotalScript optimized buffer

0.78 µl random hexamer primer

were combined to a total volume of 14 µl.

To the 14 µl reaction the following components were added for 1st strand cDNA synthesis:

1.95 µl DTT

0.39 µl dNTPs

0.78 µl RiboGuard RNase inhibitor

0.78 µl actinomycin D (250 ng/µl)

0.78 µl EpiScript reverse transcriptase.

For second strand synthesis the 18.7 µl reaction was mixed with:

0.78 µl DTT

19.5 µl 2nd strand master mix

to a total volume of 39 µl.

The complete 39 µl cDNA synthesized were used for library preparation. Tagmentation procedure, purification of the reaction and oligo replacement were performed as described in the manual. For PCR amplification 24 µl purified reaction was combined with:

1 µl TotalScript PCR primer cocktail

25 µl 2 x phusion high-fidelity PCR master mix

and 14 PCR cycles were performed. For the last purification step, 45 µl AMPure beads were added to the 50 µ PCR reaction. Following purification the sample was

eluted in 20 µl H_2O, transferred into a fresh tube and stored at -20°C until sequencing. Quality and concentration cDNA libraries were verified using the Bioanalyzer 2100 system with a high sensitivity DNA chip (Agilent) and the Qubit® dsDNA BR assay kit (Life Technologies) in combination with the Qubit® 1.0 fluorometer (Life Technologies).

Next generation sequencing and data analyses

The sequencing was performed by the NGS core facility (Bernd Timmermann, MPIMG) using the Illumina HiSeq 2500 (High Output) system for 50 bp paired end reads. Bioinformatic raw data analyses were performed by Jinhua Liu (MPIMG). The sequencing reads were mapped to the mouse genome mm10 (GRCm38) using TopHat v2.0.8b and Cuffdiff was used to calculate normalized FPKM (fragments per kilobase of transcript per million mapped reads). Heatmaps of differentially expressed genes and PCC were generated by Jinhua Liu using the R program (http://www.r-project.org). GO terms of differentially expressed genes were analyzed using the Ontologizer tool (http://compbio.charite.de/contao/index.php/ontologizer2.html).

6.2.9 t^{w18} deletion mapping by next generation sequencing

t^{w18}/+ genomic DNA sample from ESCs was prepared by Jürgen Willert and Dr. Hermann Bauer (MPIMG). t^{w18}/t^{w18} genomic DNA was isolated from embryos genotyped homozygous for the t^{w18} allele from t^{w18}/+ mouse intercrosses. Sequencing was performed by the NGS core facility (Bernd Timmermann, MPIMG) using the Illumina HiSeq 2000 system (shotgun sequencing) for 36 bp single reads. Bioinformatic data analyses were performed by Dr. Martin Werber (MPIMG).

6.3 Protein methods

6.3.1 One-step affinity purification

In order to purify Strep/HA-tagged PR65, cells that expressed the tagged protein were grown on the desired plate format. For one Strep pulldown at least 10^7 cells were needed, therefore cells were harvested from 10 cm dishes. Cells were harvested by trypsinization, counted and the cell pellet washed with PBS, transferred in a 2 ml tube and washed with PBS. The cell pellet was either frozen in dry ice and stored at -20°C or directly used for pulldown. To proceed with purification of Strep-tagged proteins, the cell pellet was resuspended in HNN lysis buffer (Table 11) and incubated on ice for 10 min. The cell lysate was cleared from cell debris by centrifugation (16.000 x g, 4°C, 20 min).

Table 11. Buffers for One-step affinity purification

Buffer	Composition
HNN buffer	50 mM HEPES; pH 7.5, 150 mM NaCl, 50 mM NaF (Sigma-Aldrich)
HNN lysis buffer	HNN buffer, 0.5% NP-40, 200 µM Na_3VO_4 (Sigma-Aldrich), 1 mM PMSF, 1 x complete protease inhibitor (Roche), 10 µg/ml avidin (iba)

Meanwhile, Bio-Spin® chromatography columns (Bio-Rad) were prepared by adding 250 µl HNN lysis buffer. 200 µl Strep-Tactin® Sepharose® 50% suspension (iba) were equilibrated in 750 µl HNN lysis buffer and added to the column. After taking an aliquot (20-50 µl) of the cleared lysate (= input sample for Western bot) the lysate was loaded to the column. Thereby, the flow through was kept for Western blot analysis. The beads were washed twice with 1 ml HNN lysis buffer and three times with HNN buffer. Afterwards, the purified proteins were eluted with 3 x 200 µl 0.5 mM biotin (Alfa Aesar)/HNN buffer. Previous to freezing on dry ice and storage at -80°C, from each of the three eluates aliquots were taken for

Western blot (20 µl). Success of the purification was checked by SDS PAGE followed by Western blot (see 6.3.3).

6.3.2 Protein quantification

Proteins were quantified using the Qubit® protein assay kit (Life Technologies) in combination with the Qubit® 1.0 fluorometer (Life Technologies) according to the manufacturer's instructions.

6.3.3 Western blot analysis

In order to analyze proteins samples by Western blot, proteins were separated by SDS PAGE. Therefore, NuPAGE® LDS sample buffer (4x, Life Technologies) and 50 mM DTT were added to protein samples and proteins were denatured by heating to 95°C for 5 min. Samples were then loaded on NuPAGE® Novex® 10% Bis-Tris protein gels (Life Technologies) and electrophoresis was performed in a XCell SureLock™ mini-cell chamber (Life Technologies) with NuPAGE® MOPS SDS running buffer (Life Technologies) at 100-150 V. When proteins were sufficiently separated, which was directly observed by using the SeeBlue® Plus2 pre-stained protein standard (Life Technologies), the gel was used for Western transfer. Western blotting was performed using iBlot™ transfer stack, PVDF mini (Life Technologies) in combination with the iBlot® gel transfer device (programm 03, 8 min transfer, Life Technologies). After disassembling the blot, the membrane was blocked with 5% skim milk/TBST for 30-60 min at RT and incubated with primary antibody (Table 12) overnight at 4°C.

On the next day, the membrane was washed three times with TBST for 7-10 min and incubated with secondary antibody coupled to HRP (Table 12) for 60-90 min at RT. The the membrane was washed again with TBST (3 x 7-10 min). Proteins were visualized with ECL Western blotting detection reagent (GE Healthcare) in

Table 12. Primary and secondary antibodies used for Western blot.

Antibody	Dilution	Supplier/Reference
α-Ppp2r1a [6F9]	1:1000 in 5% skim milk/TBST	Abcam
α-HA [Y-11]	1:2000 in 5% skim milk/TBST	Santa Cruz Biotech
α-T	1:4.000 in 5% skim milk/TBST	Kispert and Herrmann (1993)
α-rat-HRP	1:2000 in 5% skim milk/TBST	Cell Signaling Technology
α-rabbit-HRP	1:2000 in 5% skim milk/TBST	Cell Signaling Technology
α-goat-HRP	1:10.000 in 5% skim milk/TBST	Santa Cruz Biotechnology

combination with the FusionSL chemiluminescence detection system (Peqlab).

6.4 Embryo analyses and Histology

6.4.1 Whole-mount in situ hybridization (WISH)

All incubations during the WISH procedure were performed in 2 ml screw cap tubes with rotation or gentle shaking and with RNase-free solutions. Mouse embryos were dissected in cold PBS on the desired embryonic day and fixed overnight at 4°C in 4% PFA/PBS (w/v). On the next day embryos were washed twice for 5 min with PBST (PBS/0.1% Tween-20 (v/v)) and dehydrated by a MeOH series (25%, 50%, 75%, 100% MeOH/PBST (v/v), each 5-15 min) at 4°C. Embryos were then either stored in 100% MeOH at -20°C or directly further processed. To proceed, embryos were rehydrated by a reversed MeOH series (75%, 50%, 25% MeOH/PBST (v/v), each 5-15 min), washed twice for 5-10 min in PBST and bleached in 6% H_2O_2/PBST (v/v) for 30-45 min at 4°C. Then embryos were washed again for 3 times 5-10 min in PBST at 4°C. In order to improve penetration of the probe into the tissue embryos were shortly incubated in 10 µg/ml proteinase K/PBST at RT (3 min for E6.5, 5 min for E7.5-8.5, 8 min for E9.5). The proteinase K digest was stopped by a 5 min incubation in 2 mg/ml Glycine/PBST. Afterwards embryos were washed twice for 5 min, refixed for 20 min at 4°C in 0.2% glutaraldehyde/4% PFA/PBS (v/v) and

washed again twice for 5-10 min in PBST. Embryos were then either stored in storage mix (Table 13) at -20°C or used for hybridization. To proceed with hybridization embryos were pre-hybridized in pre-warmed hybridization solution (Table 13) for at least 1 h at 68°C. Then an appropriate amount of DIG-labeled probe in hybridization solution was added to the embryos and hybridization occurred overnight at 68°C. On the next day, unbound probe was washed away by incubation in pre-warmed

Table 13. Buffers for WISH.

Buffer	Composition
Storage mix	50% formamide (v/v), 2.5 x SSC; pH 4.5
Hybridization solution	50% formamide (v/v), 5 x SSC; pH 5, 1% SDS (w/v), 50 ng/ml yeast RNA (Sigma-Aldrich), 50 ng/ml heparin (Sigma-Aldrich)
Solution 1	50% formamide (v/v), 5 x SSC; pH 4.5, 1% SDS (w/v)
Solution 3T	50% formamide (v/v), 2 x SSC; pH 4.5, 0.1% Tween-20
MABT, pH 7.5	100 mM maleic acid, 150 mM NaCl, 0.8% NaOH pellets (w/v), NaOH to adjust pH, 0.1% Tween-20
NTMT	100 mM Tris; pH 9.5, 50 mM $MgCl_2$, 100 mM NaCl, 0.1% Tween-20 (v/v)
NTT	NTMT w/o $MgCl_2$

solutions at 68°C: solution 1 twice for 30 min, solution 3T for 30 min. Then a pre-warmed mix of 50% solution 3T/MABT (v/v) was added to the embryos, they were incubated at RT until they cooled down and washed 3 times for 15 min in MABT. Previous to the antibody incubation embryos were blocked for more than 1 h at RT with 2% Boehringer blocking solution/20% FCS/MABT. Then they were incubated with α-DIG-AP Fab fragments (1:2000 (Roche) in 2% Boehringer blocking solution/20% FCS/MABT) overnight at 4°C. On the next day, embryos were washed with MABT at RT: 3 x 5 min, 1 x 15min, 2 x 30 min, then every 1 h and overnight at 4°C. IF desired it was possible to prolong MABT washing for several days. To prepare embryos for the staining they were incubated in NTMT (Table 13) at RT: 2 x 10 min, 1 x 40 min. In order to visualize AP activity embryos were transferred into

BM Purple solution (Roche) in a 12 well plate and incubated at RT. When staining was clearly visible embryos were washed 3 x 5 min with PBST, documented and stored in 4% PFA/PBST at 4°C. In case that staining was not visible within one day, embryos were stored in NTT (Table 13) at 4°C and staining was proceeded on the next day.

6.4.2 Paraffin section und H&E staining

For paraffin sections of E7.5 embryos, whole deciduae were fixed overnight at 4°C in 4%PFA/PBS. Fixed deciduae were washed three times for 5min with PBS, were transferred in 70% EtOH and incubated overnight at 4°C. Further processing for embedding was was done in a Microm STP 120 spin tissue processor (Thermo Scientific) with the following program:

1. 70% EtOH, 2:00 h, agitation 2
2. 70% EtOH, 1:50 h, agitation 2
3. 80% EtOH, 1:40 h, agitation 2
4. 90% EtOH, 2:00 h, agitation 2
5. 96% EtOH, 2:00 h, agitation 2
6. 100% EtOH, 1:00 h, agitation 2
7. 100% EtOH, 1:00 h, agitation 1
8. 100% EtOH, 1:00 h, agitation 1
9. Xylene, 1:30 h, agitation 2
10. Xylene, 1:30 h, agitation 2
11. Paraffin (56°C-58°C), 2:00 h, agitation 2
12. Paraffin (56°C-58°C), 2:00 h, agitation 1

Processed specimen was then embedded in paraffin (Surgipath Paraplast Xtra, Leica) using the Microm EC 350 Modular tissue embedding center (Thermo Scientific) and stored at 4°C until sectioning. For sectioning the rotary Microm HM355S rotary microtome (Thermo Scientific) was used to generate 4-6 µm sections. Section were

transferred onto SuperFrost® plus glas slides (Menzel-Glaeser), dried at 37°C and stored at 4°C.

For hematoxylin and eosin (H&E) staining sections on slides were incubated for 30 min at 65°C, then 3 x 5 min in Xylene to remove paraffin. Sections were then hydrated in a EtOH series: 2 x 2min 100% EtOH, 2 min 96% EtOH, 2min 90% EtOH, 2 min 80% EtOH, 2min 70% EtOH, 2 min 50% EtOH, 5 min tap water. Sections were stained for 10 min with hematoxylin solution (Mayer's, Sigma-Aldrich), then washed twice for 5 min in tap water and stained with 0.5% eosin for 5-10 s. After staining sections were washed twice for 30 s in H^2O and dehydrated by incubation in 80% EtOH for 1min, 100% EtOH for 2 x 1min, Xylene for 3 x 5 min. Sections were then mounted with Entellan™.

6.5 ES cell culture

All experimental procedures were based on protocols previously described Colowick *et al.* (1993); Robertson (1987); Nagy (2003). Cell culture work was performed under sterile conditions in a laminar flow hood (HERAsafe®, Heraeus)

6.5.1 ES cell lines

ES cells used are listed in Table 14.

Table 14. ES cell lines.

ES cell line	Background	Reference
G4	F1 hybrid of maternal 129S6/SvEvTac and paternal C57BL/6Ncr	George *et al.* (2007)
t^{w18}/+	129S6/SvEv	Hermann Bauer (MPIMG, Berlin)
5H ($T^{mCherry}$ KD4-T))	G4	Shin (2011); Vidigal *et al.* (2010)

6.5.2 Maintenance of ES cells

ES cells were cultured in ES cell medium (Table 15) on a monolayer of mitomycin C-treated feeder cells (primary embryonic fibroblasts) on gelatinized dishes (0.1% gelatine (v/v), Sigma-Aldrich). ES cell culture was performed at 37°C in 5% CO2. The medium was exchanged daily and ES cells were split every two to three days. For splitting, ES cells were washed twice with PBS (Lonza) and incubated with trypsin-EDTA (0.5 g/l, Gibco) for 5-10 min. When cells detached from the plate trypsinization was stopped by adding ES cell medium.

Table 15. ES cell medium composition.

ES cell medium components	Supplier
KO DMEM (4.5 g/l D-glucose, sodium pyruvate)	Gibco
15% ES cell-qualified FCS (v/v)	PAN Biotech GmbH
2 mM L-glutamine	Lonza
50 U/ml penicillin/50 µg/ml streptomycin	Lonza
1 x non-essential amino acids	Gibco
0.1 µM β-mercaptoethanol	AppliChem
1 x nucleosides	EmbryoMax®, Millipore
1000 U/ml LIF	ESGRO®, Millipore

For regular freezing ES cells were pelleted (5 min, 200 x g) after harvesting by trypsinization. The cell pellet was resuspended in ES cell medium containing 20% FCS (v/v). After addition of 1 volume of 2 x ES cell freezing medium (ES cell medium containing 20% FCS (v/v) and 20% DMSO (v/v)) cell suspension was aliquoted into freezing vials. These were placed in a freezing box (Nalgene) and cooled overnight at -80°C. The next day freezing vials were stored in liquid nitrogen. To thaw ES cells the freezing vial was shortly placed in a 37°C water bath, transferred in fresh ES cell medium to dilute the DMSO and centrifuged (5 min, 200 x g). The cell pellet was resuspended with ES cell medium and plated on gelatinized dishes with feeder cells.

6.5.3 Generation of modified ES cell lines

Electroporation was the method of choice to modify the genome of ES cells. For this purpose cells cultured with feeder cells in ES cell medium were trypsinized and counted with a Luna^{TM} automated cell counter (Logos Biosystems). For each electroporation 3-10 x 10^6 cells were centrifuged (5 min, 200 x g) and resuspended in 800 µl PBS. The cell suspension was then mixed with the DNA (25µg linearized plasmid for homologous recombination or 5µg of linearized BAC DNA) and transferred in a electroporation cuvette (Gene Pulser Cuvette, 0.4 cm gap, Bio-Rad). For electroporation a Gene Pulser (Bio-Rad) was used at 240 V and 500µF. After electroporation cells were transferred in a 15 ml tube containing ES cell medium and plated on three 6 cm dishes (with drug resistant feeder cells) in different dilutions (1/6, 2/6 and 3/6 of the cell suspension). After 24-36 h selection was started with ES cell medium supplemented with the appropriate selection drug (Table 16). Selection medium was exchanged daily until resistant colonies were clearly visible (approximately 6-8 days after electroporation). Then colonies were picked and grown in 96- or 48-well dishes.

Table 16. Selection drugs.

Selection drug	Supplier	Resistant feeder cells
250 µg/ml G418 sulphate (Geneticin)	Gibco	EFN
150 µg/ml Hygromycin	Sigma-Aldrich	DR4

For picking ES cell colonies 30 µl trypsin were added into each well of a 96-well U-bottom plate. Single colonies were picked, transferred into the wells of a U-bottom plate and incubated for 10 min at 37°C. After trypsinization 120 µl selection medium were added to the wells and colonies were disaggregated by pipetting up and down. Cells were then transferred to prepared feeders (drug resistant) on 96- or 48-well plates. In general, 2-3 days after picking ES cells in 96-well plates were dense enough to perform splitting and freezing. It was necessary to isolate DNA from the cells in

order to analyze the clones for successful integration of the constructs. Therefore cells from one 96-well plate were split into three plates: one frozen plate and two plates for isolating DNA. For this procedure the original 96-well plate was washed twice with PBS and cells were trypsinized (30 µl trypsin/well). After trypsinization 120 µl resuspension medium (Table 17) was added to the cells. 50 µl of that cell suspension were transferred to a 96-well U-bottom plate prepared with 50 µl 2 x freezing medium per well (Table 17) and the plate was frozen in a styrofoam box at -80°C. Another 50 µl of the cell suspension were mixed with 150 µl ES cell medium (without LIF) per well of a 96-well plate coated with 0.1% gelatin (v/v). To the remaining third of the cell suspension was mixed with another 150 µl ES cell medium (without LIF). Those two resulting 96-well plates were incubated at 37°C until cells were dense enough for DNA preparation followed by Southern blot analysis (see 6.2.3).

Table 17. Media for split/freeze of ES cells in 96-well plates.

medium	components	Supplier
Resuspension medium	Bicarbonate free DMEM	Gibco
	10 mM HEPES pH7.2	Sigma-Aldrich
	20% ES cell-qualified FCS (v/v)	PAN Biotech GmbH
2 x HEPES freeze medium	Resuspension medium	
	20% DMSO (v/v)	Sigma-Aldrich

ES cells that were picked and directly grown in 48-well plates were frozen as described (see 6.5.2) with ES cell medium containing 20% FCS (v/v) and 20% DMSO (v/v). Four fifth of the cells in one well were frozen in one freezing vial and one fifth of the cells remained on the 48-well plate with ES cell medium (without LIF) for DNA preparation. Genotyping of transgenic ES cell lines by PCR is explained in section 6.2.4.

6.5.4 *in vitro* differentiation of ES cells into the mesodermal cell lineage

For differentiation ES cells have to be cultured in a feeder-free condition. For feeder depletion cells cultured in 6 cm dishes were trypsinized (500 µl trypsin). After trypsinization 3ml ES cell medium was added the plate and the cell suspension was mixed by pipetting. The cell suspension was incubated at 37°C for 20 min. Then cell suspension was transferred into a new 6 cm dish coated with gelatin. This procedure was repeated three times and feeder-free cells remained on the last dish overnight. Feeder depleted cells were trypsinized and counted. Then a cell suspension was prepared with 4 x 10^4 cells/ml in ES cell medium and 5 µl drops (200 cells/drop) were plated on 12 cm square dishes (Greiner) using an electronic 8-channel pipette (Research® pro electronic pipette, Eppendorf). The volume of the cell suspension was calculated based on the following ratios: 3 ml suspension for one 12 cm square dish, one 12 cm square plate fro 7.6 cm^2 area of fibronectin coated plate. Thus, 20 ml of 4 x 10^4 cells/ml suspension were prepared for six 12 cm square dishes, that were plated onto one 10 cm fibronectin coated dish. The 12 cm square dishes plated with drops were inverted and the cells cultured overnight as hanging drops in order to form ES cell aggregates. In parallel plates for the actual differentiation were coated with fibronectin (1% (v:v) in PBS, Calbiochem) and incubated overnight at 4°C. After 18-24 h the ES cell aggregates were washed from the square plates with 10 ml Advanced DMEM (Gibco) per plate, collected in 50 ml tubes and centrifuged (5 min, 200 x g). The pellet was washed with another 10 ml Advanced DMEM to remove as much LIF as possible. Meanwhile, the fibronectin coated plates were washed twice with PBS and left covered with PBS for further use.

After centrifugation the ES cell aggregates were resuspended in SFM (Table 18) supplemented with 20 ng/ml Bmp4 (R&D Biosystems) and plated on fibronectin coated plates and incubated at 37°C, 5% CO_2. The differentiation medium was exchanged daily with at a time freshly added growth factor. The cultivation was continued

Table 18. Serum free medium (SFM)

SFM components	Supplier
50% DMEM/F12 (v:v)	Gibco
50% Neorobasal medium (v/v)	Gibco
2 mM L-glutamine	Lonza
50 U/ml penicillin/50 µg/ml streptomycin	Lonza
1% B-27® (serum free) (v/v)	Invitrogen
0.5% N-2 (v/v)	Invitrogen
0.05% BSA fraction V (v/v)	Sigma-Aldrich
0.15 mM 1-thioglycerol	Sigma-Aldrich

until the cells were harvested on the desired differentiation day.

6.6 Mouse strains and animal husbandry

Mice used for this work were maintained in the animal facility of the Max Planck Institute for Molecular Genetics, Berlin, under conditions according to international standards and protocols.

Animal maintenance and all procedures performed on mice described in this thesis were done in accordance to the German animal welfare act (Tierschutzgesetz,TSchG) and approved by the Berlin federal office for health and social affairs (LaGeSo).

The t^{w18}/+ mouse strain was obtained from Dr. Jean Jaubert (Unité de Génétique Fonctionnelle de la Souris, Institut Pasteur, Paris, France) and kept on a 129S/SvEv and later on 129S2 backgrounds. For embryo analyses t^{w18}/+ animals were crossed to C57BL/6 mice and heterozygous female offspring was mated with t^{w18}/+ males to obtain homozygous embryos. Mice generated from ESCs carrying the *Ppp2r1a*$^{-/-}$ (*Ppp2r1a*$^{tm2a(KOMP)Mbp}$) and Tg(*Ppp2r1a* BAC) alleles were crossed to C57BL/6J to establish and maintain mouse lines. To obtain embryos for analyses transgenic mice were intercrossed or mated with t^{w18}/+ mice.

Diploid aggregation which was used to generate mice from ESCs, was performed by Karol Macura, Lars Wittler and Judith Fiedler according to described protocols (Eakin and Hadjantonakis, 2006).

6.7 General buffers and solution

Table 19. General buffers and solutions

Buffer/solution	Composition
6 x gel loading dye	1 x TAE, 60 mM EDTA, 50% Glycerol, Orange G
PBS	137 mM NaCl, 2.7 mM KCl, 10 mM Na_2HPO_4, 1.8 mM KH_2PO_4
PBST	PBS, 0.1% Tween-20
20 x SSC	300 mM trisodium citrate dihydrate, 3 M NaCl, pH 7
50 x TAE	2 M Tris, 950 mM acetic acid, 62.5 mM EDTA
TBS	50 mM Tris-HCl; pH 7.5, 150 mM NaCl
TBST	TBS, 0.1% Tween-20
TE	10 mM Tris; pH 8, 1 mM EDTA; pH 8

Supplementary

Table S1. Genes deleted in the t^{w18}-haplotype

GeneSymbol	Position on chr 17	Descripbtion
Vmn2r99	19362134	vomeronasal receptor
Vmn2r100	19504810	vomeronasal receptor
Vmn2r101	19577230	vomeronasal receptor
Vmn2r102	19660398	vomeronasal receptor
AB349811	19732845	non-coding RNA
Vmn2r103	19773362	vomeronasal receptor
Vmn2r104	20029424	vomeronasal receptor
Fpr-rs6	20182077	formyl peptide receptor, rel. seq.
Vmn2r105	20208229	vomeronasal receptor
Vmn2r106	20267546	vomeronasal receptor
Vmn2r107	20345424	vomeronasal receptor
Vmn1r224	20419162	vomeronasal receptor
Vmn2r108	20462372	vomeronasal receptor
Vmn1r225	20502298	vomeronasal receptor
Vmn2r109	20540516	vomeronasal receptor
Vmn2r110	20573828	vomeronasal receptor
Fpr-rs3	20623845	formyl peptide receptor, rel. seq.
Vmn1r226	20687507	vomeronasal receptor
Vmn1r227	20735099	vomeronasal receptor
Vmn1r228	20776252	vomeronasal receptor
Vmn1r229	20814494	vomeronasal receptor

GeneSymbol	Position on chr 17	Descripbtion
Vmn1r230	20846550	vomeronasal receptor
Vmn1r231	20889715	vomeronasal receptor
Vmn1r232	20913280	vomeronasal receptor
Ppp2r1a	20945505	PP2A subunit
Vmn1r233	20993726	vomeronasal receptor
Zfp160	21011757	zinc finger protein
Vmn1r234	21228825	vomeronasal receptor
Vmn1r235	21261414	vomeronasal receptor
Vmn1r236	21286621	vomeronasal receptor
Vmn1r237	21314016	vomeronasal receptor
Zfp677	21392521	zinc finger protein
Zfp54	21427798	zinc finger protein
Zfp51	21452499	zinc finger protein
Zfp53	21488987	zinc finger protein
Zfp52	21555045	zinc finger protein
Zfp948	21583112	zinc finger protein
3110052M02Rik	21657581	RIKEN clone
Gm10509	21690473	predicted gene
Zfp760	21707740	zinc finger protein
Zfp229	21739482	zinc finger protein
Zfp820	21818695	zinc finger protein
2210404O09Rik	21879937	RIKEN clone
Zfp942	21928185	zinc finger protein
Zfp943	21988071	zinc finger protein
AB353040	22057333	non-coding RNA
Zfp947	22145377	zinc finger protein

GeneSymbol	Position on chr 17	Descripbtion
Gm4944	22199980	predicted gene
Zfp944	22338785	zinc finger protein
Zfp758	22372058	zinc finger protein
Zfp946	22451122	zinc finger protein
DQ690785	22515536	non-coding RNA
DQ546033	22515743	non-coding RNA
DQ724532	22516242	non-coding RNA
DQ549026	22516388	non-coding RNA
DQ562017	22516560	non-coding RNA
DQ567966	22516771	non-coding RNA
DQ716783	22517043	non-coding RNA
DQ545408	22517953	non-coding RNA
DQ720899	22518025	non-coding RNA
DQ556396	22518063	non-coding RNA
Vmn2r111	22547940	vomeronasal receptor
Vmn2r112	22601147	vomeronasal receptor
Gm16386	22776229	predicted gene
Zfp945	22850601	zinc finger protein
Vmn2r113	22943183	vomeronasal receptor
Vmn2r-ps129	23004970	vomeronasal receptor
Zfp40	23175220	zinc finger protein
Vmn2r114	23290933	vomeronasal receptor
Vmn2r115	23343976	vomeronasal receptor
Vmn2r116	23384802	vomeronasal receptor
Vmn2r117	23459674	vomeronasal receptor
Zfp213	23557659	zinc finger protein

GeneSymbol	Position on chr 17	Descripbtion
Zfp13	23576056	zinc finger protein

Supplementary tables S2-S7 are provided as electronic versions on a Appendix-CD, that can be found attached to the inside of the back cover.

Table S2. Mass spectrometry data of affinity purified SH-PPP2R1A complexes

Table S3. FPKM values of genes in wild-type and t^{w18}/t^{w18} samples

Table S4. Genes dysregulated in t^{w18} ($\log_2(\text{FC}) \geq 1$)

Table S5. Genes dysregulated in t^{w18} ($\log_2(\text{FC}) \geq 1.5$)

Table S6. Genes dysregulated in t^{w18} ($\log_2(\text{FC}) \geq 2$)

Table S7. GO term analyses of genes dysregulated in t^{w18} ($\log_2(\text{FC}) \geq 1$

Literature

Abe, K., Yuzuriha, M., Sugimoto, M., Ko, M. S. H., Brathwaite, M., Waeltz, P., and Nagaraja, R. Gene content of the 750-kb critical region for mouse embryonic ectoderm lethal tcl-w5. *Mammalian genome : official journal of the International Mammalian Genome Society*, 15(4):265–76, April 2004.

Adachi, Y., Takeuchi, T., Nagayama, T., Ohtsuki, Y., and Furihata, M. Zeb1-mediated T-cadherin repression increases the invasive potential of gallbladder cancer. *FEBS letters*, 583(2):430–6, January 2009.

Andrade, M. A. and Bork, P. HEAT repeats in the Huntington's disease protein. *Nature genetics*, 11(2):115–6, October 1995.

Arnold, S. J. and Robertson, E. J. Making a commitment: cell lineage allocation and axis patterning in the early mouse embryo. *Nature reviews. Molecular cell biology*, 10(2):91–103, February 2009.

Arnold, S. J., Stappert, J., Bauer, A., Kispert, A., Herrmann, B. G., and Kemler, R. Brachyury is a target gene of the Wnt/β-catenin signaling pathway. *Mechanisms of Development*, 91(1-2):249–258, March 2000.

Arnold, S. J., Hofmann, U. K., Bikoff, E. K., and Robertson, E. J. Pivotal roles for eomesodermin during axis formation, epithelium-to-mesenchyme transition and endoderm specification in the mouse. *Development (Cambridge, England)*, 135(3): 501–11, February 2008.

Artzt, K., McCormick, P., and Bennett, D. Gene mapping within the T/t complex of the mouse. I. t-lethal genes are nonallelic. *Cell*, 28(3):463–470, March 1982.

Austin, C. P., Battey, J. F., Bradley, A., Bucan, M., Capecchi, M., Collins, F. S., Dove, W. F., Duyk, G., Dymecki, S., Eppig, J. T., Grieder, F. B., Heintz, N., Hicks, G., Insel, T. R., Joyner, A., Koller, B. H., Lloyd, K. C. K., Magnuson, T., Moore, M. W., Nagy, A., Pollock, J. D., Roses, A. D., Sands, A. T., Seed, B., Skarnes, W. C., Snoddy, J., Soriano, P., Stewart, D. J., Stewart, F., Stillman, B., Varmus, H., Varticovski, L., Verma, I. M., Vogt, T. F., von Melchner, H., Witkowski, J., Woychik, R. P., Wurst, W., Yancopoulos, G. D., Young, S. G., and Zambrowicz, B. The knockout mouse project. *Nature genetics*, 36(9):921–4, September 2004.

Avilion, A. A., Nicolis, S. K., Pevny, L. H., Perez, L., Vivian, N., and Lovell-Badge, R. Multipotent cell lineages in early mouse development depend on SOX2 function. *Genes & development*, 17(1):126–40, January 2003a.

Avilion, A. A., Nicolis, S. K., Pevny, L. H., Perez, L., Vivian, N., and Lovell-Badge, R. Multipotent cell lineages in early mouse development depend on SOX2 function. *Genes & development*, 17(1):126–40, January 2003b.

Baillat, D., Hakimi, M.-A., Näär, A. M., Shilatifard, A., Cooch, N., and Shiekhattar, R. Integrator, a multiprotein mediator of small nuclear RNA processing, associates with the C-terminal repeat of RNA polymerase II. *Cell*, 123(2):265–76, October 2005.

Bajpai, R., Makhijani, K., Rao, P. R., and Shashidhara, L. S. Drosophila Twins regulates Armadillo levels in response to Wg/Wnt signal. *Development (Cambridge, England)*, 131(5):1007–16, March 2004.

Barclay, J., King, T. F., Crossley, P. H., Barnard, R. C., Larin, Z., Lehrach, H., and Little, P. F. Physical analysis of the region deleted in the tw18 allele of the mouse tcl-4 complementation group. *Genomics*, 36(1):39–46, August 1996.

Baribault, H., Price, J., Miyai, K., and Oshima, R. G. Mid-gestational lethality in mice lacking keratin 8. *Genes & Development*, 7(7a):1191–1202, July 1993.

Baribault, H., Penner, J., Iozzo, R. V., and Wilson-Heiner, M. Colorectal hyperplasia and inflammation in keratin 8-deficient FVB/N mice. *Genes & Development*, 8(24): 2964–2973, December 1994.

Batut, J., Schmierer, B., Cao, J., Raftery, L. A., Hill, C. S., and Howell, M. Two highly related regulatory subunits of PP2A exert opposite effects on TGF-beta/Activin/Nodal signalling. *Development (Cambridge, England)*, 135(17):2927–37, September 2008.

Bauer, H., Willert, J., Koschorz, B., and Herrmann, B. G. The t complex-encoded GTPase-activating protein Tagap1 acts as a transmission ratio distorter in mice. *Nature genetics*, 37(9):969–73, September 2005.

Bauer, H., Véron, N., Willert, J., and Herrmann, B. G. The t-complex-encoded guanine nucleotide exchange factor Fgd2 reveals that two opposing signaling pathways promote transmission ratio distortion in the mouse. *Genes & development*, 21 (2):143–7, January 2007.

Beck, S., Le Good, J. A., Guzman, M., Ben Haim, N., Roy, K., Beermann, F., and Constam, D. B. Extraembryonic proteases regulate Nodal signalling during gastrulation. *Nature cell biology*, 4(12):981–5, December 2002.

Bennett, D. and Dunn, L. C. Repeated occurences in the mouse of lethal alleles of the same complementation group. *Genetics*, 49:949–58, June 1964.

Bennett, D., Dunn, L. C., and Artzt, K. Genetic Change in Mutations at the T/t-Locus in the Mouse. *Genetics*, 83(2):361–72, June 1976.

Bennett, D. The T-locus of the mouse. *Cell*, 6(4):441–454, December 1975.

Bennett, D. and Dunn, L. C. Effects on embryonic development of a group of genetically similar lethal alleles derived from different populations of wild house mice. *Journal of Morphology*, 103(1):135–157, July 1958.

Bennett, D. and Dunn, L. C. A lethal mutant (tw18) in the house mouse showing partial duplications. *Journal of Experimental Zoology*, 143(2):203–219, March 1960.

Bonhomme, F. Evolutionary relationships in the genus Mus. *Current topics in microbiology and immunology*, 127:19–34, January 1986.

Bosch, M., Cayla, X., Hoof, C., Hemmings, B. A., Ozon, R., Merlevede, W., and Goris, J. The PR55 and PR65 Subunits of Protein Phosphatase 2A from Xenopus laevis. *European Journal of Biochemistry*, 230(3):1037–1045, June 1995.

Brennan, J., Lu, C. C., Norris, D. P., Rodriguez, T. A., Beddington, R. S., and Robertson, E. J. Nodal signalling in the epiblast patterns the early mouse embryo. *Nature*, 411(6840):965–9, June 2001.

Búcan, M., Herrmann, B. G., Frischauf, A. M., Bautch, V. L., Bode, V., Silver, L. M., Martin, G. R., and Lehrach, H. Deletion and duplication of DNA sequences is associated with the embryonic lethal phenotype of the t9 complementation group of the mouse t complex. *Genes & development*, 1(4):376–85, June 1987.

Camus, A., Perea-Gomez, A., Moreau, A., and Collignon, J. Absence of Nodal signaling promotes precocious neural differentiation in the mouse embryo. *Developmental biology*, 295(2):743–55, July 2006.

Cano, A., Pérez-Moreno, M. A., Rodrigo, I., Locascio, A., Blanco, M. J., del Barrio, M. G., Portillo, F., and Nieto, M. A. The transcription factor snail controls epithelial-mesenchymal transitions by repressing E-cadherin expression. *Nature cell biology*, 2(2):76–83, February 2000.

Carver, E. A., Jiang, R., Lan, Y., Oram, K. F., and Gridley, T. The mouse snail gene encodes a key regulator of the epithelial-mesenchymal transition. *Molecular and cellular biology*, 21(23):8184–8, December 2001.

Chen, J., Ezzeddine, N., Waltenspiel, B., Albrecht, T. R., Warren, W. D., Marzluff, W. F., and Wagner, E. J. An RNAi screen identifies additional members of the Drosophila Integrator complex and a requirement for cyclin C/Cdk8 in snRNA 3'-end formation. *RNA (New York, N.Y.)*, 18(12):2148–56, December 2012.

Chesley, P. and Dunn, L. C. The Inheritance of Taillessness (Anury) in the House Mouse. *Genetics*, 21(5):525–36, September 1936.

Ciatto, C., Bahna, F., Zampieri, N., VanSteenhouse, H. C., Katsamba, P. S., Ahlsen, G., Harrison, O. J., Brasch, J., Jin, X., Posy, S., Vendome, J., Ranscht, B., Jessell, T. M., Honig, B., and Shapiro, L. T-cadherin structures reveal a novel adhesive binding mechanism. *Nature structural & molecular biology*, 17(3):339–47, March 2010.

Ciruna, B. G. and Rossant, J. Expression of the T-box gene Eomesodermin during early mouse development. *Mechanisms of Development*, 81(1-2):199–203, March 1999.

Clift, D., Bizzari, F., and Marston, A. L. Shugoshin prevents cohesin cleavage by PP2A(Cdc55)-dependent inhibition of separase. *Genes & development*, 23(6):766–80, March 2009.

Colowick, S. P., Kaplan, N. O., Wassarman, P. M., and DePamphilis, M. L. *Methods in Enzymology: Guide to techniques in mouse development / edited by Paul M. Wassarman, Melvin L. DePamphilis, Volume 225*. Academic Press, 1993.

Coucouvanis, E. and Martin, G. BMP signaling plays a role in visceral endoderm differentiation and cavitation in the early mouse embryo. *Development*, 126(3): 535–546, February 1999.

Crossley, P. and Martin, G. The mouse Fgf8 gene encodes a family of polypeptides and is expressed in regions that direct outgrowth and patterning in the developing embryo. *Development*, 121(2):439–451, February 1995.

Dallosso, A. R., Ø ster, B., Greenhough, A., Thorsen, K., Curry, T. J., Owen, C., Hancock, A. L., Szemes, M., Paraskeva, C., Frank, M., Andersen, C. L., and Malik, K. Long-range epigenetic silencing of chromosome 5q31 protocadherins is involved in early and late stages of colorectal tumorigenesis through modulation of oncogenic pathways. *Oncogene*, 31(40):4409–19, October 2012.

Dobrovolskaia-Zavadskaia, N. and Kobozieff, N. Les souris anoures et a queue filiforme qui se reproduisent entre elles sans disjonction. *CR Soc Biol*, 1932.

Dubrulle, J. and Pourquié, O. fgf8 mRNA decay establishes a gradient that couples axial elongation to patterning in the vertebrate embryo. *Nature*, 427(6973):419–22, January 2004.

Dunn, L. C. A Third Lethal in the T (Brachy) Series in the House Mouse. *Proceedings of the National Academy of Sciences of the United States of America*, 23(9):474–7, September 1937.

Dunn, L. C. Studies of the Genetic Variability in Populations of Wild House Mice. II. Analysis of Eight Additional Alleles at Locus T. *Genetics*, 42(3):299–311, May 1957.

Dunn, L. C., Bennett, D., and Beasley, A. B. Mutation and recombination in the vicinity of a complex gene. *Genetics*, 47:285–303, March 1962.

Dunwoodie, S. L., Rodriguez, T. A., and Beddington, R. S. Msg1 and Mrg1, founding members of a gene family, show distinct patterns of gene expression during mouse embryogenesis. *Mechanisms of Development*, 72(1-2):27–40, March 1998.

Dush, M. K. and Martin, G. R. Analysis of mouse Evx genes: Evx-1 displays graded expression in the primitive streak. *Developmental Biology*, 151(1):273–287, May 1992.

Eakin, G. S. and Hadjantonakis, A.-K. Production of chimeras by aggregation of embryonic stem cells with diploid or tetraploid mouse embryos. *Nature protocols*, 1(3):1145–53, January 2006.

Eichhorn, P. J. A., Creyghton, M. P., and Bernards, R. Protein phosphatase 2A regulatory subunits and cancer. *Biochimica et biophysica acta*, 1795(1):1–15, January 2009.

Fujiki, H. and Suganuma, M. Tumor Promotion by Inhibitors of ProteinZ Phosphatases 1 and 2A: The Okadaic Acid Class of Compounds. *Advances in Cancer Research*, 61:143–194, 1993.

Fujimura, N., Vacik, T., Machon, O., Vlcek, C., Scalabrin, S., Speth, M., Diep, D., Krauss, S., and Kozmik, Z. Wnt-mediated down-regulation of Sp1 target genes by a transcriptional repressor Sp5. *The Journal of biological chemistry*, 282(2):1225–37, January 2007.

George, S. H. L., Gertsenstein, M., Vintersten, K., Korets-Smith, E., Murphy, J., Stevens, M. E., Haigh, J. J., and Nagy, A. Developmental and adult phenotyping directly from mutant embryonic stem cells. *Proceedings of the National Academy of Sciences of the United States of America*, 104(11):4455–60, March 2007.

Gilbert, S. F. *Developmental Biology*. Sinauer Associates, Incorporated, 2014.

Glatter, T., Wepf, A., Aebersold, R., and Gstaiger, M. An integrated workflow for charting the human interaction proteome: insights into the PP2A system. *Molecular systems biology*, 5:237, January 2009.

Goldberg, M., Peshkovsky, C., Shifteh, A., and Al-Awqati, Q. mu-Protocadherin, a novel developmentally regulated protocadherin with mucin-like domains. *The Journal of biological chemistry*, 275(32):24622–9, August 2000.

Goris, J., Hermann, J., Hendrix, P., Ozon, R., and Merlevede, W. Okadaic acid, a specific protein phosphatase inhibitor, induces maturation and MPF formation in Xenopus laevis oocytes. *FEBS Letters*, 245(1-2):91–94, March 1989.

Götz, J., Probst, A., Ehler, E., Hemmings, B., and Kues, W. Delayed embryonic lethality in mice lacking protein phosphatase 2A catalytic subunit C. *Proceedings of the National Academy of Sciences*, 95(21):12370–12375, October 1998.

Goudreault, M., D'Ambrosio, L. M., Kean, M. J., Mullin, M. J., Larsen, B. G., Sanchez, A., Chaudhry, S., Chen, G. I., Sicheri, F., Nesvizhskii, A. I., Aebersold, R., Raught, B., and Gingras, A.-C. A PP2A phosphatase high density interaction network identifies a novel striatin-interacting phosphatase and kinase complex linked to the cerebral cavernous malformation 3 (CCM3) protein. *Molecular & cellular proteomics : MCP*, 8(1):157–71, January 2009.

Griswold-Prenner, I., Kamibayashi, C., Maruoka, E. M., Mumby, M. C., and Derynck, R. Physical and functional interactions between type I transforming growth factor beta receptors and Balpha, a WD-40 repeat subunit of phosphatase 2A. *Molecular and cellular biology*, 18(11):6595–604, November 1998.

Groves, M. R., Hanlon, N., Turowski, P., Hemmings, B. A., and Barford, D. The Structure of the Protein Phosphatase 2A PR65/A Subunit Reveals the Conformation of Its 15 Tandemly Repeated HEAT Motifs. *Cell*, 96(1):99–110, January 1999.

Hammer, M. F. and Silver, L. M. Phylogenetic analysis of the alpha-globin pseudogene-4 (Hba-ps4) locus in the house mouse species complex reveals a stepwise evolution of t haplotypes [published erratum appears in Mol Biol Evol 1994 Jan;11(1):158]. *Mol. Biol. Evol.*, 10(5):971–1001, September 1993.

Hammer, M. F., Schimenti, J., and Silver, L. M. Evolution of mouse chromosome 17 and the origin of inversions associated with t haplotypes. *Proceedings of the National Academy of Sciences*, 86(9):3261–3265, May 1989.

Hart, A. H., Hartley, L., Ibrahim, M., and Robb, L. Identification, cloning and expression analysis of the pluripotency promoting Nanog genes in mouse and human. *Developmental dynamics : an official publication of the American Association of Anatomists*, 230(1):187–98, May 2004.

Hellmuth, S., Böttger, F., Pan, C., Mann, M., and Stemmann, O. PP2A delays APC/C-dependent degradation of separase-associated but not free securin. *The EMBO journal*, 33(10):1134–47, May 2014.

Hemmings, B. A., Adams-Pearson, C., Maurer, F., Mueller, P., Goris, J., Merlevede, W., Hofsteenge, J., and Stone, S. R. .alpha.- And .beta.-forms of the 65-kDa subunit of protein phosphatase 2A have a similar 39 amino acid repeating structure. *Biochemistry*, 29(13):3166–3173, April 1990.

Hendrix, P., Turowski, P., Mayer-Jaekel, R. E., Goris, J., Hofsteenge, J., Merlevede, W., and Hemmings, B. A. Analysis of subunit isoforms in protein phosphatase 2A holoenzymes from rabbit and Xenopus. *J. Biol. Chem.*, 268(10):7330–7337, April 1993.

Hermesz, E., Mackem, S., and Mahon, K. Rpx: a novel anterior-restricted homeobox gene progressively activated in the prechordal plate, anterior neural plate and Rathke's pouch of the mouse embryo. *Development*, 122(1):41–52, January 1996.

Herrmann, B. G., Koschorz, B., Wertz, K., McLaughlin, K. J., and Kispert, A. A protein kinase encoded by the t complex responder gene causes non-mendelian inheritance. *Nature*, 402(6758):141–6, November 1999.

Herzog, F., Kahraman, A., Boehringer, D., Mak, R., Bracher, A., Walzthoeni, T., Leitner, A., Beck, M., Hartl, F.-U., Ban, N., Malmström, L., and Aebersold, R. Structural probing of a protein phosphatase 2A network by chemical cross-linking and mass spectrometry. *Science (New York, N.Y.)*, 337(6100):1348–52, September 2012.

Hinkel, I., Duluc, I., Martin, E., Guenot, D., Freund, J.-N., and Gross, I. Cdx2 controls expression of the protocadherin Mucdhl, an inhibitor of growth and β-catenin activity in colon cancer cells. *Gastroenterology*, 142(4):875–885.e3, April 2012.

Holland, A. J., Böttger, F., Stemmann, O., and Taylor, S. S. Protein phosphatase 2A and separase form a complex regulated by separase autocleavage. *The Journal of biological chemistry*, 282(34):24623–32, August 2007.

Hombauer, H., Weismann, D., Mudrak, I., Stanzel, C., Fellner, T., Lackner, D. H., and Ogris, E. Generation of active protein phosphatase 2A is coupled to holoenzyme assembly. *PLoS biology*, 5(6):e155, June 2007.

Hu, M.-W., Wang, Z.-B., Jiang, Z.-Z., Qi, S.-T., Huang, L., Liang, Q.-X., Schatten, H., and Sun, Q.-Y. Scaffold subunit Aalpha of PP2A is essential for female meiosis and fertility in mice. *Biology of reproduction*, 91(1):19, July 2014.

Huang, J., Gong, Z., Ghosal, G., and Chen, J. SOSS complexes participate in the maintenance of genomic stability. *Molecular cell*, 35(3):384–93, August 2009.

Huelsken, J., Vogel, R., Brinkmann, V., Erdmann, B., Birchmeier, C., and Birchmeier, W. Requirement for beta-Catenin in Anterior-Posterior Axis Formation in Mice. *The Journal of Cell Biology*, 148(3):567–578, February 2000.

Janssens, V. and Goris, J. Protein phosphatase 2A: a highly regulated family of serine/threonine phosphatases implicated in cell growth and signalling. *Biochem. J.*, 353:417–439, February 2001.

Jho, E.-h., Zhang, T., Domon, C., Joo, C.-K., Freund, J.-N., and Costantini, F. Wnt/beta-catenin/Tcf signaling induces the transcription of Axin2, a negative regulator of the signaling pathway. *Molecular and cellular biology*, 22(4):1172–83, February 2002.

Jones, C., Kuehn, M., Hogan, B., Smith, J., and Wright, C. Nodal-related signals induce axial mesoderm and dorsalize mesoderm during gastrulation. *Development*, 121(11):3651–3662, November 1995.

Jurica, M. S. and Moore, M. J. Pre-mRNA Splicing: Awash in a Sea of Proteins. *Molecular Cell*, 12(1):5–14, July 2003.

Kapp, L. D., Abrams, E. W., Marlow, F. L., and Mullins, M. C. The integrator complex subunit 6 (Ints6) confines the dorsal organizer in vertebrate embryogenesis. *PLoS genetics*, 9(10):e1003822, October 2013.

Katz, D. F., Erickson, R. P., and Nathanson, M. Beat frequency is bimodally distributed in spermatozoa from T/t12 mice. *The Journal of experimental zoology*, 210 (3):529–35, December 1979.

Kelly, O. G., Pinson, K. I., and Skarnes, W. C. The Wnt co-receptors Lrp5 and Lrp6 are essential for gastrulation in mice. *Development (Cambridge, England)*, 131(12): 2803–15, June 2004.

Kimura-Yoshida, C., Nakano, H., Okamura, D., Nakao, K., Yonemura, S., Belo, J. A., Aizawa, S., Matsui, Y., and Matsuo, I. Canonical Wnt signaling and its antagonist regulate anterior-posterior axis polarization by guiding cell migration in mouse visceral endoderm. *Developmental cell*, 9(5):639–50, November 2005.

Kinoshita, N., Ohkura, H., and Yanagida, M. Distinct, essential roles of type 1 and 2A protein phosphatases in the control of the fission yeast cell division cycle. *Cell*, 63(2):405–415, October 1990.

Kispert, A. and Herrmann, B. G. The Brachyury gene encodes a novel DNA binding protein. *The EMBO journal*, 12(8):3211–20, August 1993.

Kitajima, T. S., Sakuno, T., Ishiguro, K.-i., Iemura, S.-i., Natsume, T., Kawashima, S. A., and Watanabe, Y. Shugoshin collaborates with protein phosphatase 2A to protect cohesin. *Nature*, 441(7089):46–52, May 2006.

Klein, J., Sipos, P., and Figueroa, F. Polymorphism of t-complex genes in European wild mice. *Genetical Research*, 44(01):39, April 1984.

Kondoh, H. and Kuroiwa, A. *New Principles in Developmental Processes*. Springer, 2014.

Kremmer, E., Ohst, K., Kiefer, J., Brewis, N., and Walter, G. Separation of PP2A core enzyme and holoenzyme with monoclonal antibodies against the regulatory A subunit: abundant expression of both forms in cells. *Mol. Cell. Biol.*, 17(3):1692–1701, March 1997.

Kumar, A., Novoselov, V., Celeste, A. J., Wolfman, N. M., ten Dijke, P., and Kuehn, M. R. Nodal signaling uses activin and transforming growth factor-beta receptor-regulated Smads. *The Journal of biological chemistry*, 276(1):656–61, January 2001.

Kuphal, S., Martyn, A. C., Pedley, J., Crowther, L. M., Bonazzi, V. F., Parsons, P. G., Bosserhoff, A. K., Hayward, N. K., and Boyle, G. M. H-cadherin expression reduces invasion of malignant melanoma. *Pigment cell & melanoma research*, 22(3): 296–306, June 2009.

Lawson, K. A. Fate mapping the mouse embryo. *The International journal of developmental biology*, 43(7):773–5, January 1999.

Lee, S. H-cadherin expression inhibits in vitro invasiveness and tumor formation in vivo. *Carcinogenesis*, 19(6):1157–1159, June 1998.

Lenington, S., Franks, P., and Williams, J. Distribution of T-Haplotypes in Natural Populations of Wild House Mice. *Journal of Mammalogy*, 69(3):489, August 1988.

Li, X., Yost, H. J., Virshup, D. M., and Seeling, J. M. Protein phosphatase 2A and its B56 regulatory subunit inhibit Wnt signaling in Xenopus. *The EMBO journal*, 20 (15):4122–31, August 2001.

Liu, P., Wakamiya, M., Shea, M. J., Albrecht, U., Behringer, R. R., and Bradley, A. Requirement for Wnt3 in vertebrate axis formation. *Nature genetics*, 22(4):361–5, August 1999.

Liu, P., Jenkins, N. A., and Copeland, N. G. A highly efficient recombineering-based method for generating conditional knockout mutations. *Genome research*, 13(3): 476–84, March 2003.

Lohnes, D. The Cdx1 homeodomain protein: an integrator of posterior signaling in the mouse. *BioEssays : news and reviews in molecular, cellular and developmental biology*, 25(10):971–80, October 2003.

Longin, S., Jordens, J., Martens, E., Stevens, I., Janssens, V., Rondelez, E., De Baere, I., Derua, R., Waelkens, E., Goris, J., and Van Hoof, C. An inactive protein phosphatase 2A population is associated with methylesterase and can be re-activated by the phosphotyrosyl phosphatase activator. *The Biochemical journal*, 380(Pt 1): 111–9, May 2004.

Lustig, B., Jerchow, B., Sachs, M., Weiler, S., Pietsch, T., Karsten, U., van de Wetering, M., Clevers, H., Schlag, P. M., Birchmeier, W., and Behrens, J. Negative feedback loop of Wnt signaling through upregulation of conductin/axin2 in colorectal and liver tumors. *Molecular and cellular biology*, 22(4):1184–93, February 2002.

Lyon, M. F. Transmission ratio distortion in mouse t-haplotypes is due to multiple distorter genes acting on a responder locus. *Cell*, 37(2):621–628, June 1984.

Lyon, M. F. Male sterility of the mouse t-complex is due to homozygosity of the distorter genes. *Cell*, 44(2):357–363, January 1986.

Lyon, M. F. Transmission ratio distortion in mice. *Annual review of genetics*, 37:393–408, January 2003.

Lyon, M. F. and Phillips, R. J. S. Crossing-over in mice heterozygous for t-alleles. *Heredity*, 13(1):23–32, February 1959.

Macneil, L. T. and Walhout, A. J. M. Gene regulatory networks and the role of robustness and stochasticity in the control of gene expression. *Genome research*, 21 (5):645–57, May 2011.

Martin, G. R., Silver, L. M., Fox, H. S., and Joyner, A. L. Establishment of embryonic stem cell lines from preimplantation mouse embryos homozygous for lethal mutations in the t-complex. *Developmental Biology*, 121(1):20–28, May 1987.

Mitsui, K., Tokuzawa, Y., Itoh, H., Segawa, K., Murakami, M., Takahashi, K., Maruyama, M., Maeda, M., and Yamanaka, S. The Homeoprotein Nanog Is Required for Maintenance of Pluripotency in Mouse Epiblast and ES Cells. *Cell*, 113 (5):631–642, May 2003.

Morita, T., Kubota, H., Murata, K., Nozaki, M., Delarbre, C., Willison, K., Satta, Y., Sakaizumi, M., Takahata, N., and Gachelin, G. Evolution of the mouse t haplotype: recent and worldwide introgression to Mus musculus. *Proceedings of the National Academy of Sciences*, 89(15):6851–6855, August 1992.

Moser, G. C. and Gluecksohn-Waelsch, S. Developmental genetics of a recessive allele at the complex T-locus in the mouse. *Developmental Biology*, 16(6):564–576, December 1967.

Nagy, A. *Manipulating the Mouse Embryo: A Laboratory Manual*. Cold Spring Harbor Laboratory Press, 2003.

Nakaya, Y., Sukowati, E. W., Wu, Y., and Sheng, G. RhoA and microtubule dynamics control cell-basement membrane interaction in EMT during gastrulation. *Nature cell biology*, 10(7):765–75, July 2008.

Nichols, J., Zevnik, B., Anastassiadis, K., Niwa, H., Klewe-Nebenius, D., Chambers, I., Schöler, H., and Smith, A. Formation of Pluripotent Stem Cells in the Mammalian Embryo Depends on the POU Transcription Factor Oct4. *Cell*, 95(3): 379–391, October 1998.

Nizetić, D., Figueroa, F., and Klein, J. Evolutionary relationships between the t and H-2 haplotypes in the house mouse. *Immunogenetics*, 19(4):311–20, January 1984.

Norris, D. P. and Robertson, E. J. Asymmetric and node-specific nodal expression patterns are controlled by two distinct cis-acting regulatory elements. *Genes & Development*, 13(12):1575–1588, June 1999.

Norris, D. P., Brennan, J., Bikoff, E. K., and Robertson, E. J. The Foxh1-dependent autoregulatory enhancer controls the level of Nodal signals in the mouse embryo. *Development*, 129(14):3455–3468, July 2002.

Obata, S., Sago, H., Mori, N., Rochelle, J., Seldin, M., Davidson, M., St John, T., Taketani, S., and Suzuki, S. Protocadherin Pcdh2 shows properties similar to, but distinct from, those of classical cadherins. *J. Cell Sci.*, 108(12):3765–3773, December 1995.

Olds-Clarke, P. and Johnson, L. R. t haplotypes in the mouse compromise sperm flagellar function. *Developmental biology*, 155(1):14–25, January 1993.

Oosterveen, T., Meijlink, F., and Deschamps, J. Expression of retinaldehyde dehydrogenase II and sequential activation of 5′ Hoxb genes in the mouse caudal hindbrain. *Gene expression patterns : GEP*, 4(3):243–7, May 2004.

Osoegawa, K., Tateno, M., Woon, P. Y., Frengen, E., Mammoser, A. G., Catanese, J. J., Hayashizaki, Y., and de Jong, P. J. Bacterial artificial chromosome libraries for mouse sequencing and functional analysis. *Genome research*, 10(1):116–28, January 2000.

Pearce, J. J. and Evans, M. J. Mml, a mouse Mix-like gene expressed in the primitive streak. *Mechanisms of Development*, 87(1-2):189–192, September 1999.

Pfister, S., Steiner, K. A., and Tam, P. P. L. Gene expression pattern and progression of embryogenesis in the immediate post-implantation period of mouse development. *Gene expression patterns : GEP*, 7(5):558–73, April 2007.

Piccolo, S., Agius, E., Leyns, L., Bhattacharyya, S., Grunz, H., Bouwmeester, T., and De Robertis, E. M. The head inducer Cerberus is a multifunctional antagonist of Nodal, BMP and Wnt signals. *Nature*, 397(6721):707–10, February 1999.

Rattani, A., Wolna, M., Ploquin, M., Helmhart, W., Morrone, S., Mayer, B., Godwin, J., Xu, W., Stemmann, O., Pendas, A., and Nasmyth, K. Sgol2 provides a regulatory platform that coordinates essential cell cycle processes during meiosis I in oocytes. *eLife*, 2:e01133, January 2013.

Rivera-Pérez, J. A. and Magnuson, T. Primitive streak formation in mice is preceded by localized activation of Brachyury and Wnt3. *Developmental biology*, 288(2):363–71, December 2005.

Robb, L., Hartley, L., Begley, C. G., Brodnicki, T. C., Copeland, N. G., Gilbert, D. J., Jenkins, N. A., and Elefanty, A. G. Cloning, expression analysis, and chromosomal localization of murine and human homologues of a Xenopus mix gene. *Developmental dynamics : an official publication of the American Association of Anatomists*, 219 (4):497–504, December 2000.

Robertson, E. J. *Teratocarcinomas and embryonic stem cells: a practical approach*. IRL Press, 1987.

Russ, A. P., Wattler, S., Colledge, W. H., Aparicio, S. A., Carlton, M. B., Pearce, J. J., Barton, S. C., Surani, M. A., Ryan, K., Nehls, M. C., Wilson, V., and Evans, M. J. Eomesodermin is required for mouse trophoblast development and mesoderm formation. *Nature*, 404(6773):95–9, March 2000.

Sambrook, J. and Russel, D. W. *Molecular cloning: a laboratory manual*. Cold Spring Habor Laboratory Press, New York, 3 edition, 2001.

Schier, A. F. and Shen, M. M. Nodal signalling in vertebrate development. *Nature*, 403(6768):385–9, January 2000.

Schoenwolf, G. C. Tail (end) bud contributions to the posterior region of the chick embryo. *Journal of Experimental Zoology*, 201(2):227–245, August 1977.

Seeling, J. M. Regulation of -Catenin Signaling by the B56 Subunit of Protein Phosphatase 2A. *Science*, 283(5410):2089–2091, March 1999.

Sents, W., Ivanova, E., Lambrecht, C., Haesen, D., and Janssens, V. The biogenesis of active protein phosphatase 2A holoenzymes: a tightly regulated process creating phosphatase specificity. *The FEBS journal*, 280(2):644–61, January 2013.

Shimono, A. and Behringer, R. R. Angiomotin Regulates Visceral Endoderm Movements during Mouse Embryogenesis. *Current Biology*, 13(7):613–617, April 2003.

Shin, E. Transcriptome analysis of Bmp4-induced mesoderm formation in vitro. *PhD thesis*, 2011.

Silver, L. M. Mouse t haplotypes. *Annual review of genetics*, 19:179–208, January 1985.

Silver, L. M., White, M., and Artzt, K. Evidence for unequal crossing over within the mouse T/t complex. *Proceedings of the National Academy of Sciences*, 77(10): 6077–6080, October 1980.

Silver, L. M. The peculiar journey of a selfish chromosome: mouse t haplotypes and meiotic drive. *Trends in Genetics*, 9(7):250–254, July 1993.

Silver, L. M. and Artzt, K. Recombination suppression of mouse t-haplotypes due to chromatin mismatching. *Nature*, 290(5801):68–70, March 1981.

Silver, L. M., Artzt, K., Barlow, D., Fischer-Lindahl, K., Lyon, M. F., Klein, J., and Snyder, L. Mouse Chromosome 17. *Mammalian Genome*, 3(S1):S241–S260, 1992.

Skaar, J. R., Richard, D. J., Saraf, A., Toschi, A., Bolderson, E., Florens, L., Washburn, M. P., Khanna, K. K., and Pagano, M. INTS3 controls the hSSB1-mediated DNA damage response. *The Journal of cell biology*, 187(1):25–32, October 2009.

Slack, J. M. W. *Essential Developmental Biology*. John Wiley & Sons, 2009.

Smith, L. J. A morphological and histochemical investigation of a preimplantation lethal (t12) in the house mouse. *Journal of Experimental Zoology*, 132(1):51–83, June 1956.

Snaith, H. A., Armstrong, C. G., Guo, Y., Kaiser, K., and Cohen, P. T. Deficiency of protein phosphatase 2A uncouples the nuclear and centrosome cycles and prevents attachment of microtubules to the kinetochore in Drosophila microtubule star (mts) embryos. *J. Cell Sci.*, 109(13):3001–3012, December 1996.

Snow, M. H. L. and Bennett, D. Gastrulation in the mouse: assessment of cell populations in the epiblast of twl8/tw18 embryos. *J Embryol Exp Morphol*, 47(1):39–52, October 1978.

Suganuma, M., Fujiki, H., Suguri, H., Yoshizawa, S., Hirota, M., Nakayasu, M., Ojika, M., Wakamatsu, K., Yamada, K., and Sugimura, T. Okadaic acid: an additional non-phorbol-12-tetradecanoate-13-acetate-type tumor promoter. *Proceedings of the National Academy of Sciences*, 85(6):1768–1771, March 1988.

Sugimoto, M., Kondo, M., Hirose, M., Suzuki, M., Mekada, K., Abe, T., Kiyonari, H., Ogura, A., Takagi, N., Artzt, K., and Abe, K. Molecular Identification of tw5: Vps52 Promotes Pluripotential Cell Differentiation through Cell-Cell Interactions. *Cell Reports*, 2(5):1363–1374, 2012.

Swindell, E. C., Thaller, C., Sockanathan, S., Petkovich, M., Jessell, T. M., and Eichele, G. Complementary domains of retinoic acid production and degradation in the early chick embryo. *Developmental biology*, 216(1):282–96, December 1999.

Tam, P. P. L. and Loebel, D. A. F. Gene function in mouse embryogenesis: get set for gastrulation. *Nature reviews. Genetics*, 8(5):368–81, May 2007.

Thomas, P., Brown, A., and Beddington, R. Hex: a homeobox gene revealing peri-implantation asymmetry in the mouse embryo and an early transient marker of endothelial cell precursors. *Development*, 125(1):85–94, January 1998.

Threadgill, D., Dlugosz, A., Hansen, L., Tennenbaum, T., Lichti, U., Yee, D., LaMantia, C., Mourton, T., Herrup, K., Harris, R., and Et, A. Targeted disruption of mouse EGF receptor: effect of genetic background on mutant phenotype. *Science*, 269(5221):230–234, July 1995.

Tortelote, G. G., Hernández-Hernández, J. M., Quaresma, A. J. C., Nickerson, J. A., Imbalzano, A. N., and Rivera-Pérez, J. A. Wnt3 function in the epiblast is required

for the maintenance but not the initiation of gastrulation in mice. *Developmental biology*, 374(1):164–73, February 2013.

Toyama, R., O'Connell, M. L., Wright, C. V., Kuehn, M. R., and Dawid, I. B. Nodal induces ectopic goosecoid and lim1 expression and axis duplication in zebrafish. *Development (Cambridge, England)*, 121(2):383–91, February 1995.

Vafai, S. B. and Stock, J. B. Protein phosphatase 2A methylation: a link between elevated plasma homocysteine and Alzheimer,Äôs Disease. *FEBS Letters*, 518(1-3):1–4, May 2002.

Vidigal, J. A., Morkel, M., Wittler, L., Brouwer-Lehmitz, A., Grote, P., Macura, K., and Herrmann, B. G. An inducible RNA interference system for the functional dissection of mouse embryogenesis. *Nucleic acids research*, 38(11):e122, June 2010.

Virshup, D. M. Protein phosphatase 2A: a panoply of enzymes. *Current Opinion in Cell Biology*, 12(2):180–185, April 2000.

Wassarman, D. A., Solomon, N. M., Chang, H. C., Karim, F. D., Therrien, M., and Rubin, G. M. Protein phosphatase 2A positively and negatively regulates Ras1-mediated photoreceptor development in Drosophila. *Genes & Development*, 10(3): 272–278, February 1996.

Weidinger, G., Thorpe, C. J., Wuennenberg-Stapleton, K., Ngai, J., and Moon, R. T. The Sp1-related transcription factors sp5 and sp5-like act downstream of Wnt/beta-catenin signaling in mesoderm and neuroectoderm patterning. *Current biology : CB*, 15(6):489–500, March 2005.

Wolpert, L. *Principles of Development*. Oxford University Press, 3rd edition, 2007.

Xu, Z., Cetin, B., Anger, M., Cho, U. S., Helmhart, W., Nasmyth, K., and Xu, W. Structure and function of the PP2A-shugoshin interaction. *Molecular cell*, 35(4): 426–41, August 2009.

Yamamoto, H., Hinoi, T., Michiue, T., Fukui, A., Usui, H., Janssens, V., Van Hoof, C., Goris, J., Asashima, M., and Kikuchi, A. Inhibition of the Wnt signaling pathway by the PR61 subunit of protein phosphatase 2A. *The Journal of biological chemistry*, 276(29):26875–82, July 2001.

Yamashita, K., Yasuda, H., Pines, J., Yasumoto, K., Nishitani, H., Ohtsubo, M., Hunter, T., Sugimura, T., and Nishimoto, T. Okadaic acid, a potent inhibitor of type 1 and type 2A protein phosphatases, activates cdc2/H1 kinase and transiently induces a premature mitosis-like state in BHK21 cells. *The EMBO journal*, 9(13):4331–8, December 1990.

Yang, J., Wu, J., Tan, C., and Klein, P. S. PP2A:B56epsilon is required for Wnt/beta-catenin signaling during embryonic development. *Development (Cambridge, England)*, 130(23):5569–78, December 2003.

Zhang, W., Yang, J., Liu, Y., Chen, X., Yu, T., Jia, J., and Liu, C. PR55 alpha, a regulatory subunit of PP2A, specifically regulates PP2A-mediated beta-catenin dephosphorylation. *The Journal of biological chemistry*, 284(34):22649–56, August 2009.

List of Tables

List of Figures

Danksagung

Zuallererst möchte ich mich bei Prof. Dr. Bernhard G. Herrmann bedanken, mir die Möglichkeit gegeben zu haben, meine Promotion in seiner Abteilung durchführen zu dürfen. Ich danke ihm auch für die Betreuung sowohl beim praktischen Teil als auch beim schriftlichen Verfassen der Arbeit. Bei Prof. Dr. Rupert Mutzel bedanke ich mich für Begutachtung meiner Arbeit als Universitäts-interner Betreuer.
Mein ganz besonderer Dank gilt Matthias Marks für seine ständige Hilfe und Geduld, für jegliche Ratschläge und seine Unterstützung auch außerhalb des Labors, die diese Arbeit erst ermöglicht haben.
Außerdem danke ich Sandra Währisch, Manuela Scholze und Gaby Bläß nicht nur für ihre tatkräftige Hilfe in der Zellkultur und bei allen anderen Problemen und Fragen im Labor, sondern auch für die schöne Zeit, die sie mir bereitet haben. Ich bin Dr. Tracie Pennimpede, Dr. Hermann Bauer, Dr. Lars Wittler, Dr. Frederic Koch, Dr. Phillip Grote und Dr. Heiner Schrewe sehr dankbar für die vielen, vielen Ratschläge, fachliche Diskussionen und jegliche Hilfe. Tracie danke ich auch für die tolle Atmosphäre, mit der sie die Abteilung durch ihr sonniges Gemüt bereichert hat und ihr superschnelles Korrekturlesen. Dr. Pavel Tsaytler danke ich für die Einführung in die Differenzierung von ES-Zellen. Ich bin Karol Macura, Judith Fiedler und Dr. Lars Wittler für die Generierung von Mäusen aus ES-Zellen dankbar. Bei Carolin Willke und Sonja Banko bedanke ich mich für die exzellente Pflege der Mauslinien. Außerdem danke ich Dr. Matthias Gstaiger für die Bereitstellung des SH-Tags und die Durchführung der Massenspektrometrieversuche.
Ich möchte mich auch bei allen jetzigen und ehemaligen Mitgliedern der Abteilung nicht nur für die freundliche und angenehme Arbeitsatmosphäre bedanken, sondern auch viele Gespräche und tolle Kuchen. Ich habe es sehr genossen, mit euch zusammenzuarbeiten und hoffe sehr, auch in meinem zukünftigen Karriereweg solch starken Zusammenhalt und gegenseitige Hilfe zu erleben.

Zuletzt danke ich auch meiner Familie für ihre Unterstüzung, Liebe und Geduld.